TÉCNICO LISBOA

A three-dimensional regression model of the shoulder rhythm in a wide-ranging envelope of humeral postures

Gil Perdigão Gonçalves

Thesis to obtain the Master of Science Degree in

Biomedical Engineering

Supervisor(s): Prof. Jorge Alberto Cadete Ambrósio

Prof. Carlos Miguel Fernandes Quental

Examination Committee

Chairperson: Prof. Fernando Manuel Fernandes Simões

Supervisor: Prof. Carlos Miguel Fernandes Quental

Member of the Committee: Prof. Miguel Pedro Tavares da Silva

July 2021

Preface

The work presented in this dissertation was performed at the Lisbon Biomechanics Laboratory of Instituto Superior Técnico (Lisbon, Portugal), during the period September 2020 - July 2021, under the supervision of Prof. Jorge Alberto Cadete Ambrósio and Prof. Carlos Miguel Fernandes Quental.

Declaration

I declare that this document is an original work of my own authorship and that it fulfills all the requirements of the Code of Conduct and Good Practices of the Universidade de Lisboa.

Acknowledgments

Antes de mais, o meu mais sentido agradecimento ao Professor Jorge Alberto Cadete Ambrósio. A sua paixão e experiência iluminaram o meu trabalho e motivaram-me quando mais precisava. Sempre pude contar com o seu apoio, vastos conhecimentos e boa-disposição. As nossas reuniões semanais forneceram-me importantes lições, que certamente me acompanharão ao longo do meu percurso profissional. Por último (mas não menos importante!), agradeço-lhe as reflexões atentas e por me dar a conhecer inspirações extra-académicas, como Naná Vasconcelos ou Egberto Gismonti. Agradeço-lhe por todos estes exemplos e, mais marcadamente, pelo seu.

Muito agradeço ao Professor Carlos Miguel Fernandes Quental pelo seu acompanhamento pormenorizado e orientação diligente. A sua disponibilidade, rigor científico e comunicação cuidadosa foram exemplares e um porto seguro nas etapas de maior hesitação. Desde sessões de esclarecimento espontâneas a idas ao AKI, sempre senti que podia contar com a sua ajuda. Espero vir a incorporar na minha carreira algumas das suas virtudes e saberes.

Ao Sérgio Gonçalves pela participação em todo o processo de aquisição laboratorial. Agradeço-lhe a disponibilidade, paciência, sentido prático e diálogos formativos. O meu reconhecimento também para todos os doze voluntários que, em plena pandemia e confinamento, cederam parte do seu tempo e simpatia para me auxiliar de forma essencial. À Rita pelo amparo nas representações gráficas.

Aos meus amigos da faculdade. Obrigado por terem enriquecido e povoado de memórias um percurso académico que nem sempre foi alegre. Agradeço ao Cristiano, ao Rodrigo, à Joana, ao Alex Silva, Pedro Constantino, Salústio, João Champ, Gouveia, Jean “Il Chivo” Baptista e a todos aqueles que foram o meu suporte durante todos estes anos do curso. Reconheço também o trabalho da Ana Barbosa, do Núcleo de Mobilidade, que agilizou os meus dois períodos de intercâmbio, cujo impacto em mim será eterno.

Aos meus amigos e amigas de todos os tempos e vivências. São o meu melhor escape, o meu refúgio, o meu deleite. A minha mais arrebatadora surfada, empática jam ou terno piquenique.

Finalmente, à minha família. Avós queridas e bem-intencionadas. E aos meus pais. Devo-lhes tudo. Sãos os meus melhores amigos e confidentes. São quem por mim mais se esforçou e esforça. Foram eles que tornaram todo este percurso possivel. Levo-os em mim. Gosto muito de vocês. Sempre.

Resumo

O objetivo deste trabalho é desenvolver modelos de regressão para o ombro capazes de estimar a orientação da clavícula e da escápula a partir da orientação do úmero considerando um conjunto mais alargado de posturas do braço do que o disponível na literatura. Foram concebidos dois tipos de modelos de regressão: um que usa exclusivamente a orientação do úmero como preditor e outro que também usa dados antropométricos como preditores.

Usou-se um sistema de tracking optoelectrónico, complementado por unidades de medida inerciais e uma estrutura externa de suporte. A cinemática do ombro de 8 sujeitos saudáveis registou-se usando um procedimento não-invasivo com marcadores cutâneos e um localizador da escápula. Obtiveram-se equações de regressão. Naquelas que usam fatores individuais, foi detetada multicolinearidade acentuada, tendo sido feito um processamento estatístico. Os modelos de regressão validaram-se usando um conjunto de dados independente referente a 4 sujeitos saudáveis.

O modelo sem fatores individuais revelou um ajuste aos dados nos intervalos indicados na literatura. Os modelos com fatores individuais apresentam um melhor ajuste ao conjunto inicial de dados de teste do que o modelo sem fatores individuais. A inclusão de fatores individuais na regressão tem, porém, resultados variáveis quando os modelos são aplicados ao conjunto de validação. Tal pode ser explicado pela elevada multicolinearidade encontrada entre os preditores. Esta faz com que os coeficientes de regressão sejam muito sensíveis a pequenas alterações no modelo.

Palavras-Chave: Ombro; Cinemática; Ritmo escápulo-humeral; Ritmo do ombro; Modelo de regressão.

Abstract

The aim of this work is to develop regression models for the shoulder which predict the orientation of the clavicle and the scapula from the humeral orientation for a wider envelope of arm postures than the one available in the literature. Two types of regression models are built: one using exclusively the humeral orientation as a predictor and another one which also uses anthropometry data as predictors.

An optoelectronic tracking system, complemented with inertial measurement units and an external frame, is used. Shoulder kinematics from 8 healthy subjects are assessed using a non-invasive procedure with cutaneous markers and a scapula locator. Regression equations are obtained for the two types of regression models. For the one which uses individual factors as predictor variables, multicollinearity is detected and thus a statistical processing is made. The models are validated using an independent dataset obtained from 4 healthy subjects.

The model without individual factors shows a fit to the data in the range of the preceding literature. The models with individual factors show a better fit to the test dataset than the model without. The inclusion of individual factors has, however, varying results when the models are applied to the validation dataset. This can be explained by the high multicollinearity found among the predictors. This causes the regression coefficients to be very sensitive to small changes in the model.

Keywords: Shoulder; Kinematics; Scapulo-humeral rhythm; Shoulder rhythm; Regression model.

Contents

List of Tables

List of Figures

Glossary

AC acromioclavicular joint
AI angulus inferior of the scapula
BMI body mass index
C7 spinous process of the seventh cervical vertebra
EL most caudal point on the lateral epicondyle
EM most caudal point on the medial epicondyle
GH glenohumeral joint
HT1 plane of elevation angle of the thoracohumeral joint
HT2 elevation angle of the thoracohumeral joint
HT3 axial rotation angle of the thoracohumeral joint
IJ deepest point of the incisura jugularis
IMU inertial measurement units
ISB International Society of Biomechanics
M0 regression model 0
M1 regression model 1
M2 regression model 2
MEMS micro electro mechanical systems
PX processus xiphoideus of the sternum
RMSE root-mean-square error
SC sternoclavicular joint
SC1 retraction/protraction of sternoclavicular joint
SC2 elevation/depression of sternoclavicular joint
SHR scapulohumeral rhythm
ST scapulothoracic
ST1 retraction of the scapulothoracic joint
ST2 lateral/medial rotation of the thorascoscapular joint
ST3 anterior/posterior tilt of the scapulothoracic joint
T8 spinous process of the eighth thoracic vertebra
VDP variance-decomposition proportions
VIF variable inflation factors

List of Symbols

Convention

a, A, α	Scalar
$\mathbf{a}$	Vector
$\mathbf{A}$	Matrix

Superscript

x^A, y^A, z^A	Body A coordinate system
x^B, y^B, z^B	Body B coordinate system

Latin Symbols

R	Rotation matrix
$\mathbf{R}_i$, $\mathbf{R}_j$, $\mathbf{R}_k$	Rotational transformation about axis *i, j* and *k*
$\mathbf{T}$	Homogeneous transformation matrix
$\mathbf{TL}$	Translation matrix of a frame with respect to another frame
R	Rotation matrix of a frame with respect to another frame
X, *Y*, *Z*	Cartesian coordinates

Greek Symbols

$\Theta_1, \Theta_2, \Theta_3$	Euler angles

Chapter 1

Introduction

1.1 Motivation and Objectives

The shoulder is, from a biomechanical standpoint, the most complex structure in the human body. It is also the most mobile joint in the body, relying on an intricate system that allows motion in six degrees of freedom. It is comprised of four joints. The rounded humeral head articulates with the glenoid cavity of the scapula, forming the glenohumeral joint. The acromioclavicular joint is formed by the junction of the lateral clavicle and the acromion process of the scapula. The sternoclavicular joint results from the articulation of the medial aspect of the clavicle with the manubrium of the sternum. Finally, the scapulothoracic joint, which is not a true anatomic joint, since it does not display the usual joint characteristics, i.e., union by fibrous, cartilaginous, or synovial tissues, is formed by the articulation of the scapula with the thorax. The shoulder joint plays an important role in many daily activities as well as in sports performances.

The shoulder girdle is is composed of three bones, the clavicle, the scapula, and the humerus. Together they form a kinematic chain: during movement of the upper limb a defined relation between their individual motions has been observed (Hogfors et al., 1991; Inman et al., 1944). This movement pattern has been called the shoulder rhythm (de Groot & Brand, 2001; Grewal & Dickerson, 2013; Xu et al., 2014a). Assessing the orientation of the shoulder girdle bones using in vivo non-invasive methods can be difficult due to the soft tissue overlying the bones (Brochard et al., 2011; Karduna et al., 2001; Prinold et al., 2011; van Andel et al., 2009): inaccuracies arise relating to the placement of the markers (Leardini et al., 2005). Differences of up to 87 mm have been found between the position of markers along the medial border of the scapula and the actual position of the scapula, and these discrepancies tend to accentuate as the arm reaches full elevation (Matsui et al., 2006). One way to surpass this challenge is to use bone-fixed pins, attaching the sensors to surgically placed pins (Ludewig et al., 2009). This provides a direct bone tracking but is extremely invasive and thus not always practical.

Nowadays, the application of a scapula locator is considered the optimum method for non-invasively tracking the movement of the scapula (Meskers et al., 2007). This devices helps in determining the locations of three scapula landmarks simultaneously. It reduces the inaccuracies caused by soft tissue displacement, requiring, however, a strictly static tracking of the different postures. Multiple studies have used this technique (Johnson et al., 1993; Ludwig et al., 2002; Meskers et al., 1998; Meskers et al., 2007 Ogston et al., 2007; Pronk, 1991; van der Helm, 1995). Van Andel et al. (2009) found that dynamic recording lead to general underestimation of scapula position and also overestimation of two scapular movements (protraction and external rotation during forward flexion of the humerus), when compared to static tracking using a scapula locator. Static measurements using this device were found to provide more accurate data when compared to a dynamic acquisition, as the mismatches due to skin deformation are minimized (van Andel et al.,2009). Soft tissue displacement on the scapula region may

induce displacements between the markers and the corresponding anatomical landmarks as severe as 2 cm and, thus, too highly unreliable data (de Groot et al., 1998).

Some studies have taken a regression-based shoulder rhythm approach (de Groot & Brand, 2001; Grewal & Dickerson, 2013; Hogfors et al., 1991), using the easily measurable humeral orientation to estimate the orientations of the scapula and clavicle. Some of these studies also consider readily available anthropometric factors as covariates in the regression process. This results in a set of regression equations, or lookup tables, that help define the shoulder rhythm. However, these regression equations have a limited range of application due to the considered envelope of humeral postures. De Groot & Brand (2001) studied 23 different arm postures in four planes of elevation and six elevation angles, but axial rotation of the humerus was not considered. Grewal & Dickerson (2013) measured 39 static postures with three arm elevation planes, five elevation angles, and three axial rotation angles of the humerus. To the author's knowledge, Xu et al. (2014a) provided the study with the highest angular resolution: for each participant, 118 arm postures were examined with a 30º interval in each rotation axis. Past studies have, however, neglected arm postures in negative planes of elevation, which are particularly prevalent in sport performances such as swimming. Extrapolating shoulder rhythms to an untested range may result in poor prediction of the scapula and clavicle orientation (Xu et al., 2014a).

The main objective of this thesis was to extend current regression models available in the literature to a wider envelope of arm postures. To do so, an optoelectronic tracking system, complemented with inertial measurement units (IMU) and an external frame, was used to acquire shoulder kinematics. This external frame was built with the goal of improving the consistency of arm positioning and the comfort of the subjects. Shoulder kinematics were assessed using a non-invasive procedure with cutaneous markers and a 3-D printed scapula locator. Two types of regression models were built to predict the 3-D orientations of the clavicle and scapula. The first model used exclusively the humerus orientation as a predictor. The other two regression models used as input the humerus orientation as well as readily available anthropometry data as predictors. The regression models were validated using an independent dataset.

1.2 Literature Review

1.2.1 Kinematic Analysis

Biomechanics is the study of the movement of living things using the science of mechanics (Hatze, 1974). Mechanics is a branch of physics that is concerned with how forces create motion and with the description of motion. These forces can produce different effects on biological tissues, including healthy growth stimulus or hazardous tissue damage.

Biomechanics as a written out scientific field is generally considered to have begun with a series of Aristotle's (384–322 B.C.) essays, *De Motu Animalium* (*Movement of Animals*). Here, Aristotle first defined animal's bodies as mechanical systems and analysed the geometry and the action of muscular tissues. Archimedes (287–212 B.C.) later established concepts such as his homonymous Principle, fundamental to the field of fluid mechanics and the basis for today's sport of swimming (Innocenti, 2018)

Later, Leonardo da Vinci (1452–1519) focused on functional anatomy. Over the course of the following centuries, many other brilliant scientists, namely Galileo (1564–1642), Newton (1642–1726), and Borelli (1608–1679), advanced this scientific field. The first motion-picture project to study human and animal motion was developed by Eadweard Muybridge (1830-1904). His contemporary, Julies Wolff described the relationship between trabecular bone geometries and mechanical stimuli on bone (Innocenti, 2018). Later on, during the 1960s and 1970s, biomechanical principles started to permeate surgical practice, namely through the work of AI Burstein et al. (1976). Biomedical engineering, alongside orthopaedics, has expanded the mathematical modelling of physiological systems and applied this knowledge to solve clinically relevant problems, improving patient treatment and clinical outcomes.

With the advancement of technology, and specifically the exponential growth of computational power, the more rudimentary organ-specific two-dimensional representations of a part of the human body evolved to more elaborate full body three-dimensional models (Farron et al., 2006; Quental et al., 2012a, 2012b, 2013; Silva et al., 2002; Van der Helm, 1994a, 1994b). Biomechanical models can be used, for instance, when direct or in vitro measurements are invasive, expensive or simply unavailable (Favre et al., 2009). In the future, these models are expected to impact areas such as orthopaedics, sports science, and medical rehabilitation.

Initial kinematic studies on human motion focused on the movement of the lower limbs as upper limb motions tend not to be cyclic. Furthermore, often the same arm movement can be achieved by different joint adaptations which leads to redundancy issues. The first use of photography as a shoulder kinematics tracking technique happened with Taylor & Blaschke (1951). In this study, the subject was fitted with landmarks and photographed behind a Cartesian coordinate grid framework. Two diagonally placed mirrors allowed for two different views on the performed functional movements. The aim of this study was to improve arm and hand prostheses through the motion analysis of the markers path across time. Thirty years later, Langrana (1981) further expanded this study by dividing the upper extremity in different segments and characterizing them with four points in a three-dimensional space using biplanar videotaping and subsequent analysis by computer-aided descriptive geometry. Engin et al. (1984) introduced a sonic digitizing technique. Here sensors (microphones), an electronic control unit, and a generator determined the direction and location of the segments, through the principle of sound triangulation. Johnson & Anderson (1990) first introduced an electromagnetic movement sensor to measure spatial motion. The source generated an electromagnetic field and a sensor detected the magnetic field. This information was integrated allowing the calculation of the relative position and orientation with the full six degrees of freedom required in 3-D (Johnson & Anderson, 1990). The results of this study showed that electromagnetic tracking systems, along with spherical polar coordinates, could be applied to a clinical setting (Johnson & Anderson, 1990).

Some electromagnetic tracking system sensors use direct skeletal tracking, with surgically placed bone-fixed placed pins (Lawrence et al., 2014; (Ludewig et al., 2009). This highly invasive procedure can be replaced by surface sensors, as Cook et al. (2002) proved that for certain movements it is possible to use this less invasive approach with minimal errors at slow velocities. This method is currently the most used one due to its simplicity.

Hogfors et al. (1991) first studied the relationship between the movement of the humerus and the scapular and clavicular orientations. This relative motion, resulting from the interaction between the sternoclavicular, acromioclavicular, scapulothoracic and glenohumeral joints is known as scapulohumeral rhythm or shoulder rhythm. He applied a roentgenographic technique, which consists of X-rays passing through the body producing a shadow image on specially sensitized film, to track the arm abduction in the frontal plane. Spherical tantalum balls were inserted percutaneously on the shoulder. The shoulder rhythm was described by a polynomial model fit.

More studies on the shoulder rhythm followed, using 3-D regression models. De Groot and Brand (2001) studied 23 different arm postures in four planes of elevation and six elevation angles but axial rotation of the humerus was not considered. Grewal and Dickerson (2013) measured 39 static postures with three arm elevation planes, five elevation angles, and three humerus axial rotation angles. Xu et al. (2014a) provided a study with higher angular resolution: for each participant, 118 arm postures were examined with a 30º interval in each rotation axis. These studies focused, however, on a limited envelope of humeral postures (Table 1.1), excluding for instance negative planes of motion (i.e., those involving shoulder joint hyperextension (Figure 1.1).

Table 1.1: Arm postures discretization in past regression based 3-D models

ARTICLE	PLANE OF ELEVATION	ANGLE OF ELEVATION	AXIAL ROTATION
de Groot et al. (2001)	(30°, 60°, 90°, 120°)	(0°, 30°, 60°, 90°, 120°, 150°)	Non-defined
Grewal et al. (2013)	(0º, 45º and 90º)	(0º, 45º, 90º, 135º, 180º)	maximum internal, neutral, and maximum external
Xu et al. (2014a)	(0º, 30º, 60º, 90º, and 120º)	(0º, 30º, 60º, 90º, 120º,150º)	(-90º, -60º, -30º, 0º, 30º, 60º, 90º)

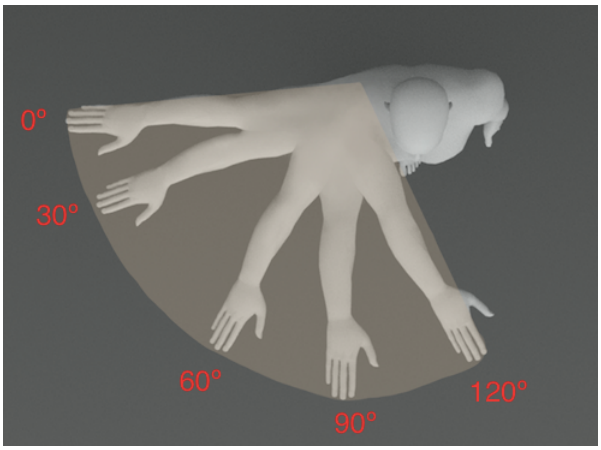

Figure 1.1: Top view of the envelope of humeral postures studied by Xu et al. (2014a) regression equations, on the elevation planes (0º, 30º, 60º, 90º, and 120º)

Finally, a more recent technique for studying the motion of the shoulder employs inertial and magnetic measurement units. The working principle of these sensors mimics the human vestibular system, located in the inner ear. This system senses rotations and linear accelerations and reacts maintaining the position of the eyes. Artificial sensors replicate this mechanics through MEMS (micro electro mechanical systems) technology which are miniaturized sensors, accelerometers and gyroscopes integrated into small wearable units capable of estimating variations in body segment position. Results showed that the root mean square difference in this estimation is 2º with respect to a stereophotogrammetric system (Roetenberg et al., 2005). However, the orientation estimation can be worsened by environmental conditions, such as the effect of magnetic distortions on the output of magnetometers. If these are not accounted for, the root mean square difference can reach 10º (Roetenberg et al., 2005). Inertial and magnetic measuring units can be connected together to form a network which sends synchronized data via cable or wireless to a data logger communicating with a computer. Zhou et al. (2018) used this motion tracking unit to measure real-time movements of upper limb as the basis of a home-rehabilitation service system, which assessed the outcomes of rehabilitation during daily activities. Full body systems are also available, like the Functional Assessment of Biomechanics (Biosyn, Canada). These sensors are non-visual systems and thus can avoid occlusion problems associated with camera-based motion capture systems. They can also be integrated into wearable devices. Due to this, motion analysis using inertial measurement units has emerged as an alternative to optical motion capture (Höglund et al., 2021). Their complementary use also provides helpful perspectives. The optical motion capture systems readily track body segments positioning, while the inertial measurement units offer a quick assesment of their relative movement.

1.3 Thesis Organization

The current work is structured in six main chapters.

Chapter 1 states the motivation and objectives behind this dissertation and reviews past developments in kinematic analysis, focusing on movement tracking and past shoulder rhythm models. Lastly, this chapter states the novel contributions of this work.

Chapter 2 details key concepts related to the anatomy of the upper limb to better understand the kinematic chain responsible for the shoulder movement. It also describes the glenohumeral joint movements and expands on the concept of shoulder rhythm.

Chapter 3 concerns the experimental and computational methods used in this work. It first states the participants selection criteria, the experimental protocol which included the usage of IMU and the development of an external frame and a 3-D printed palpatory device, the scapula locator. Afterwards, the shoulder kinematics data analysis is described, stating the Euler decomposition orders used to describe the orientations of the clavicle, scapula, and humerus with respect to the thorax, according to ISB standards (Wu et al., 2005). The anthropometrical characteristics of the participants used to collect these data are also presented. Afterwards, the two types of regression models are explained, the first type including only the three thoracohumeral angles as predictor variables and the second type including

the three thoracohumeral angles as well as a selection of individual factors as predictors. For the second type, the statistical methods used to detect and reduce multicollinearity problems (Belsley collinearity diagnostics, Pearson correlation coefficients and variable inflation factors) are described. Lastly, the characteristics of the independent dataset used to validate the models are enunciated.

Chapter 4 first presents the obtained regression equations for the three derived models. It then discusses the obtained models, analysing the influence of each of the predictor variables on the studied joint angles. The model's predictability and goodness of fit is assessed and the correlation between the measured angles from the validation dataset and the corresponding predicted angles is studied. For the models including individual factors, the statistical processing findings are introduced.A comparison between the three derived models is stated, as well as the comparison between this work's models and others present in the existing literature (de Groot and Brand, 2001; Grewal and Dickerson, 2013; Xu et al., 2014a). Lastly, the quality of postural standardization achieved by the developed external frame is quantified.

Finally, Chapter 5 pinpoints the major conclusions of the current work and identifies its limitations, suggesting future improvements in the experimental protocol, body orientation definition and in the development of the 3-D regression models.

1.4 Novel Contributions of this Work

The main contributes of this thesis are:

- The development of a scapula locator to lock the scapula configuration and facilitate the alignment of the markers on the anatomical landmarks;
- The development of an external frame to efficiently stabilize and standardize the orientation of the arm along the three descriptive Euler angles;
- The formulation of regression equations to predict the orientation of the clavicle and the scapula using a larger envelope of arm postures than the one currently available in the literature;
- The study of the influence of anthropometric variables on the shoulder rhythm, as well as the underlying multicollinearity among them.

Chapter 2

Shoulder Anatomy and Biomechanics

An anatomical perspective of the shoulder complex is important to better understand the kinematic chain responsible for the shoulder movement. The main anatomical landmarks of the shoulder components are detailed in this chapter. Due to the wide range of motion it enables, the shoulder has an intricate stabilizing mechanism, mostly achieved through muscle action (Lugo et al., 2018).

The range of motion of the upper extremity depends on the glenohumeral joint which interacts with the shoulder girdle. This interaction between the sternoclavicular, acromioclavicular, scapulothoracic and glenohumeral joints constitutes the shoulder rhythm and underlies the full range of motion of the upper limb, which is detailed in this chapter (Culham and Peat, 1986; Forte et al., 2009; McQuade and Smidt, 1998; Moore et al., 2010).

2.1 Bones

The shoulder girdle is formed by the clavicle and scapula. Along with the humerus they constitute the osteological foundation of the shoulder complex. The sternum and rib cage then add to form the entire shoulder complex. (Hendrickson 2009).

2.1.1 Scapula

The scapula, presented in Figure 2.1, is a large, triangular, flat bone located on the superior posterior portion of the thorax at the level of the first seven ribs. It articulates with the humerus, forming the glenohumeral (sometimes simply called shoulder) joint, and with the clavicle, forming the acromioclavicular joint.

It also constitutes a third separate joint, the scapulothoracic joint, as it interacts with the thorax and vertebral column through muscular connections which hold the scapula in place, since it is not attached to the axial skeleton through bony structures. This provides remarkable mobility to the upper limp, with a wide range of positions available to the scapula across the posterior thoracic wall.

The scapula has two surfaces, three borders, three angles and three processes.

Regarding the surfaces, the costal surface is concave and presents three longitudinal ridges. This part of the bone plays an important role in the overhead abduction of the arm, leveraging the action of serratus anterior. The dorsal surface is divided between infraspinous fossa, located below the spine of the scapula, and supraspinous fossa, the area above the spine of the scapula (Gray and Lewis, 1918**).** The first displays a convex shape, being the insertion point for the infraspinatus muscle, while the second, also convex, is the origin of the supraspinatus muscle.

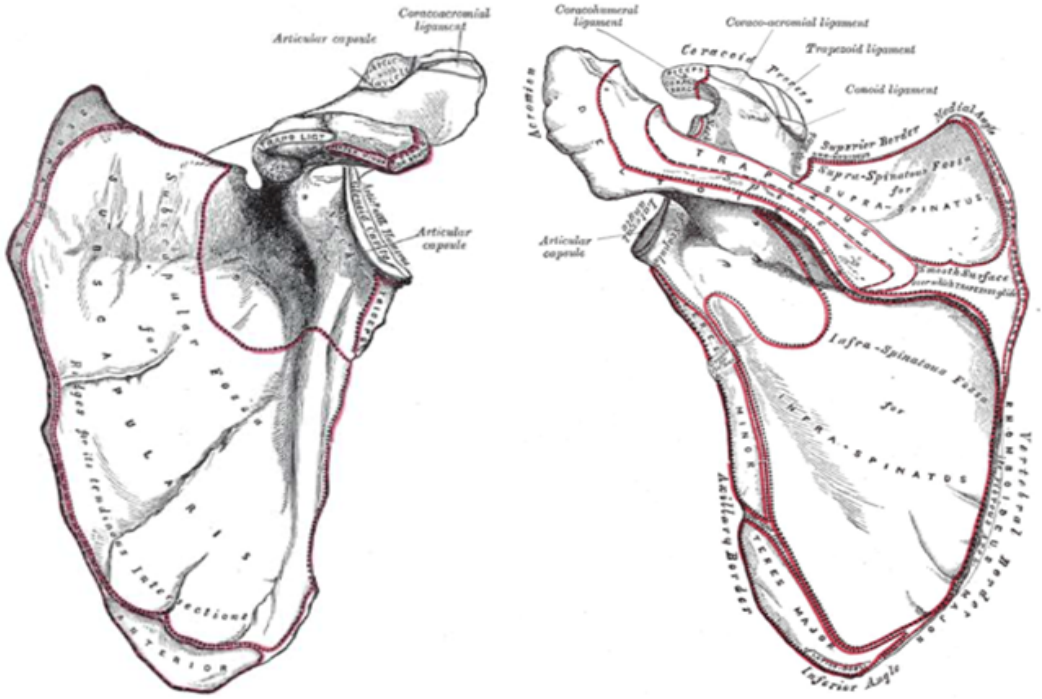

Figure 2.1: Anterior (a) and posterior (b) surfaces of the left scapula (Gray and Lewis, 1918)

Regarding the borders, the scapula presents the medial border, the lateral border and the superior border. The superior border is the shortest, thinnest and presents the suprascapular notch near the root of the coracoid process. The lateral border is thick and presents an infraglenoid tubercle at the upper end. Finally, the medial border is, when in the standard anatomical position, located parallel to the vertebral column (Gray and Lewis, 1918).

The scapular angles can be divided into superior, inferior and lateral angles. The superior angle between the superior and medial borders of the scapula is covered by the trapezius muscle. The inferior angle, on the lower portion of the scapula, is covered by the latissimus dorsi and moves forwards when arm abduction occurs. The lateral or glenoid angle of the scapula is also known as the head of the scapula and presents the glenoid cavity or fossa, directed forward, laterally and upwards. It is the thickest part of the scapula (Gray and Lewis, 1918). The scapula presents three processes. The spine or spinuous process is the triangular plate that divides the dorsal surface of the scapula into supraspinous and infraspinous fossae.

The acromion process has two borders, medial and lateral; 2 surfaces and a facet where the clavicle attaches (Gray and Lewis, 1918**).** Finally, the coracoid Process projects anterolaterally from the superior border and has three ligaments attached: the coracohumeral ligament, the coracoclavicular ligament and the coracoacromial ligament.

2.1.2 Clavicle

The clavicle, presented in Figure 2.2 is an S-shape elongated bone, located across the upper portion of the ribcage, between the manubrium of the sternum and the acromion of the scapula. Its medial portion is convex, and the lateral aspect concave. Morphologically, it is divided into a sternal end, a shaft, and an acromial end (Gray and Lewis, 1918**).**

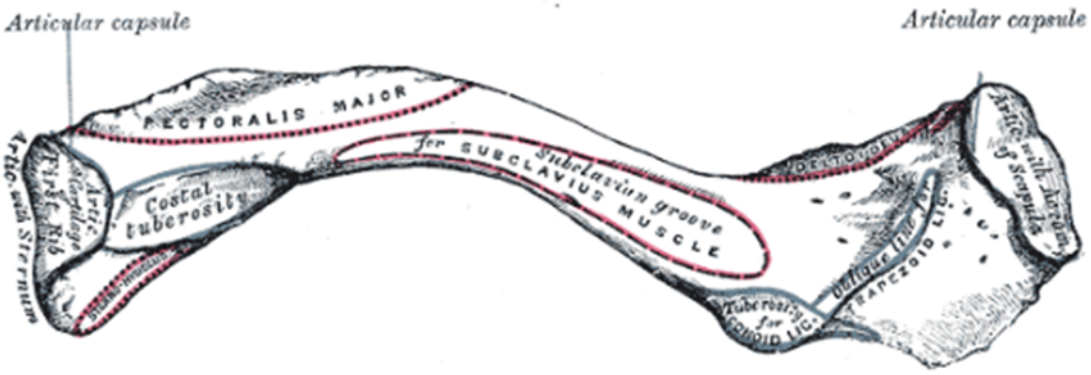

(a)

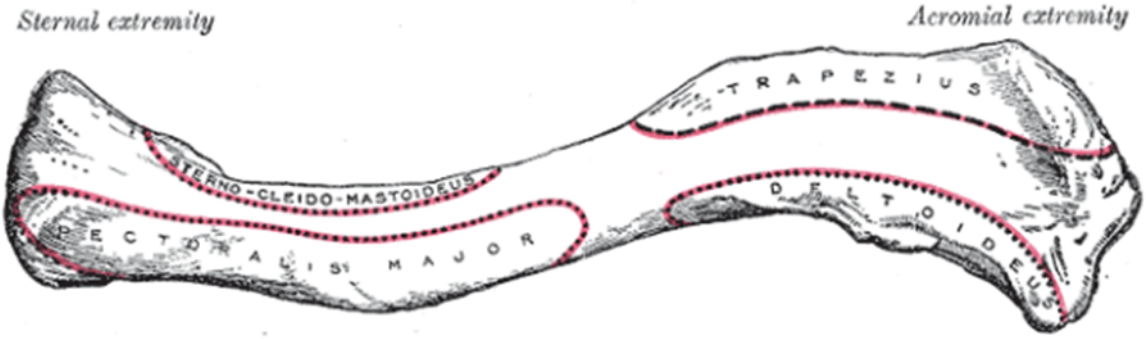

(b)

Figure 2.2: Anterior (a) and posterior (b) view of the clavicle (Gray and Lewis, 1918)

The sternal end presents a large facet and articulates with the manubrium of the sternum, forming the sternoclavicular joint. On the other hand, the inferior surface of the sternal end presents an oval depression, suitable for the insertion of the costoclavicular ligament (a ligament of the sternoclavicular joint joint). The shaft of the clavicle is where muscles such as the deltoid, trapezius, subclavius, pectoralis major, sternocleidomastoid and sternohyoid attach. Finally, the acromial end presents a small facet and articulates with the acromion of the scapula, forming the acromioclavicular joint. Two ligaments attach to this portion of the clavicle: the conoid tubercle and the trapezoid line. The first is the medial part of the coracoclavicular ligament, where the second is the attachment point of the trapezoid

ligament, the lateral part of the coracoclavicular ligament. (Drake et al., 2009; Tortora & Derrickson, 2017).

The clavicle plays a vital role in the functional movement of the human skeleton, so much it is the first bone in the human body to begin intramembranous ossification directly from mesenchyme during the fifth week of fetal stage. This bone connects the upper limb of the appendicular skeleton – shoulder girdle - to the axial skeleton, allowing for the transfer of loads. The clavicle is easy to identify in a laboratory context as it is palpable through its entire length.

2.1.3 Humerus

The humerus, shown in Figure 2.3, is the largest bone of the upper limb. It consists of a proximal end, a shaft and a distal end (Gray and Lewis, 1918**).**

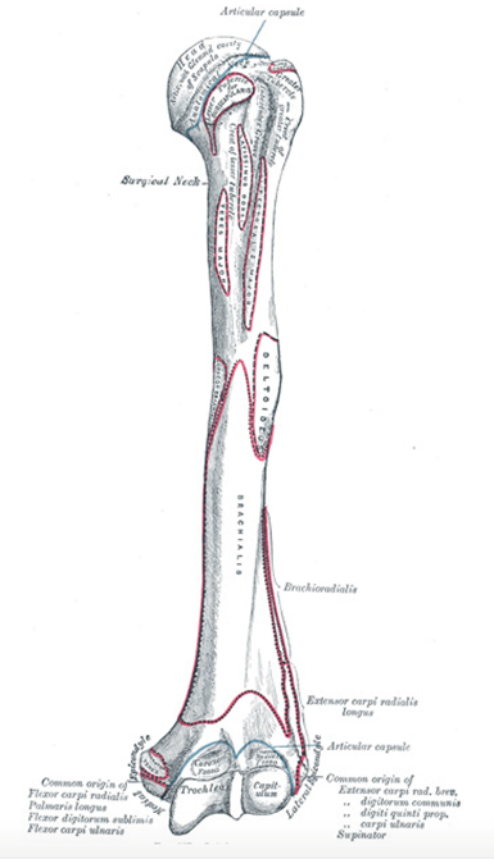

Figure 2.3: Anterior view of the humerus (Gray and Lewis, 1918)

The proximal end of the humerus consists of a head, an anatomical neck and tubercles. The head is a hyaline cartilage covered hemispheroidal articular surface. This rounded head articulates with the glenoid cavity of the scapula, forming the glenohumeral joint, depicted in Figure 2.4. Below it there is a slight narrowing portion deemed the anatomical neck, where the joint capsule of the shoulder joint is attached. Regarding the tubercles, the greater tubercle is the most lateral portion of the proximal end of the humerus. It consists of three impressions where several muscles are attached to and has its lateral

portion covered by the deltoid muscle. The lesser tubercle is located anterior to the anatomical neck and has a smooth, palpable muscular impression. The subscapularis muscle and the transverse ligament attach at this tubercle. Between the two tubercles there is a depression named intertubercular sulcus or bicipital groove (Moore et al., 2010). In it attaches laterally the tendon of the pectoralis major muscle, medially the teres major tendon and posteriorly the tendon of latissimus dorsi.

Concerning the shaft, it displays a cylindrical shape in its proximal half, and a triangular one on its distal half. It consists of three borders (anterior, lateral and medial) and three surfaces (anterolateral, proximal and posterior).

The anterior border runs from the greater tubercle almost to the end of the bone. The lateral border begins distal to the greater tubercle of the humerus. The medial border forms the medial supracondylar ridge distally. Between the anterior and lateral borders there is the anterolateral surface. Covered by the deltoid muscle, it has a smooth proximal surface. Between the anterior and medial borders of the shaft/body is located the anteromedial surface. Its distal half is mostly covered by the medial portion of the brachialis muscle. The posterior surface, bounded by the medial and lateral borders, also presents a muscular layer, in this case by the medial head of the triceps brachii muscle (Tortora & Derrickson, 2017).

At the distal end, the humerus articulates with the ulna and radius, composing the elbow joint. This distal portion consists of both articular and non-articular parts. The articular part is a modified condyle and the non-articular part consists of the medial and lateral epicondyles and of three fossae (the radial, coronoid and olecranon fossae). The radial fossa, receives the anterior border of the head of the radius, when the forearm is flexed. The coronoid fossa receives the coronoid process of the ulna during flexion of the forearm. Finally, the olecranon fossa accommodates the ulna during full extension of the elbow (Gray and Lewis 1918).

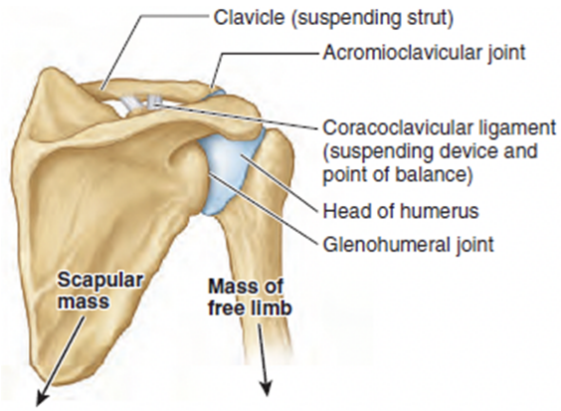

Figure 2.4: Representation of the articulation between humerus and scapula. Adapted from (Moore et al., 2014)

2.2 Joints

A joint is a connection between two bones, between bone and cartilage, or between bone and teeth. Joints can be characterized according to the type of connective tissue that binds the bones together and

also depending on the existence of a space between the articulating bones, that is, the synovial cavity (Tortora & Derrickson, 2017). This gap between the bones influences both the joint´s mobility and stability: more separation increases mobility but reduces stability.

The shoulder is composed of four joints, three anatomical and one physiological: the glenohumeral, the acromioclavicular, the sternoclavicular and the scapulothoracic joints. It is the interaction between them that allows the wide range of movements in the upper extremity, in all three planes of motion.

2.2.1 Glenohumeral Joint

The glenohumeral (GH) joint, present in Figure 2.5, is a true synovial ball-and-socket or spheroidal joint that is responsible for connecting the upper extremity to the trunk. It results from the combination of the humeral head and the glenoid fossa of the scapula.

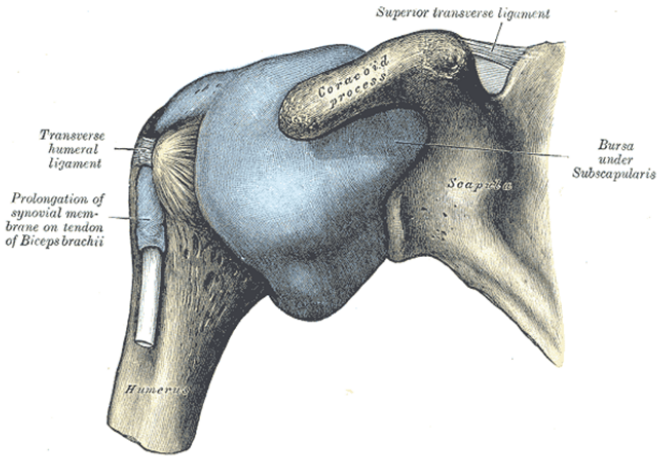

Figure 2.5: Glenohumeral joint (Gray and Lewis 1918)

The articular surface of the pear-shaped glenoid fossa is only one third to one fourth of that of the humeral head, and, due to this, only 25% to 30% of the humeral head contacts the glenoid cavity for any given position (Moore et al., 2010; Palastanga et al., 2002; Terry and Chopp, 2000; Wilk et al., 2009). This gives the joint its wide range of motion. Such freedom of movement leads however to less stability, making it the most commonly dislocated synovial joint (Wilk et al., 1997). To increase the joint´s stability, a fibrocartilaginous structure, named glenoid labrum, deepens the glenoid cavity, contributing approximately to 50% of the total depth of the socket (Culham and Peat, 1993; Standring, 2008; Wilk et al., 2009). The base of the labrum attaches to the fossa, the inner surface is lined by cartilage and the outer surface attaches to the joint capsule posteriorly and superiorly. It is reinforced by the tendons of the biceps brachii and triceps brachii muscles. If the labrum was removed, the forces required to dislocate the joint would decrease by 20%, showcasing its importance role as a stabilizing agent of the glenohumeral joint (Finnoff et al., 2004; Terry and Chopp, 2000; VandenBerghe et al., 2005).

The GH joint allows abduction in the frontal plane, flexion in the sagittal plane, as well as elevation in the scapular plane, situated midway between the previous two. It also allows horizontal abduction

(movement in a medial direction) and flexion, extension, internal and external rotation of the humerus. During these wide-ranging movements, and to keep the humeral head in contact with the glenoid fossa, the joint capsule and ligaments of the joint act passively. The joint capsule is a loose fibrous capsule that gives support to the GH joint. For example, with the arm in a resting position, the inferior and anterior portions of the capsule are relaxed, while the superior portion is tense. It attaches to the margin of the glenoid cavity medially and, laterally, to the anatomical neck of the humerus. However, due to its laxity, the capsule contributes, by itself, little to the glenohumeral joint stability and the bones can, in fact, separate 2 to 3 cm (Palastanga et al., 2002; Standring, 2008; Wilk et al., 2009).

The capsule has an opening between the tubercles of the humerus for the biceps brachii and between the superior and medial glenohumeral ligaments. Sometimes a third opening exists, allowing communication between the joint cavity and the infraspinatus bursa. The capsule's action is reinforced by the ligaments' muscular assistance. The muscles of the rotator cuff also act to reinforce the joint capsule superiorly, posteriorly, and anteriorly. The ligaments include the superior glenohumeral ligament, the middle glenohumeral ligament, inferior glenohumeral ligament, coracohumeral ligament, transverse humeral ligament.

To sum up, the glenohumeral joint is a very mobile joint and has passive and active mechanisms of stabilization. The main passive stabilizers are bony, the glenoid labrum, intra-articular pressure, joint cohesion, the glenohumeral capsule and the glenohumeral ligaments. Active mechanisms involve mainly joint compression, dynamic ligament tension, neuromuscular control and the action of the scapulothoracic joint itself (Wilk et al., 1997).

2.2.1.1 Glenohumeral Joint Movements and Shoulder Rhythm

The axes about which the movements of the glenohumeral joint occur are depicted in Figure 2.6. They can be defined in relation to the cardinal planes of the body or the plane of the scapula, located approximately 30º to 45º anteriorly from the frontal plane (Quental, 2013).

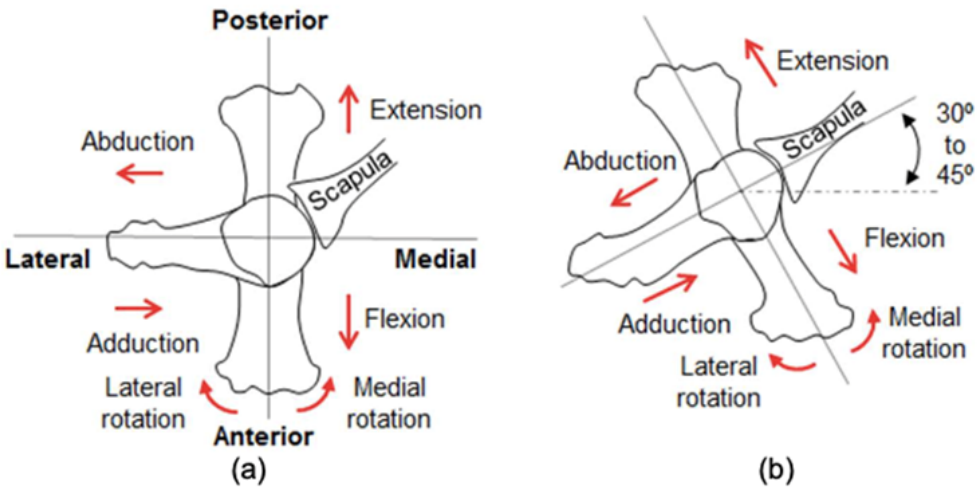

Figure 2.6: Axes of movement at the shoulder joint in relation to the cardinal planes of the body (a) and in relation to the plane of the scapula (b) (Quental, 2013).

The motion of abduction consists in the lateral elevation of the arm and adduction is its return to the original position. When the plane of elevation corresponds to the frontal plane and the humerus exhibits axial internal rotation, the glenohumeral abduction is limited to 60º due to the impingement of the greater tubercle of the humerus on the coracoacromial arch and the tension in the inferior glenohumeral ligament (Culham and Peat, 1993; Moore et al., 2010). In order to elevate this abduction to the 90º to 120º range, the humerus can laterally rotate which causes the tubercles to rotate posteriorly.

The plane of humerus elevation coincident with the plane of the scapula is sometimes referred as scaption (Culham and Peat, 1993; Lippert, 2006; McMahon et al., 1996). In this plane there is greater conformity of the joint surfaces, no need for humeral rotation to prevent the contact between the greater tubercle and the coracoacromial arch, as described for the abduction in the frontal plane, and the alignment of the deltoid and supraspinatus muscles for arm elevation is less constrained. This “optimal” plane is, in fact, the plane of elevation in which most daily activities happen (Culham and Peat, 1996; Lippert, 2006; Oatis, 2004; Wilk et al., 2009).

The flexion and extension of the arm are similar to the abduction-adduction movement but the arm moves anteriorly and posteriorly, respectively. The glenohumeral joint is also capable of 45º of hyperextension in the sagittal plane (Lippert, 2006), from the standard anatomical position, and 90º in each direction in the transverse plane (Lippert, 2006; Palastanga et al., 2002).

These movements are depicted in Figure 2.7.

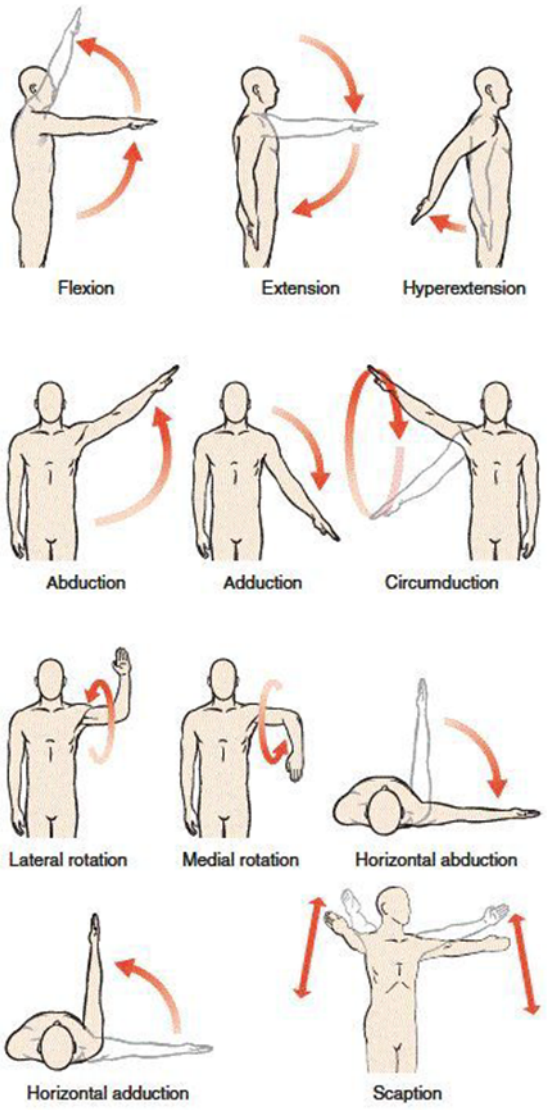

Figure 2.7: Shoulder joint movements (https://passtheot.com)

The glenohumeral joint movements do not occur independently but are accompanied by the shoulder girdle movements. This interaction between the sternoclavicular, acromioclavicular, scapulothoracic and glenohumeral joints is known as shoulder or scapulohumeral rhythm (SHR) and underlies the full range of motion of the upper limb (Culham and Peat, 1986; Forte et al., 2009; McQuade and Smidt, 1998; Moore et al., 2010). It also preserves the length-tension relationships of the glenohumeral muscles and preventing impingement between the humerus and acromion (Vizniak, 2010). Inman et al. (1944) were the firsts to study it (McQuade and Smidt, 1998; Scibek and Carcia, 2012). During the first 30º of abduction and 60º of flexion, the scapula may remain still or it may slightly rotate medially or laterally. As the elevation angle increases, there is a 2:1 ratio between the glenohumeral and scapular rotation. This means that for every 2º of humeral rotation, there is approximately 1º of scapular rotation (Clarkson, 1999). Some more recent studies present different ratios, some of them variable along the full elevation range (Oatis, 2004; Scibek and Carcia, 2012) (Table 2.1).

Table 2.1: SHR values found in the literature, representing the ratio of the glenohumeral movement to the scapulothoracic movement during arm elevation

ARTICLE	PLANE OF MOTION	SHR	TOTAL RANGE OF ELEVATION
Yoshizaki et al., (2009)	Scapular and sagittal	3.0 - 4.0	[Min - Max]
Ludewig & Cook (2000)	Scapular plane	2.3 - 3	[30º - 120º]
McClure et al., (2001)	Scapular plane	1.7	[Min - Max]
Matsuki et al., (2011)	Scapular plane	2.6 - 2.7	[Min - Max]
Braman (2010)	Without a controlled plane	2.3	Without a controlled elevation angle

The exact ratio is also hypothesized to be subject specific and even possibly vary with the plane of elevation, the elevation angle and muscle activity (Oatis, 2004).

In the same plane of motion, for instance in the scapular plane, SHR can range from 1.7 to 3.4 (Yoshizaki et al., 2009; Ludewig & Cook, 2000; Struyf et al., 2011; Matsuki et al., 2011; Braman, 2010). Within the same plane of elevation, variations have also been observed (Inman, 1944; Braman, 2010; Mell et al., 2005; Hosseinimehr et al., 2015; Turgut et al., 2016b; Scibek et al., 2008). This led to studies determining SHR by dividing the motion in elevation intervals. Braman (2010), for instance, divided each movement intervals of 30◦ increment: [Min,30◦]; [30◦,60◦]; [60◦,90◦]; [90◦,120◦] and [Min,120◦].

2.2.2 Acromioclavicular Joint

The acromioclavicular joint (AC joint), depicted in Figure 2.8, is formed by the junction of the lateral clavicle and the acromion process of the scapula and is a gliding, or plane style synovial joint. Its exact configuration varies: it might be flat, reciprocally concave-convex, or reversed (Alderink, 2006). Given the variable articular configuration, intra-articular movements for this joint are not predictable. (Neumann et al., 2009). It serves as the main articulation that suspends the upper extremity from the trunk and allows the scapula to change its position during the movement of the humerus (Alderink, 2006). It also allows transmission of forces from the upper extremity to the clavicle.

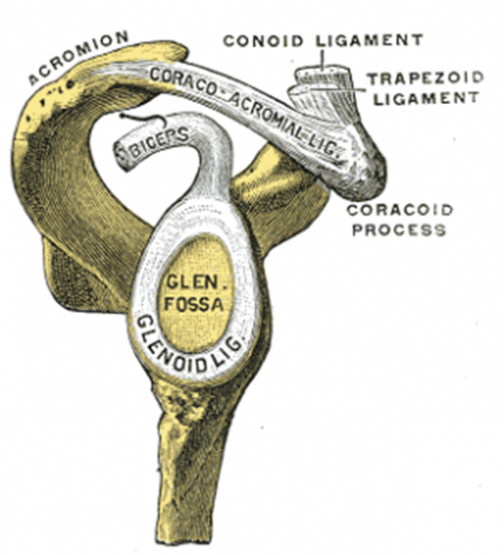

Figure 2.8: Acromioclavicular joint (Gray and Lewis 1918)

The AC joint capsule and ligaments surrounding it work to keep the clavicle in contact with the acromion process of the scapula. The capsule is strengthened inferiorly and superiorly by ligaments which are reinforced through muscular attachments from the deltoid and trapezius. (Neumann et al., 2009). The supporting ligaments are the coracoclavicular and acromioclavicular ligaments. The coracoclavicular ligament is composed of the conoid and trapezoid ligaments and is the primary support ligament of the AC Joint. It provides rotation of the clavicle during elevation of the humerus. The acromioclavicular ligament strengthens the joint capsule and serves as the primary constraint to posterior translation and posterior axial rotation at the AC joint. Finally, this joint can possess another anatomical feature, the disc. It is variable in size, or even non-existent. Through the first two years of age, the joint is a fibro-cartilaginous union. With recurrent upper extremity motion, a joint space develops at each articulating surface and may possibly leave a meniscoid fibrocartilage remnant within the joint (Alderink, 2006).

It has six degrees of motion: upward/downward rotation, about an axis directed perpendicular to the scapular plane facing anteriorly and medially, internal/external rotation, about an approximately vertical axis, and anterior/posterior tipping or tilting, about an axis directed laterally and anteriorly.

2.2.3 Sternoclavicular Joint

The sternoclavicular joint (SC joint), present in Figure 2.9, results from the articulation of the medial aspect of the clavicle with the manubrium of the sternum. It is a plane style synovial joint with a fibrocartilage joint disk. The SC joint is the only true articulation connecting the upper limb to the axial skeleton and is an extremely mobile joint. It is reinforced by very strong ligaments (Tortora & Derrickson, 2017).

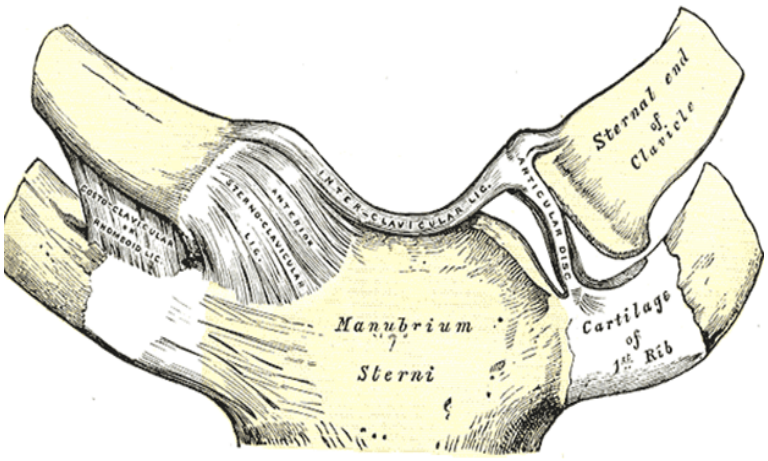

Figure 2.9: Sternoclavicular joint (Gray and Lewis 1918)

The SC joint is formed by the articulation of three bones: the manubrium (the superior portion of the sternum), the clavicle and the articulation between the first rib costal cartilage. Similarly, to the previous shoulder joints, it is supported by the joint capsule and by the important action of several ligaments: the anterior and posterior sternoclavicular, the costoclavicular and the interclavicular. Anatomically speaking, a fibrocartilaginous intra-articular disc may be present. It enhances the joint's congruency as the curvatures of the articular surfaces differ. This disc is located between the clavicular and sternal surfaces, separating the joint in two portions, and the disc is held in place by several attachments (Tortora & Derrickson, 2017).

Even though the SC joint is classified as a saddle joint it has the functional features of a ball-and-socket joint, having three degrees of freedom, whose ranges of motion are, on average: elevation – depression (40°); protraction – retraction (35°); axial rotation (20°- 40°) (Palastanga & Soames, 2012).

2.2.4 Scapulothoracic Joint

The scapulothoracic (ST) joint, depicted in Figure 2.10, is formed by the articulation of the scapula with the thorax. It is not a true anatomic joint, not displaying the usual joint characteristics (union by fibrous, cartilaginous, or synovial tissues). It relies heavily on the SC and AC joints, meaning that any scapula movement is supported by the interdependence of these three joints. The SC and AC joints are related with the ST joint because the scapula is attached by its acromion process to the lateral end of the clavicle through the AC joint; sub sequentially the clavicle is attached to the axial skeleton at the manubrium of the sternum through the SC joint. The ST joint does not have specific articular surfaces, ligaments or the joint capsule (Tortora & Derrickson, 2017).

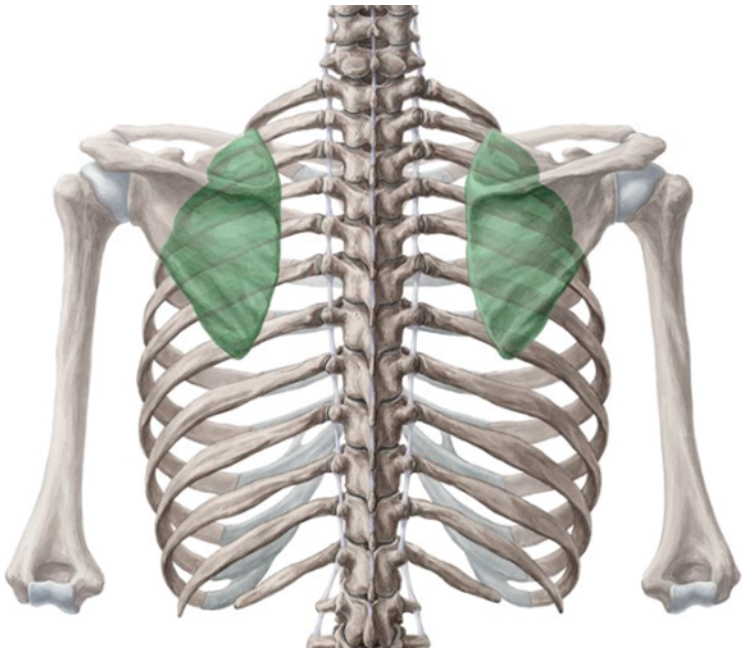

Figure 2.10: Scapulothoracic joint (https://www.kenhub.com)

The ST junction is a connection between the concave anterior surface of scapula and the convex superolateral surface of the thoracic wall. These two surfaces are not connected, being instead separated by the serratus anterior muscle which attaches to the thoracic wall, the subscapularis muscle that fills the subscapular fossa on the anterior surface of scapula, and the fascial space between these two muscles. This fascial space is filled with loose connective tissue in order to facilitate the different scapular movements. This scapulothoracic junction is stabilized by the action of three main muscles group: the trapezius muscle, the serratus anterior muscle and the medial stabilizers of the scapula; levator scapulae and rhomboid muscles (Tortora & Derrickson, 2017).

The scapular movement, essential for the different shoulder postures, occurs as the scapula moves around the fulcrum of the acromioclavicular joint, enabled by the scapulothoracic joint. This movement occurs in three degrees of freedom, here followed by their respective estimated ranges of motion (ROM): elevation (ROM: motion 40°) /depression (ROM: 10°), protraction (ROM: 20°)/ retraction (ROM: 15°), external (ROM: 60°)/internal rotation (ROM: 30°) (Palastanga & Soames, 2012).

From all these movements, scapular involvement is primarily focused on the range of elevation of the upper extremity, as the scapula displays upward rotation on the thorax (Alderink, 2006). Essentially, the scapular motion orients the glenoid fossa for optimal contact with the manoeuvring arm; increases the elevation range of the humerus; and provides a stable base for the interaction between the humeral head and glenoid fossa (Alderink, 2006).

Chapter 3

Experimental and Computational Methods

The present dissertation focuses on the relationship between the movement of the humerus, the clavicle and the scapula. To study it a series of arm postures was performed by a group of participants. The shoulder was tracked using the experimental protocol detailed in this chapter, which included the usage of an external frame, IMU and a 3-D printed palpatory device, the scapula locator. For each arm posture, joint angles were calculated using software developed in-house (Quental, 2013) and coded in MATLAB (MathWorks, Natick, MA). The shoulder rhythm was described by regression equations, built using a two-step regression procedure and a statistical processing of predictor variables was done in order to minimize multicollinearity among the predictors. These methods are explained over the course of this chapter.

3.1 Participants

Twelve participants were selected for this study. They were previously informed about the protocol and signed a written informed consent form prior to the beginning of the experiments. The protocol was approved by an ethics committee (Comissão de Ética of Instituto Superior Técnico).

Literature shows alterations in scapular and glenohumeral kinematics are not always related with diagnosed shoulder pathology (Kibler, 1998; Kebaetse et al., 1999; Gupta et al., 2013). Hence, it is also important to identify and use benign factors of kinematic alterations as exclusion criteria (Nunes, 2019). The used inclusion criteria required that the subject:

1. Self-reported right-hand dominance;
2. Did not present shoulder pain or pathology history;
3. Did not practice frequently overhead movements, as sports or work-related activities;
4. Was not obese;

First of all, only right-handed participants were selected. Nelson et al. (2017) showed that left-handers are not reversed right-handers when compared on interlimb kinematics for reach-to-place tasks. Hence only one type of hand dominance was selected, chosen as right-hand dominance for being the most frequent across our participant recruitment group. This aimed at an homogeneous group, minimizing possible hand-dominance-specific kinematic alterations The second criteria required the subjects not to present history of previous surgery to the shoulder, or pain while performing arm elevations. This was particularly relevant as the goal of this study was to assess shoulder kinematics in the total arm range of motion. Furthermore, overhead athletes have shown asymmetrical shoulder kinematics, due to

muscle adaptations that affect scapular kinematics (Hosseinimehr et al., 2015; Oyama et al., 2008). No professional (or active competing) athletes were selected for this study. Finally, body overweight results in increased arm weight which can also lead to kinematic alterations. There is an increased scapula upward rotation, compensating for the greater inertia of the arm with increased mass (Gupta et al., 2013). Cau et al. (2017) detected significant range of motion limitations in lateral and frontal upper arm elevation in obese patients. Thus, no obese people were included in this study.

Globally, the collected data came from 12 right-hand-dominant subjects (6 females and 6 males, 26.4 years ± 9.8, height: 1.72 ± 0.1 m; weight: 66.1 ± 10.5 kg) with no acute or chronic upper extremity musculoskeletal disorders. Their anthropometrical data are represented in Table 3.1.

Table 3.1: Average anthropometry data for the 12 subjects that participated in this study

Anthropometry Data	Definition	Average (mm)	SD (mm)
Length Thorax	IJ-PX	191.2732	26.5123
Depth Thorax	PX-T8	237.2062	21.6918
Length Clavicle	SC-AC	155.3850	13.0864
Length Scapular Spine	AA-TS	127.2294	10.8616
Length Scapula	AA-AI	189.3719	14.5157
Upper Arm Length	AC-EL	347.2010	16.2983

3.2 Experimental methods

The 3D-kinematics of the shoulder rhythm was collected using the precision motion capture and 3-D positioning tracking system Qualisys Tracking Manager (QTM), at the Lisbon Biomechanics Laboratory (LBL). It utilized 14 digital infrared cameras (Pro Reflex MCU 1000), pointed at, and interacting with, 22 retro-reflective markers (each with a diameter of 19 mm) and two marker clusters per arm. The cameras were set at a sampling frequency of 100 Hz.

The retro-reflective markers were attached to the bony landmarks of the thorax, clavicle, scapula, humerus, and forearm, of each subject's right arm. Table 3.2 indicates the used anatomical landmarks and Figure 3.1 shows their location.

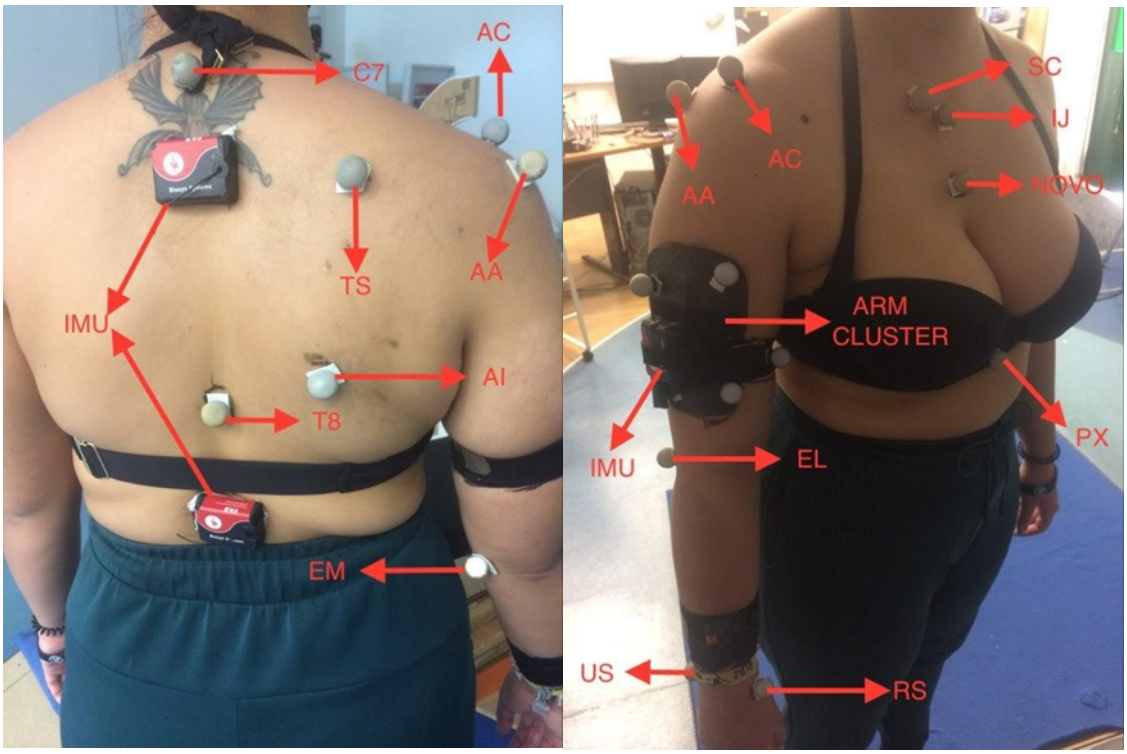

(a) (b)

Figure 3.1: Posterior, in (a) and anterior, in (b), views of the upper limb bony landmarks

On the upper arm, a passive four-marker cluster, made of copolymer polypropylene, was placed laterally and held in position using elastic bands. The use of clusters placed at sites which showcase minimal overlying skin movement aims at reducing skin movement artefacts associated with standard motion analysis techniques (Cappozzo et al., 1995). This arm cluster can be seen in Figure 3.1 (arm cluster).

Table 3.2: Anatomical landmarks proposed by the ISB (Wu et al., 2005)

Bone	Bony Landmark	Description
Thorax	C7	Spinous process of the seventh cervical vertebra
	T8	Spinous process of the eighth thoracic vertebra
	IJ	Deepest point of Incisura Jugularis
	PX	Processus Xiphoideus, most caudal point on the sternum
	NOVO	Replacement for IJ
Clavicle	SC	Most ventral point on the SC joint
	AC	Most dorsal point on the AC joint
Scapula	TS	Trigonium Spinae, the midpoint of the triangular surface on the medial border of the scapula in line with the scapular spine; root of the scapular spine
	AI	Angulus Inferior, most caudal point of the scapula
	AA	Angulus Acromialis, most laterodorsal point of the scapula
Humerus	EL	Most caudal point on the lateral epicondyle
	EM	Most caudal point on the medial epicondyle
Forearm	RS	Most caudal–lateral point on the radial styloid
	US	Most caudal–medial point on the ulnar styloid

The scapula locator uses two adjustable beams to locate the positions of the angulus acromialis, trigonum spinae, and angulus inferior. After adjusted to the individual scapula, the rods are fixed into rigid triangular position. At each new position, the scapula locator was readjusted to the bony landmarks of the scapula and a new recording was made. The scapula locator was after 3-D printing, as detailed in section 3.2.1.

Another consequence of tracking static postures was the need for a stabilizing mechanism, in order to provide both consistency to the humeral elevations as well as comfort for the participants. In response to this, an external frame was built, as detailed in section 3.2.2.

Finally, inertial measurement units, detailed in section 3.2.3, were used during the data acquisition. These sensors had an important role in estimating in real time the humeral axial rotation, which allowed the participant to be directed to the neutral axial rotation. They also estimated in real time the participants thorax tilts and thus gave important feedback on the need to correct the postures. The sensors also estimated the thoracohumeral joint's elevation before kinematic data were processed.

3.2.1 Scapula Locator

The scapula locator functions as a way of locking the scapula configuration of each participant. It is set before the acquisition and, after each posture change, it facilitates the correct alignment of the scapula markers. The markers are inserted through the scapula locator at the following positions: Trigonum Spinae (TS), the midpoint of the triangular surface on the medial border of the scapula in line with the scapular spine; Angulus Inferior (AI), most caudal point of the scapula; and Angulus Acromialis (AA), most laterodorsal point of the scapula.

The scapula locator was designed using *SolidWorks* and then 3-D printed. After 9 designs with various flexion angles, thicknesses, lengths and edges profiles, the final design, shown in Figure 3.2, was reached. The two segments of the scapula locator were printed with 17º of curvature to better adjust to the natural curvature of the participant's scapula region. This value was chosen following the average curvature of the upper thoracic spine of 16.5º (Wakimoto et al., 2018).

This device had to be able to change the angle between its two segments and maintain it, in order to lock the subject specific scapula configuration. This is achieved by the locking mechanism of a screw, nut and washer (Figure 3.3). The through holes were extended which allowed different scapula border's length. The corners of the apparatus were rounded to improve ergonomics. Figure 3.2 shows the two parts drawn on *SolidWorks* and Figure 3.3 shows the final assembly.

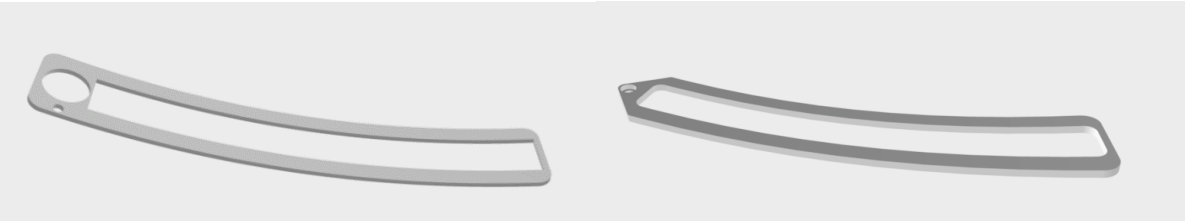

Figure 3.2: The two parts of the scapula locator, with a flexion angle of 17 º, drawn on *SolidWorks*.

Figure 3.3: (a) Final assembly of the two 3-D printed parts and (b) scapula locator in use, locking the subject specific scapula configuration

3.2.2 External Frame

To systematize the wide ranging, and sometimes uncomfortable, arm postures an external frame was used. This frame was cut from a 150 × 62 × 1.8 cm pine construction panel. It consisted of a vertical support in the shape of a “question mark”. The arc had an amplitude of 180º and a radius of 22 cm and was located at the end of a linear 78 cm segment. The discretized elevation angles were painted on this arc. The vertical support was fixed (encastre) in a 30 × 1.8 × 10 cm wood block, stabilized by two blocks. This platform block was allowed to rotate around the axis of a 20 cm steel screw, fixed (encastre) in a panel laid on the floor. This rotation allowed the entire vertical frame to rotate to the selected thoracohumeral elevation plane, painted on the floor panel. Figure 3.4 presents a close-up of the vertical support and Figure 3.5 displays the overview of the external frame.

Figure 3.4: Close-up of the fixed vertical support (*encastre*), stabilized by two blocks. This platform block then rotated around the axis of a 20 cm steel screw

Figure 3.5: Overview of the built external frame, which rotated around the axis of a 20 cm steel screw, fixed (*encastre*) in the panel laid on the laboratory's floor, where marks had been drawn signalling the different elevation planes. In front of the frame the height adjustable bench and the support for the participant's feet, which aimed at minimizing thorax flexion, are displayed

The accuracy of this external frame (i.e., the degree to which it standardized the humeral postures) was assessed. This study was done by evaluating the differences between frame defined angles and the measured joint angles.

3.2.3 Inertial and Magnetic Measurement Unit

A wireless inertial sensor system Biosyn F.A.B. System-Functional Assessment of Biomechanics, from Biosyn, Canada, similar to the one presented in Figure 3.6, was used.

Figure 3.6: FAB system from Biosyn, Canada. This inertial measurement units setup was used, with the exception of the sensors in the lower limbs

The IMU were placed over the skin or clothes using elastic bands. The sensor data were transmitted in real time to a receiver (F.A.B Belt Clip receiver) and then to the computer to which it was connected. Here, an avatar was animated and displayed in real time, providing immediate visual feedback for both the laboratory technician and the participant. This helped detect thorax tilts and readjust the participant's posture or the bench's height. These sensors also estimated in real time the humeral axial rotation. This information was used to direct the participant to the neutral axial rotation. Finally, the IMU also estimated the thoracohumeral joint's elevation before kinematic data were processed.

Another advantage of inertial sensors is that, since they are non-visual systems, occlusion problems are avoided. This was important in this study since the acquisition was constrained by the external frame. The fact that these sensors are wearable and present robust results in joint estimation further made them a suitable option for this study.

3.3 Experimental Protocol

The experimental protocol can be divided into 4 phases:

1. Camera calibration;

2. Placement of markers, cluster and IMU;

3. Definition of scapula locator's configuration and initial calibration;

4. Tested arm postures;

The initial stage consisted on the calibration of the tracking system, QTM. The QTM software must determine the orientation and position of each infrared camera in order to track and transform the 2-D data into 3-D data. This procedure used an L-shaped reference structure and a calibration wand. The L-shaped calibration frame was placed in the centre of the laboratory, surrounding one of the ground force plates. The arms of the frame defined the axes of the Global Coordinate System (GCS). The long arm defined the x-axis, the short arm defined the y-axis, and the z-axis was perpendicular to the x and y axes, pointing vertically upwards. The calibration wand was moved inside the measurement volume, filling the entire space with calibration points, especially the regions where many markers were going to be placed. This action took on average 30 seconds.

Afterwards, the bony landmarks were palpated and the markers and arm cluster were put in place. The 3 IMU were placed over the skin or clothes using elastic bands. The sensor data were transmitted in real time to a receiver (F.A.B Belt Clip receiver) and then to a computer. The subject assumed a standing position, with straight posture, arms relaxed and palms facing the thighs. The IMU system software algorithms estimated the positions of the IMU relative to the adjacent body joints and defined the described humeral position as the humeral neutral axial rotation. Combining measurements of each IMU, the joint axes were calculated, allowing the tracking of the joint angles in a reliable and clinically interpretable way (Salehi et al., 2015).

In the third step, the scapula locator's configuration was defined. This apparatus locked the subject specific scapula configuration, using the AI, TS and AA markers as reference points. The subject then performed two static positions followed by a small amplitude movement. The first static position consisted of the anatomical standard position. In the second position, the participant was also standing up, but the elbows were close to the thorax, with approximately a 90º angle and the hand pronated. During these two postures, all markers were placed on the subject. Afterwards, the markers were kept the same, and the subject was instructed to make movements with small arm elevation angles. These movements were made so that the algorithm of Gamage and Lasenby (2002), implemented in MATLAB (MathWorks, Natick, MA) could estimate the GH average centre of rotation using a least squares method. The small amplitude of these motions aimed at minimizing scapular movement, reducing errors in the estimation.

Phase 4 consisted of the series of tested arm postures. The subjects were given instructions on how to perform each posture and then asked to practice it before the actual acquisition. The arm was kept straight in all tested postures, that is, the cubital angle, formed between the humerus and forearm axes, was at its normal value of approximately 10° in men and 13° in women (Snell et al., 2003). Subjects were allowed to rest at any time during the protocol if desired. All the postures were stabilized with the aid of an external frame. This frame had the goal of providing both consistency to the performed humeral elevations and comfort to the participant. Its development is detailed in section 3.2.2.

The participants were asked to avoid thorax´s lateral flexion and rotation, as not to interfere with the thoracohumeral joint angles, guided by the frame. A platform was set for their feet and the bench's height was adjusted as the postures succeeded. The subject aligned his estimated glenohumeral joint rotation centre with the centre of the arc. The GH centre of rotation was visually approximated as the centre of a sphere through the glenoid surface, with the radius of the humeral head (Veeger et al., 2000). In the context of the present work, the location of this centre was important, as the participant had to be aligned with the centre of the external frame, in order to correctly attain each humeral posture described by the three Euler angles. The non-invasive nature of the protocol required, however, a simplified visual approximation. The location was marked, palpating the coracoid process region and using the geometrical reference detailed above. To avoid significant mismatches between the articular centre and the arc centre, the height of the bench was adjusted progressively as the elevation reached its highest values (120º and 160º). An extra frame, shown in Figure 3.7, was set next to the participant's left arm to provide extra support and minimize lateral flexion of the thorax. This was important especially in the more uncomfortable postures, which concentrated on the lowest thoracohumeral plane of elevation angles (-60º and -90º) and on the highest thoracohumeral elevation angles (120º and 160º).

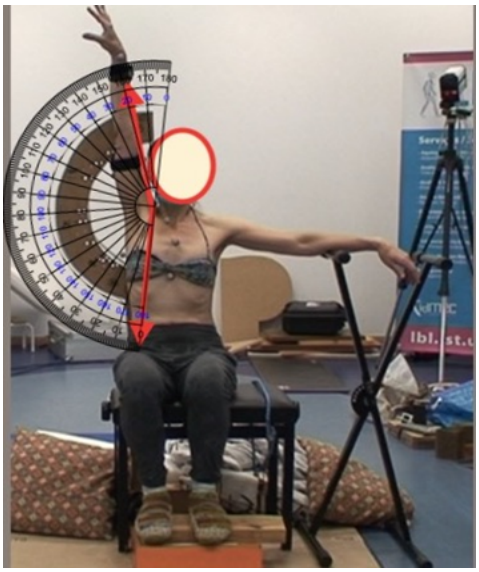

Figure 3.7: Data acquisition for a humeral posture in the 0º elevation plane and with 160º elevation angle and maximum internal rotation, with the aid of the two external frames. The digitally superimposed protractor has the goal of visually estimating the joint elevation angle and assuring it matched the given frame elevation angle

The participant was asked to initiate every arm position in the same way. The initial position had the participant sat, looking straight forward and with the hands either laying on his lap or in the standard anatomical position. The humerus elevation had to be performed along the designated plane of elevation. The participant was asked to gently touch the frame's wood, while raising the humerus along the elevation plane. Even though the studied positions were static, the motion was controlled to minimize possible path-dependent intersubject variability.

Once the humerus was at the chosen elevation angle, a metal platform (protected with a latex cover for comfort as seen in Figure 3.8) was inserted under the humerus through the back of the external frame. This provided the needed stability and was important for the participant to maintain its shoulder configuration while the scapula markers were adjusted.

Figure 3.8: Close up of the platform where the participant laid his arm, at the selected elevation angle. The latex cover reduced skin abrasion

This process required some seconds because of the scapula palpation and the positioning of the scapula locator. More strenuous arm positions difficulted the palpation of the three scapula markers, due to the vigorous contraction of the back muscles, namely the rhomboid major, rhomboid minor and latissimus dorsi. Thus, for these postures, the markers positioning was a more time-consuming process.

Once at the selected humeral elevation angle, three positions were registered. First the participant axially rotated the humerus in order to achieve the neutral position, as indicated by the IMU interface. Once the scapula markers had been set and the configuration tracked, the participant then rotated his humerus into maximum internal axial rotation. Afterwards, the same process was repeated for maximum external axial rotation. For some frame configurations, the axial rotation naturally displayed by the humerus, i.e., the most comfortable position with which the participant could set his arm on the frame, was already significantly rotated in relation to the IMU defined neutral axial rotation, sometimes up to 50º in either the internal or external rotation. For these positions, and especially for those in the superior frame elevation angles, sometimes the neutral position was not attainable for the participant. In these cases, the most comfortable axial rotation for that given posture was tracked, even though it did not correspond to the neutral position.

The laboratory acquisition was done respecting the following order of the planes of elevation: 0º, -30º-60º, -90, 90º and 45º, depicted in Figure 3.9. In agreement with the ISB standardization (Wu et al., 2005), the negative planes of elevation correspond to those involving shoulder joint hyperextension (Figure 2.7). The plane defined as 0º corresponds to the frontal plane. The 45º plane forms a 45º angle with the frontal plane and a 45º angle with the saggital plane. The 90º and -90º planes correspond to the sagittal plane. The -30º plane forms a 30º angle with the frontal plane and a 60º angle with the saggital plane. The -60º plane forms a 30º angle with the sagittal plane and a 60º angle with the frontal plane. These planes are represented in Figure 3.9.

For each plane of elevation, the angles of elevation discretized were 40º, 80º, 120º and 160º, as shown in Figure 3.10, and attained only if possible. The 0º was also tracked, corresponding to the position with the arm relaxed by the side. For the negative planes of elevation, the highest elevation angles were unattainable. If the maximum elevation attained by the participant was $< 80º$, the discretization followed was instead 20º, 40º and 60º. This was done to increase the number of tracked shoulder configurations. It is worth noting that the angle of elevation of 0º, with its corresponding three axial rotation positions, was recorded once, at the beginning of each acquisition.

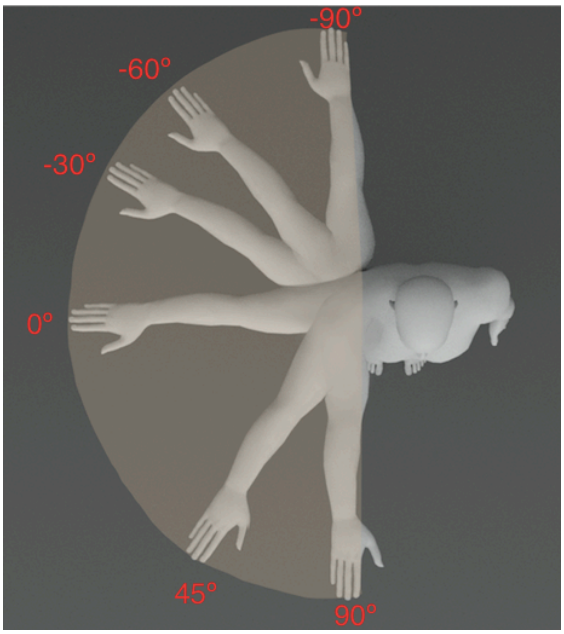

Figure 3.9: Top view of the envelope of humeral postures studied by the present work's regression equations, on the elevation planes (-90º, -60º, - 30º, 0º, 45º, 90º). A comparison can be made with the envelope of humeral postures studied in the work of Xu et al. (2014a) (Figure 1.1)

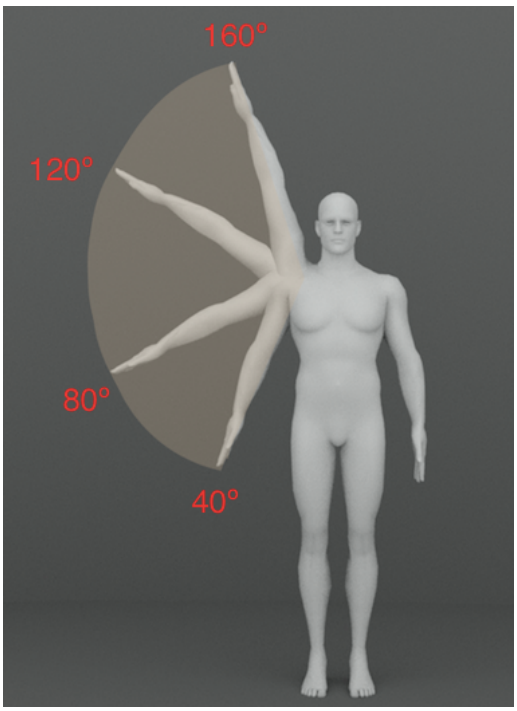

Figure 3.10: Front view of the envelope of humeral postures studied by the present work's regression equations, on the elevation angles (0, 40º, 80º, 120º, 160º)

3.4 Data Analysis

Software developed in-house (Quental, 2013) was used to generate the anatomical coordinate systems for each bone segment. The used upper limb model follows the standardization of the upper limb data proposed by the Standardization and Terminology Committee of the International Society of Biomechanics (ISB) (Wu et al., 2005).

To parametrise shoulder movement the distal segment is always described relative to the proximal segment, which is known as the relative kinematics problem (Krishnan et al., 2019). In the context of the present work, the sternoclavicular, the scapulothoracic and the thoracohumeral joint have as reference body the thorax . In order to represent the relative kinematics between the moving body B and reference body A, depicted in Figure 3.11, the homogeneous transformation matrix **T** can be used, as presented in Equation (1) :

$$\begin{bmatrix} x^A \\ y^A \\ z^A \\ 1 \end{bmatrix} = \begin{bmatrix} \mathbf{R}_{3\times3} & \mathbf{TL}_{3\times1} \\ \mathbf{0}_{1\times3} & 1 \end{bmatrix} \begin{bmatrix} x^B \\ y^B \\ z^B \\ 1 \end{bmatrix} = \mathbf{T} \begin{bmatrix} x^B \\ y^B \\ z^B \\ 1 \end{bmatrix} \tag{1}$$

where **R** and **TL** represent the rotation and translation of frame B with respect to frame A, respectively.

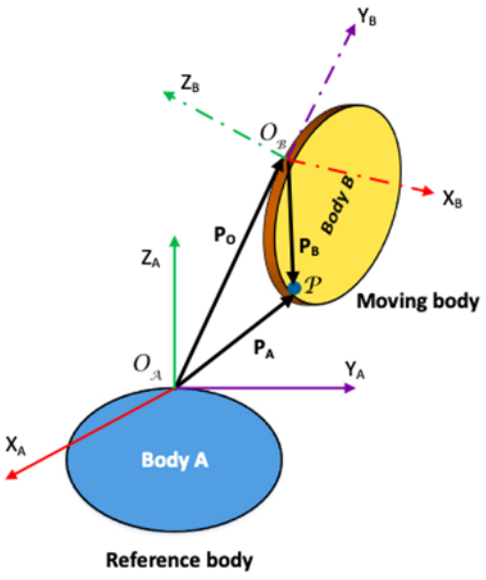

Figure 3.11: Generalised relative kinematics (Krishnan et al., 2019)

In this work, these frames are defined using anatomical landmarks. The interpretation of kinematic data is sensitive to the choice of these frames of reference (Krishnan et al., 2018) and kinematic representations differ in how elements of **T** are computed (Zatsiorsky, 1998).

In this work the representation uses the Euler angles or Tait–Bryan (also named Cardan) angles. The last represent rotations about three distinct axes while proper Euler angles use the same axis for both the first and third elemental rotations. In the Euler angles, the rotation matrix **R**, present in Equation (1), is the product of three sequential rotational transformations $\mathbf{R_i}$, $\mathbf{R_j}$, and $\mathbf{R_k}$ about the axes ***i***, ***j***, and ***k***:

$$\mathbf{R}_{(i,j,k)} = \mathbf{R}_i\,(\theta_1)\,\mathbf{R}_j\,(\theta_2)\,\mathbf{R}_k\,(\theta_3) \qquad (2)$$

where, $i, j, k \in \{X, Y, Z\}$, provided $i \neq j$, $j \neq k$, resulting in 12 different sequences of Euler/Cardan angles. When $i \neq k$, the resulting asymmetric Euler angles are called Cardan angles (Zatsiorsky,1998). The International Society of Biomechanics (ISB) recommends a symmetric Euler sequence, YXY, for describing HT kinematics (Wu et al., 2005).

For each arm posture, body orientations were calculated using the three-dimensional coordinates of relevant markers. The glenohumeral joint centre was estimated using the algorithm of Gamage & Lasenby (2002). The thoracohumeral, scapulothoracic and sternoclavicular joint angles were decomposed using the Euler angle sequence recommended by the ISB (Wu et al., 2005), as presented in Table 3.3. For the thoracohumeral joint, the ISB standardization offers two possible coordinate systems. The second option, using the forearm orientation to estimate axial rotation, was followed. This alternative coordinate system was defined in response to the high error sensitivity of the direction connecting EL and EM due to the short distance between them (Wu et al., 2005). Only two angles were calculated for the sternoclavicular joint because only two landmarks can be identified on the clavicle (SC and AC).

Table 3.3: Euler decomposition orders and their interpretations according to ISB standards (Wu et al., 2005) describing the orientation of clavicle, scapula, and humerus orientation with respect to the thorax.

Joint	Euler decomposition order	Rotation description	Designation
Sternoclavicular	Y X	Retraction/protraction Elevation/depression	SC1 SC2
Scapulothoracic	Y X Z	Retraction/protraction Lateral/medial rotation Anterior/posterior tilt	ST1 ST2 ST3
Thoracohumeral	Y X Y	Plane of elevation Elevation Axial rotation	HT1 HT2 HT3

3.4.1 Regression Models

Out of the 12 subjects (6 females and 6 males), 4 females and 4 males (age: 27.8 ± 12.0 years, height: 1.72 ± 0.04 m, weight: 66.4 ± 9.5 kg) were randomly selected to build the regression models.

Two types of regression models were developed using MATLAB (Math Works, Natick, MA, USA): the first type included only the three thoracohumeral angles as predictor variables; and the second type included the three thoracohumeral angles as well as a selection of individual factors as predictors. Each

regression model was built through a two-step regression process, in agreement with previous studies (de Groot and Brand, 2001; Grewal and Dickerson, 2013).

In the first step, all predictors were centred to reduce multicollinearity (Aiken et al., 1991) and the *z*-score of each variable´s measurement was calculated. The three thoracohumeral angles were treated as continuous variables, and, in the models that included individual factors, gender was treated as a nominal variable while the remaining individual factors were treated as continuous variables. A linear regression model was used to assess the influence of the independent variables, detailing the p-value for each variable and defining the significant variables.

In the second step, the significant variables from the first step were treated as continuous variables to build the regression equation by forward and backward stepwise regression. In previous studies (Grewal and Dickerson, 2013; Xu et al., 2014a), only the thoracohumeral angles, if deemed significant in the first step, had their quadratic and interaction terms evaluated in the second step. In this study, this analysis was extended to all significant variables, in order to better understand the influence of individual factors on the shoulder rhythm as well as the dependency between predictor variables. The output model may contain an intercept, linear and squared terms for each significant predictor, and all products of pairs of significant distinct predictors.

For the stepwise regression, the p-value required for a term to be entered in the model (i.e., considered a predictor variable) was 0.05. The p-value for a term to be retained in the model (i.e., maintained as a predictor variable once successive new variables are included in the model) was 0.10 . These values are in alignment with the work of Xu et al. (2014a). To assess the model's fit to the data, the root-mean-square error (RMSE), the coefficient of determination (R^2), the F-statistic vs. constant model (F vs C), the p-value, and the Akaike information criterion (AIC) were calculated to evaluate the predictability of the model. AIC estimates the quality of each model, relative to each of the other models. A model with a lower AIC is a better-fit model and more parsimonious than one with a higher AIC, as AIC penalizes models that use more parameters. F vs C tests whether the model fits significantly better than a degenerate model consisting of only a constant term: the higher its value the better the model performance.

Three regression models were developed: Model 0 (M0), Model 1 (M1) and Model 2 (M2).

Model 0 included only the three thoracohumeral angles as predictor variables.

Model 1 was developed with the intention of estimating the influence of individual factors on the shoulder rhythm. This model included as predictors the three thoracohumeral parameters plus a comprehensive set of 10 individual factors: gender, age, height, weight, thorax length, thorax depth, clavicular length, scapular spine length, scapular length, upper arm length. de Groot and Brand (2001) used as predictors height, thorax depth, thorax length, clavicular length, and scapular spine length. Grewal and Dickerson (2013) estimated the impact of gender, age, height and weight. Xu et al. (2014a) included age and gender, plus the thorax length, clavicular length, scapular length and upper arm length. By including a combination of all these variables, this second model employed a wider range of individual factors than the ones previously developed.

The anthropometric data include segments that are constrained by their relation in a closed chain mechanism. For instance, the thorax length may be related with the thorax length. If predictors are correlated among themselves, multicollinearity is said to exist among them. Correlation between predictor variables does not exclude the ability to obtain a good model fit, neither does it tend to affect inferences about mean responses or predictions of new observations. However, the estimated regression coefficients tend to have large sampling variability and thus the estimated regression coefficients tend to vary widely from one sample to the next when predictor variables are highly correlated (Kutner et al., 2005). The coefficients become very sensitive to small changes in the model. Generally, coefficients are considered to measure the change in the response variable when the given predictor variable is increased by one unit and all the other predictor variables are held constant. This notion is not fully applicable when multicollinearity exists since some predictor variables are highly correlated (Kutner et al., 2005).

Due to the interconnected nature of the shoulder components, some of the individual factors may be redundant co-variates (i.e., their explanatory variables can be closely correlated). Variable inflation factors (VIF) were estimated to assess the strength and sources of collinearity among the variables in this multiple linear regression model. These factors determine the strength of the correlation between the independent variables. They were calculated by selecting each variable and then regressing it against every other variable. Each predictor variable has a VIF assigned to it, representing how well the variable is explained by the other independent variables. The higher the VIF, the more serious the multicollinearity, thus requiring correction i.e., predictor exclusion from the model).

The condition indices were also estimated. The data (i.e., all the values for all the variables) were decomposed into linear combinations of variables. The linear combinations are chosen in such a way that the first combination has the largest possible variance; the second combination has the next largest variance, subject to being uncorrelated with the first; the third combination has the largest possible variance, subject to being uncorrelated with the first and second, and so forth. The variance of each of these linear combinations is called an eigenvalue. The square root of the ratio of the maximum eigenvalue to each eigenvalue from the correlation matrix of standardized explanatory variables is referred to as the condition index. These indices identify the number and strength of any near dependencies between variables in the variable matrix. Multicollinearity is suspected when the condition indices are higher than 10 to 30 (Kim, 2019).

The three variables with the highest VIF corresponding to a common condition index higher than 30 were excluded from the second step of the regression analysis. The remaining variables were included as predictors.

Lastly, a third model, Model 2, was devised to address the multicollinearity problem. The adopted strategy involved performing Belsley collinearity diagnostics (Belsley, 1991) and analysing the Pearson correlation coefficients. Belsley collinearity diagnostics assess the strength and sources of collinearity among variables in a multiple linear regression model. These diagnostics consist of a two-step procedure. First, singular values of the scaled variable matrix are computed and converted into condition indices. These values represent the collinearity of combinations of variables in the dataset, through the

relative size of the eigenvalues of the matrix. Afterwards, the variance of the ordinary least squares estimates of the regression coefficients in terms of the singular values (variance-decomposition proportions) is computed. These values indicate the proportion of variance for each regression coefficient (and associated variable) attributable to each condition index (eigenvalue). These identify groups of variables involved in dependencies, and the extent to which the dependencies degrade the regression.

On the matrix rows that have a condition index larger than the default tolerance of 30, the variables that had variance-decomposition proportions (VDP) above the default tolerance of 0.5 were singled out as exhibiting multicollinearity. When two or more VDP corresponding to a common condition index higher than 10 to 30 are higher than 0.8 to 0.9, their associated explanatory variables are considered to be involved in severe multicollinearity (Kim et al., 2019).

In this model, the predictor variables selected to integrate the stepwise regression were decided following an analysis of the Pearson correlation coefficients. Each of the Pearson correlation coefficients is the ratio between the covariance of two variables and the product of their standard deviations and thus act as an assessment of linear correlation between two sets of data.

If two variables had a Pearson correlation coefficient > 0.75, one of them was dropped. This process was repeated until only variables with correlation coefficients (between them) < 0.75 existed. These final variables were then included as predictors in the stepwise regression.

3.5 Model Validation

The data of the remaining 4 participants not chosen to integrate the model building (2 females and 2 males, age: 23.8 ± 1.3 years, height: 1.73 ± 0.11 m, weight: 65.5 ± 14.1 kg) were used to validate the regression models. The root-mean-square error (RMSE), the coefficient of determination (R^2) were calculated to evaluate the predictability of the model.

Lastly,the model developed by Xu et al. (2014a) that only included thoracohumeral angles and the model developed by Grewal and Dickerson (2013) were applied to this work's validation dataset. This was made to assess how well the regression equations developed by other authors, which exclude thoracohumeral negative planes of elevation, estimate the wider-ranging dataset of joint rotations contained in the present work.

Chapter 4

Results and Discussion

4.1 Regression Equations for Developed Models

The following tables 4.1, 4.2 and 4.3 indicate the obtained regression equations for Model 0 (M0), Model 1 (M1) and Model (2), whose specifications are detailed in sections 3.4.1. All the equations are in Wilkinson notation (Wilkinson et al., 1973), sometimes called the Wilkinson-Rogers notation. This notation allows the quick computation of regression equations containing multiple predictor variables. It is used by common commercial software including MATLAB (Math Works, Natick, MA, USA), Octave and R to indicate relationships between variables. In this notation, each term is multiplied by the coefficient associated with it. A colon (:) between two variables indicates a two-way interaction, that is, the interaction (product) of the two independent variables. The intercept (often labelled the constant) is the expected mean value of the response variable when all predictor variables equal 0 and is added to all the other variables predictors as its value, the intercept's coefficient.

The joint angle is then calculated in the form: Joint Rotation = Intercept's coefficient + $Term_1$ * Coefficient $_1$ + Term $_2$ * $Coefficient_2$ + … Term $_n$ * Coefficient $_n$, where the terms 1 to *n* are the terms listed in each row of the following table and the coefficients 1 to *n* are their corresponding coefficients.

4.1.1 Regression Equations for Model 0

Table 4.1: Regression equations obtained for the scapular retraction/protraction (ST1), scapular lateral/medial rotation (ST2), scapular anterior/posterior tilt (ST3), clavicular retraction/protraction (SC1) and clavicular elevation/depression (SC2) for Model 0 (M0)

Joint Rotation	Term	Coefficient
ST1(**M0**)	Intercept	37.625
	HT1	0.14212
	HT3	0.1085

Joint Rotation	Term	Coefficient
ST2(**M0**)	Intercept	5.439
	HT1	0.22365
	HT2	0.60913
	HT3	0.11633
	HT1:HT2	0.0025723
	HT2:HT3	-0.00086994
	$HT2^2$	0.0022037
	$HT3^2$	0.0010033

Joint Rotation	Term	Coefficient
ST3(**M0**)	Intercept	-8.6489
	HT1	0.043321
	HT2	0.1057
	HT3	0.0095627
	HT1:HT2	0.00057578
	HT2:HT3	0.0012797
	$HT1^2$	0.00061026
	$HT2^2$	0.00066838

Joint Rotation	Term	Coefficient
SC1(**M0**)	HT1	0.20188
	HT2	0.040005
	HT3	0.15876
	HT1:HT2	0.0019354
	HT1:HT3	-0.0013034
	$HT2^2$	-0.0011866

Joint Rotation	Term	Coefficient
SC2(**M0**)	Intercept	-4.4813
	HT2	0.4926
	HT3	0.0012678
	HT2:HT3	-0.00066918
	$HT2^2$	0.0025672
	$HT3^2$	0.0010362

4.1.2 Regression Equations for Model 1

Table 4.2: Regression equations obtained for the scapular retraction/protraction (ST1), scapular lateral/medial rotation (ST2), scapular anterior/posterior tilt (ST3), clavicular retraction/protraction (SC1) and clavicular elevation/depression (SC2) for Model 1 (M1)

Joint Rotation	Term	Coefficient
ST1(**M1**)	Intercept	-3584.8
	HT1	-1.4881
	HT3	-1.2679
	Age	-0.41617
	Height	3919.8
	LengthThorax	3.5065
	LengthClavicle	0.13733
	HT1:Height	0.92271
	HT3:Height	0.77326
	$HT1^2$	0.00040604
	$Height^2$	-1171.1
	$LengthThorax^2$	-0.0090076

Joint Rotation	Term	Coefficient
ST2(**M1**)	Intercept	-220.25
	HT1	0.30868
	HT2	0.13334
	HT3	0.1731
	Age	0.089883
	LengthClavicle	2.8015
	HT1:HT2	0.0020497
	HT1:Age	-0.0040594
	HT2:LengthClavicle	0.0024806
	$HT2^2$	0.0012891
	$HT3^2$	0.00083255
	$LengthClavicle^2$	-0.0088142

Joint Rotation	Term	Coefficient
ST3(**M1**)	Intercept	373.5
	HT1	0.22672
	HT2	0.047529
	HT3	0.0777
	Weight	-0.65702
	LengthThorax	-2.7636
	LengthClavicle	-0.1558
	LengthScapularSpine	-0.68857
	HT1:LenghtClavicle	-0.0013056
	HT2:HT3	0.0012667
	HT2:Weight	0.0038596
	HT2:LenghtThorax	0.0012819
	HT2:LenghtScapularSpine	-0.004206
	HT3:LenghtThorax	0.00071073
	HT3:LenghtScapularSpine	-0.0014355
	$HT1^2$	0.00042391
	$Weight^2$	0.0084557
	$LengthThorax^2$	0.0070335

Joint Rotation	Term	Coefficient
SC1(**M1**)	Intercept	21.299
	HT1	0.409
	HT2	0.099103
	HT3	0.15257
	Gender	244.03
	Height	-80.408
	LengthClavicle	0.59722
	HT1:HT2	0.0017871
	HT1:HT3	-0.00065256
	HT1: Gender	0.095278
	HT1:LengthClavicle	-0.0017409
	HT2:Gender	0.068999
	Gender:Height	-136.23
	$HT2^2$	-0.00060118
	$HT3^2$	0.00052902

Joint Rotation	Term	Coefficient
SC2(**M1**)	Intercept	-515.72
	HT2	0.065868
	HT3	-0.16164
	Age	10.288
	LengthThorax	-0.26689
	LengthClavicle	5.6162
	LenghtScapularSpine	0.56309
	HT2:LengthScapularSpine	0.0027958
	HT3:Age	0.0021178
	HT3:LengthClavicle	0.00099873
	Age:LengthClavicle	-0.075438
	$HT2^2$	0.0019164
	$HT3^2$	0.0010169
	$LengthClavicle^2$	-0.014404

4.1.3 Regression Equations for Model 2

Table 4.3: Regression equations obtained for the scapular retraction/protraction (ST1), scapular lateral/medial rotation (ST2), scapular anterior/posterior tilt (ST3), clavicular retraction/protraction (SC1) and clavicular elevation/depression (SC2) for Model 2 (M2)

Joint Rotation	Term	Coefficient
ST1(**M2**)	Intercept	3117.5
	HT1	0.97919
	HT3	0.5838
	Age	-74.423
	DepthThorax	-8.2565
	LenghtScapularSpine	-0.16576
	UpperArmLength	-5.7584
	HT1:Age	-0.0047428
	HT1:DepthThorax	-0.0030871
	HT3:Age	-0.0031637
	HT3:DepthThorax	0.0017992
	Age:UpperArmLength	0.21556
	$HT1^2$	0.00034112
	$DepthThorax^2$	0.015826

Joint Rotation	Term	Coefficient
ST2(**M2**)	Intercept	642.14
	HT1	0.25548
	HT2	1.1392
	HT3	1.2062
	Age	-19.742
	LengthScapularSpine	-0.50505
	UpperArmLength	-1.6496
	HT1:HT2	0.0013968
	HT1:HT3	-0.0013124
	HT1:Age	-0.0052936
	HT2:Age	-0.003537
	HT2:LengthScapularSpine	-0.0038282
	HT3:UpperArmLenght	-0.031106
	Age:UpperArmLenght	0.057224
	$HT1^2$	-0.00073989
	$HT2^2$	0.001318

Joint Rotation	Term	Coefficient
ST3(**M2**)	Intercept	-154.97
	HT1	-0.039031
	HT2	0.67123
	HT3	-0.092566
	Age	6.5428
	DepthThorax	0.6078
	UpperArmLength	0.033197
	HT1:Age	0.0023588
	HT2:HT3	0.0011436
	HT2:Age	-0.0032685
	HT2:UpperArmLength	-0.0016215
	HT3:DepthThorax	-0.00046138
	Age:DepthThorax	-0.029464
	$HT1^2$	0.0004699

Joint Rotation	Term	Coefficient
SC1(**M2**)	Intercept	1528
	HT1	0.53355
	HT2	-2.1723
	HT3	-0.14505
	Age	-0.18676
	DepthThorax	0.835
	LengthClavicle	-24.975
	LengthScapularSpine	-0.34333
	UpperArmLength	0.61038
	HT1:HT2	0.0013606
	HT1:HT3	-0.00053046
	HT1Age	-0.043227
	HT1:DepthThorax	-0.0038112
	HT1:LenghtScapularSpine	0.0053292
	HT2:DepthThorax	0.0031456
	HT2:UpperArmLength	0.042351
	H3:LenghtScapularSpine	0.0023203
	$HT2^2$	-0.0010446
	$HT3^2$	0.00050131
	$LengthClavicle^2$	0.080888

Joint Rotation	Term	Coefficient
SC2(**M2**)	Intercept	315.68
	HT2	0.22318
	HT3	0.050851
	Weight	0.34562
	DepthThorax	-0.21574
	LengthClavicle	-3.4244
	HT2:DepthThorax	0.00082935
	$HT2^2$	0.0019409
	$HT3^2$	0.00098148
	$LenghtClavicle^2$	0.0098947

4.2 Analysis of Developed Models

When interpreting the regression equations, special attention has to be given to the distinction between the second thoracohumeral Euler angle, HT2, and the humeral elevation. Following ISB standardization HT2 decreases as humeral elevation increases. The used decomposition of the rotation matrix computes HT2 in the range [-180º,0º]. Humeral elevation is, on the other hand, a positive value corresponding to the modulus of HT2.

Futhermore, the third thoracohumeral Euler angle, HT3, is a measure of the axial rotation, but is also weighed by the plane of elevation in which the arm posture occurs. This is a direct consequence of the ISB convention for the thoracohumeral joint angles. This convention is based on the Euler angles decomposition. Thoracohumeral angles follow a symmetric Euler sequence YXY, as shown in Table 3.3. Following this sequence, the plane of elevation is selected by an angle around the initial y axis (Yh axis, shown in the leftmost representation of Figure 4.2, which is the axis fixed to the thorax and coincident with the Yt axis of the thorax coordinate system, shown in Figure 4.1). The elevation angle constitutes the second rotation by an angle around the new position (Xh in the central representation of the Figure 4.2) of the initial x axis. Axial rotation happens around the final position of the Yh axis

(depicted as Yh axis in the rightmost representation in Figure 4.2. Yt is defined as the line connecting the midpoint between PX and T8 and the midpoint between IJ and C7, and pointing upward. Yh is defined as the line connecting GH and the midpoint of EL and EM, pointing to GH. It is, depending on the elevation angle, possible for the selection of the plane of elevation and the axial rotation to occur around the same axis (that is, for the Yt, displayed in Figure 4.1 and Yh axis, displayed in Figure 4.2, to coincide). Using the same axis for both the first and third elemental rotations explains why a positive HT3 can be found in an externally rotated arm posture and, reciprocally, a negative HT3 can be calculated for an internally rotated humerus. For instance, an arm posture with neutral axial rotation in the 90 º plane of elevation and 0º elevation angle registers and HT3 of 90º, even though it is neither internally nor externally rotated. This has to be kept in mind while interpreting the regression equations.

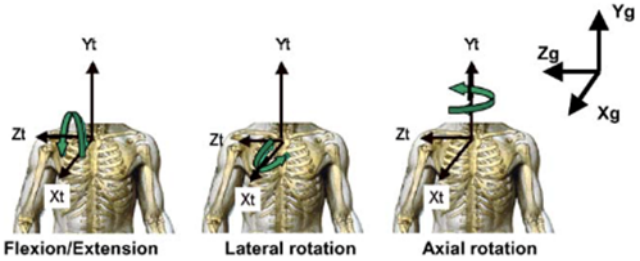

Figure 4.1: ISB thorax coordinate system and definition of motions (Wu et al., 2004)

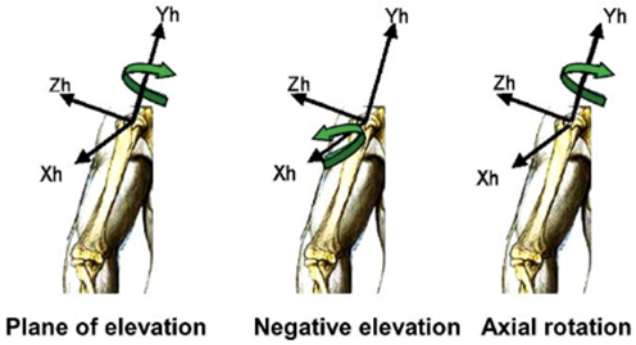

Figure 4.2: ISB definition of thoracohumeral rotations (Wu et al., 2004)

Lastly, it is important to recall the signal convention according to the ISB standardization. For the sternoclavicular joint, retraction is negative and protraction positive, elevation is negative and depression positive. For the scapulothoracic joint, retraction is a negative angle and protraction positive, lateral rotation is negative and medial rotation is positive, anterior tilt is negative and posterior is positive.

4.2.1 Analysis of Model 0

For the first model, excluding all individual factors, the first step of the regression analysis indicated that all thoracohumeral predictors contributed to all sternoclavicular and scapulothoracic joint angles. The

second step eliminated HT2 as a predictor of retraction/protraction of the scapula and HT1 as a predictor of the elevation/depression of the clavicle.

Globally, lateral/medial rotation of the scapulothoracic joint had the greatest R^2, of 0.81, while the retraction/protraction of the scapulothoracic joint had the least R^2, of 0.26. The RMSE of the model ranged between 5.26º, for the anterior/posterior tilt of the scapula, and 8.36º , for the retraction/protraction of the scapula. For the validation dataset, R^2 ranged between 0.05, for the retraction/protraction of the scapula, and 0.75 for the retraction/protraction of the clavicle, while the RMSE ranged from 5.05º, for the anterior/posterior tilt of the scapula, and 10.80º, for the lateral/medial rotation of the scapula.

Quadratic prediction models were obtained for the lateral/medial rotation and anterior/posterior tilt of the scapula and for both clavicular retraction/protraction and elevation/depression. Figures 4.3, 4.4, 4.5, 4.6 and 4.7 present the plots of the adjusted response functions, describing the relationship between, respectively, the fitted ST1, ST2, ST3, SC1 and SC2 responses and the model predictors. These graphs include: the scatter plot of adjusted response values against adjusted predictor variable values, a fitted line for adjusted response values as a function of adjusted predictor variable values and a 95% confidence bounds of the fitted line. The adjusted values are equal to the average of the variable plus the residuals of the variable fit to all predictors except the selected predictor.

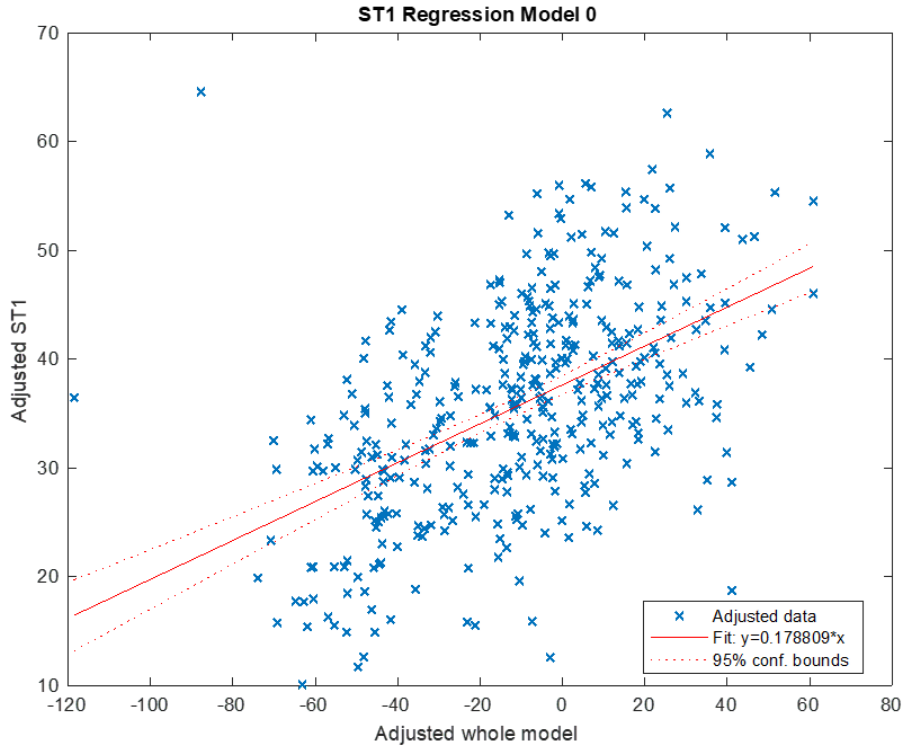

Figure 4.3: Adjusted response function describing the relationship between the fitted ST1 response and the model predictors

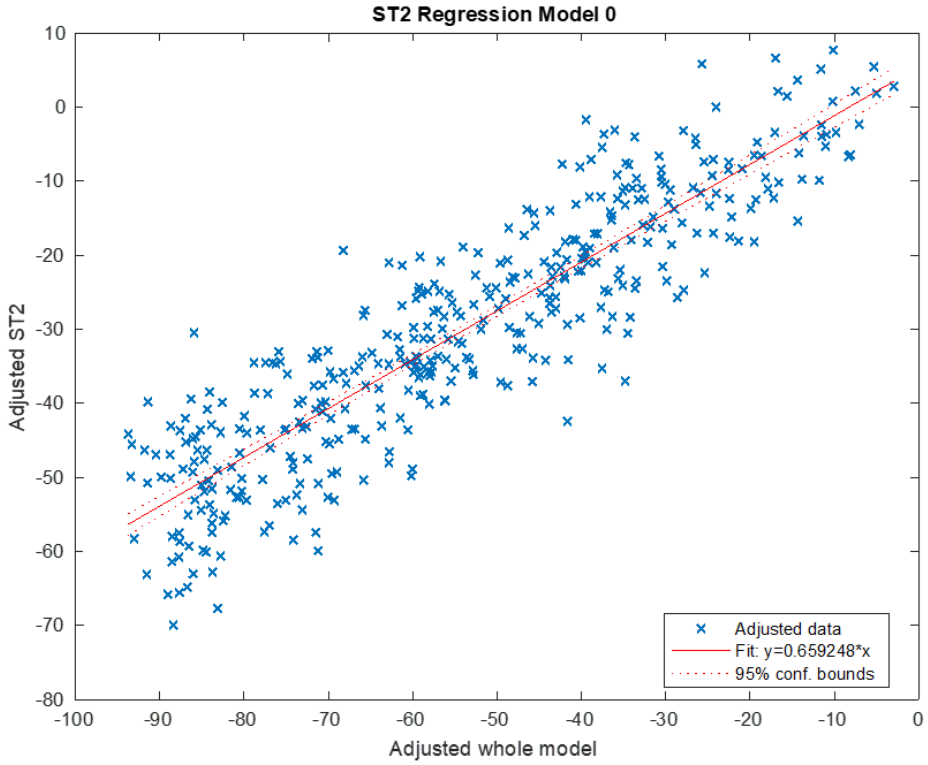

Figure 4.4: Adjusted response function describing the relationship between the fitted ST2 response and the model predictors

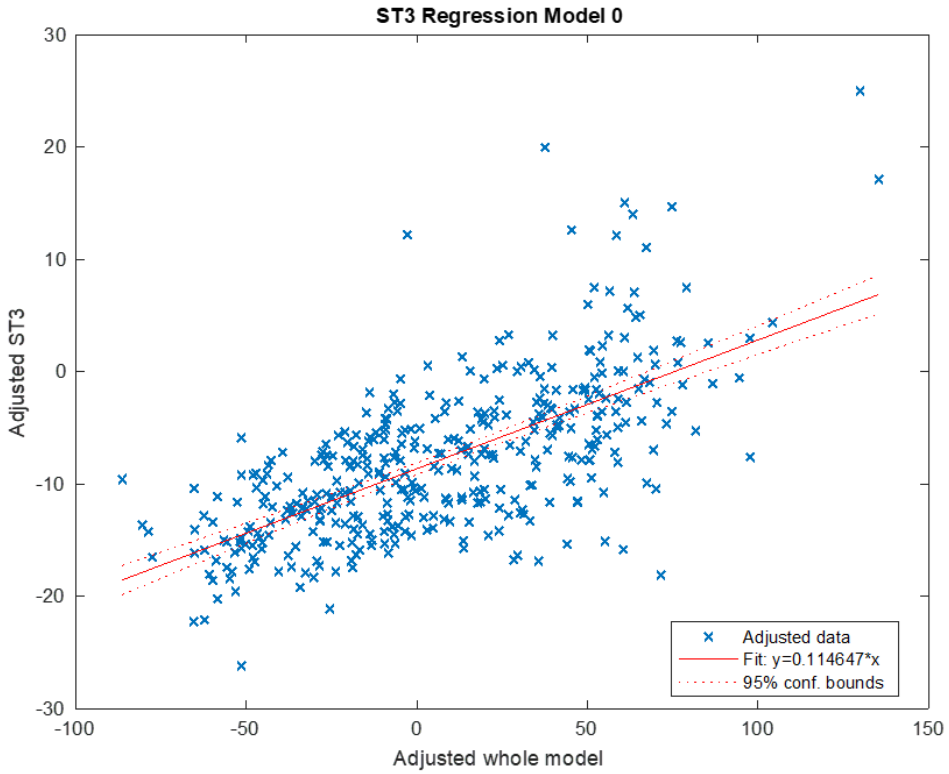

Figure 4.5: Adjusted response function describing the relationship between the fitted ST3 response and the model predictors

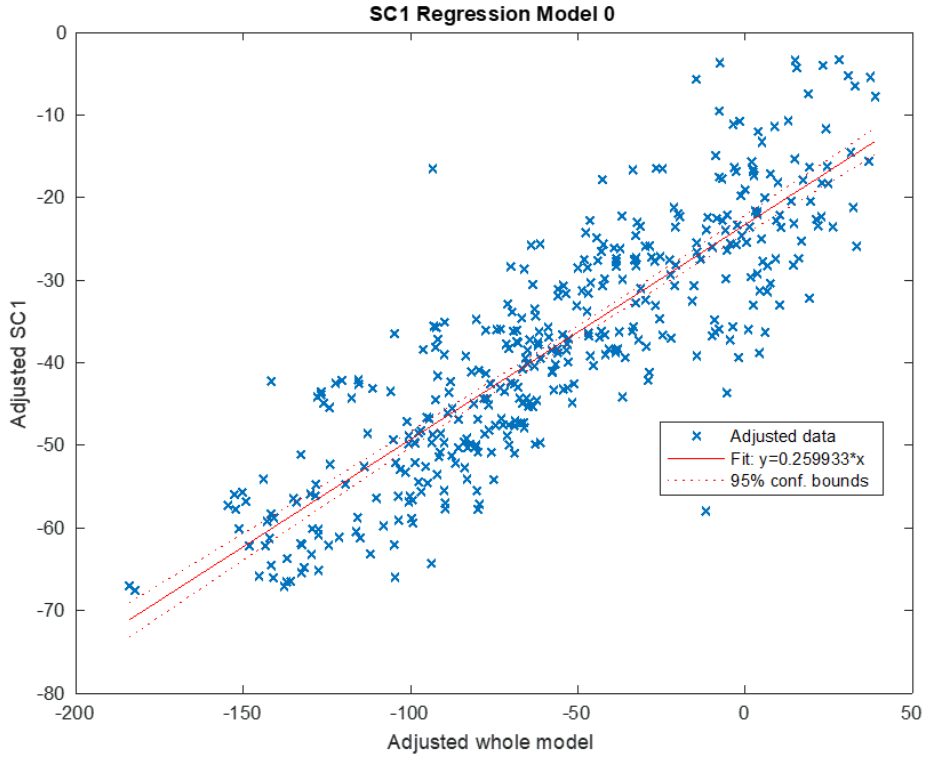

Figure 4.6: Adjusted response function describing the relationship between the fitted SC1 response and the model predictors

Figure 4.7 Adjusted response function describing the relationship between the fitted SC2 response and the model predictors

Analyzing the regression equations derived for Model 0, it is observed that the scapula protracted with increasing humeral plane of elevation and increasing humeral axial rotation.

HT1 and HT2 interacted in such a way that the scapula medially rotated with increasing humeral elevation plane, if HT2 was > -87°. For elevation angles below this value, the scapula laterally rotated with increasing humeral elevation plane. HT2 also interacted with HT3. Medial rotation increased with increasing HT2 regardless of axial rotation. Finally, medial rotation increased with increasing axial rotation.

Concerning scapular tilting, and in general, for positive elevation planes, posterior tilting increases with increasing elevation plane. For negative elevation planes, as HT1 increases from -90° to 0° the scapula tilts anteriorly. This interaction is, however, affected by the interaction between HT1 and HT2. For the postures with the highest humeral elevation, i.e., lowest HT2, the scapula tilts anteriorly with increasing elevation plane for a range of positive elevation planes. The higher the elevation the wider this positive range of motion. For instance, for the maximum recorded humeral elevation (HT2 = -155°) the scapula tilts anteriorly as HT1 increases from -90° to 38°. The scapula tilts anteriorly with increasing axial rotation, regardless of the elevation angle.

Clavicular protraction increased with increasing HT2, regardless of the elevation plane, which interacted with HT2. Protraction also increased with increasing axial rotation, regardless of the elevation plane. The influence of HT3 on clavicular protraction depends on a more delicate balance between axial rotation and elevation angle. For most of the HT2 and HT3 configurations protraction increases with increasing elevation plane. However, for high humeral elevation (HT2 $\leq$ -90) in positive HT3 configurations, protraction decreases with increasing elevation plane, and this decrease is more pronounced the higher the elevation angle and the more internally rotated the humerus is.

Clavicular depression was influenced by a quadratic HT2 term. It increased with increasing HT2, past a certain HT2 value, and decreased for lower HT2 values. This inflexion value was affected by the displayed axial rotation. The more internal the axial rotation, the higher the inflexion value. For instance, for an HT3 of -70º clavicular depression increased with increasing HT2 for HT2 values > -102º. For lower HT2 clavicular protraction decreased with increasing HT2. However, for a higher HT3 value of 70º clavicular protraction increased with increasing HT2 for HT2 values > -86º, and decreased with increasing HT2 for HT2 values below that.

The model's goodness of fit was summarized by the obtained p-values, R-squared (R^2) values, root-mean-square error (RMSE), F-statistic vs. constant model and Akaike information criterion (AIC) values, shown on Table 4.4.

Table 4.4: The obtained p-values, R-squared (R^2) values, root-mean-square error (RMSE), F-statistic vs. constant model and Akaike information criterion (AIC) values to estimate the scapular and the clavicular angles using Model 0

Model 0	RMSE (°)	R^2	F vs C	p-value	AIC
ST1	8.36	0.26	72	$p < 0.001$	2.85×10^3
ST2	7.39	0.81	238	$p < 0.001$	2.76×10^3
ST3	5.26	0.44	45	$p < 0.001$	2.48×10^3
SC1	7.57	0.74	185	$p < 0.001$	2.77×10^3
SC2	6.63	0.42	57	$p < 0.001$	2.67×10^3

For Model 0, the retraction/protraction of the scapula presented the lowest R^2 (R^2 = 0.26), whereas the lateral/medial rotation of the scapula presented the highest R^2 (R^2 = 0.81). The scapular anterior/posterior tilt had the lowest root-mean-square error (RMSE = 5.26°), and thus the lowest error in predicting the quantitative data. Scapular retraction/protraction, scapular lateral/medial rotation and clavicular retraction/protraction displayed the largest errors, with RMSE > 7°). These larger errors could be explained by the fact that these three joint angles had the widest range of measured and observed values meaning erroneously estimated angles were also spread across a larger set of values, increasing the unit-dependent relative measure of fit, the RMSE value. The AIC ranged from 2.48×10^3 for the scapular anterior/posterior tilt to 2.85×10^3 for the scapular retraction/protraction. The F vs C ranged from 45 for scapular anterior/posterior tilt to 238 for scapular lateral/medial rotation. The p-value was $p < 0.001$ for all the studied joint angles indicating statistical significance.

4.2.1.1 Validation of Model 0

The dataset of the remaining 4 subjects (2 females and 2 males) was used to validate the regression models. The subjects followed the same experimental protocol and performed the same arm postures. The root-mean-square error and the coefficient of determination were calculated to evaluate the predictability of the model, as seen on Table 4.5.

Table 4.5: Validation of Model 0

Model 0	R^2	RMSE (°)
ST1	0.05	8.13
ST2	0.66	10.80
ST3	0.39	5.05
SC1	0.75	6.62
SC2	0.32	6.54

For the validation dataset, retraction/protraction of the scapula had the lowest R^2 (0.05), which means that only approximately 10% of the observed variation can be explained by the model's inputs. Clavicular retraction/protraction, on the other hand, had the highest R^2 (0.75), which means that approximately 75% of the observed variation can be explained by the model's inputs.

A scatter plot is presented in Figure 4.8 to visually assess the correlation between the measured angles and the data computed with the regression equations.

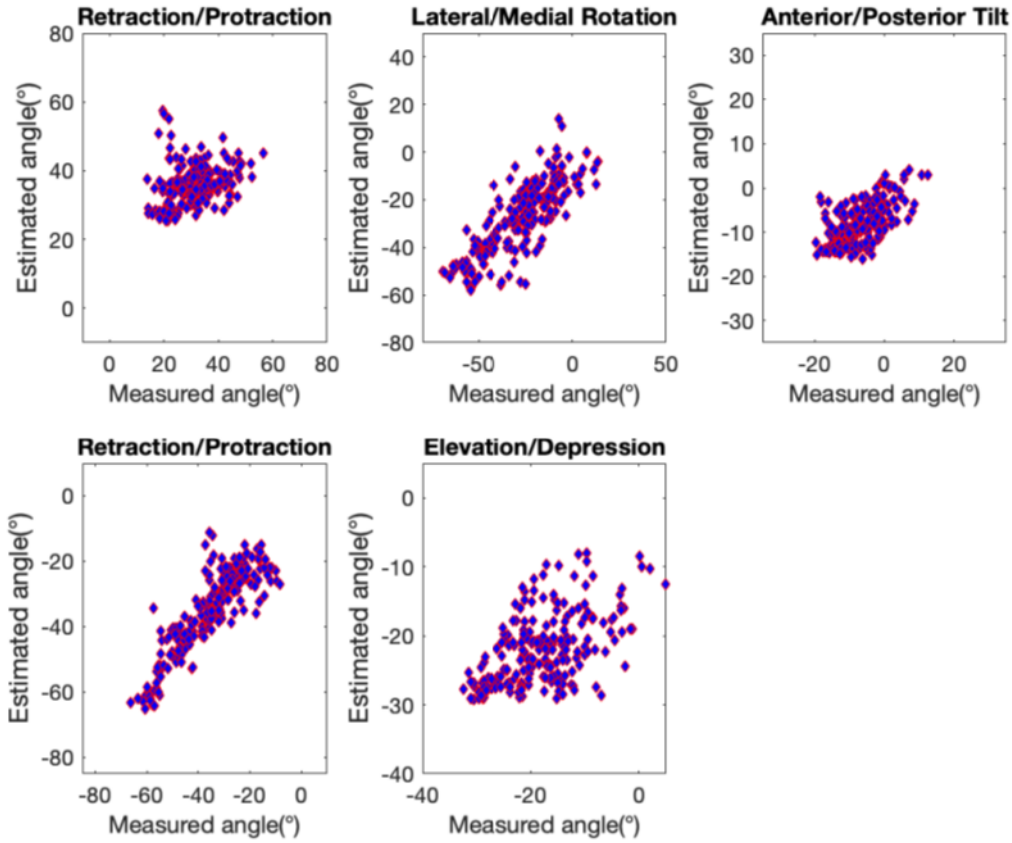

Figure 4.8: The correlation between the measured and the predicted sternoclavicular and scapulothoracic joint angles for Model 0

The scapular anterior/posterior tilt predicted angles were under-estimated for some tilt angles, especially for the higher ones. Even though, scapular anterior/posterior tilt had the lowest root-mean-square error (RMSE = 5.05°). Clavicular elevation/depression was over-estimated for lower elevation angles and under-estimated for higher elevation angles.

4.2.2 Analysis of Model 1

Model 1 considered the three thoracohumeral angles as well as the individual factors, as detailed in section 3.4.1. After the statistical processing, thorax depth, scapular length and upper arm length were the three variables with the highest VIF and were thus excluded from the second step of the regression analysis (Figure 4.9).

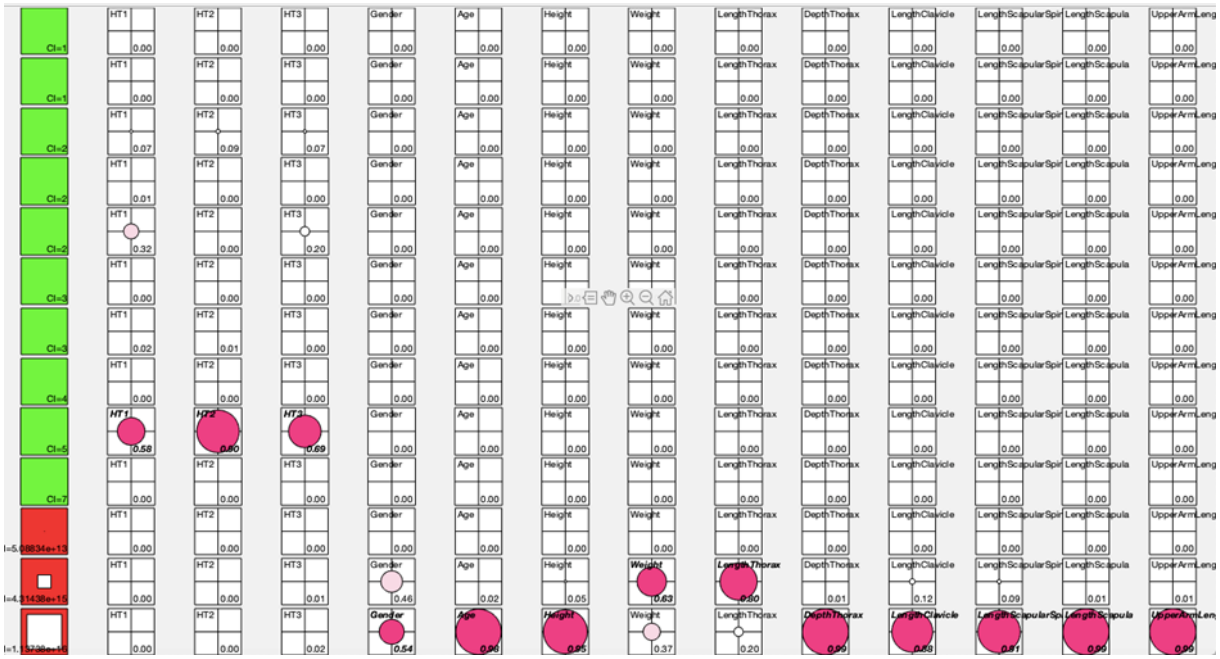

Figure 4.9: Visual representation of each predictor variable's condition indices and VIF. Variables 1 to 13 denoted, respectively: thoracohumeral angle HT1, thoracohumeral angle HT2, thoracohumeral angle HT3, gender, age, height, weight, thorax length, thorax depth, clavicular length, scapular spine length, scapular length, upper arm length. The rows index indicates the condition index, green if below the threshold of 30 and highlighted in red if above it, indicating strong variable dependence. VIF are represented for each matrix entry, signifying the strength of correlation between each pair of variables. The highest VIF correspond to the bigger and darker pink circles; the three variables with the highest value are thorax depth, scapular length and upper arm length

Quadratic prediction models were obtained for all sternoclavicular and scapulothoracic joint angles. Figures 4.10, 4.11, 4.12, 4.13 and 4.14 present the plots of the adjusted response functions, describing the relationship between, respectively, the fitted ST1, ST2, ST3, SC1 and SC2 responses and the model predictors.

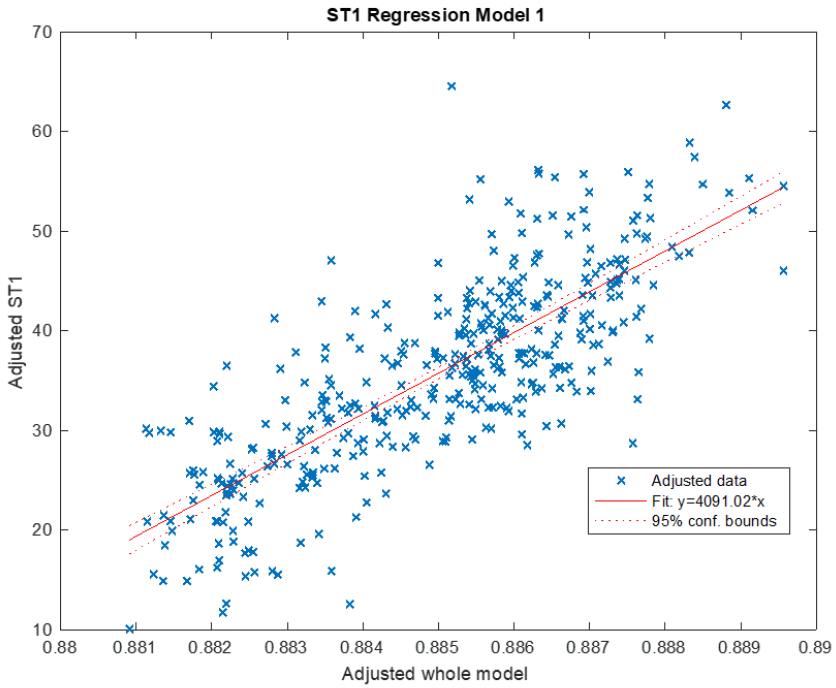

Figure 4.10: Adjusted response function describing the relationship between the fitted ST1 response and the model predictors

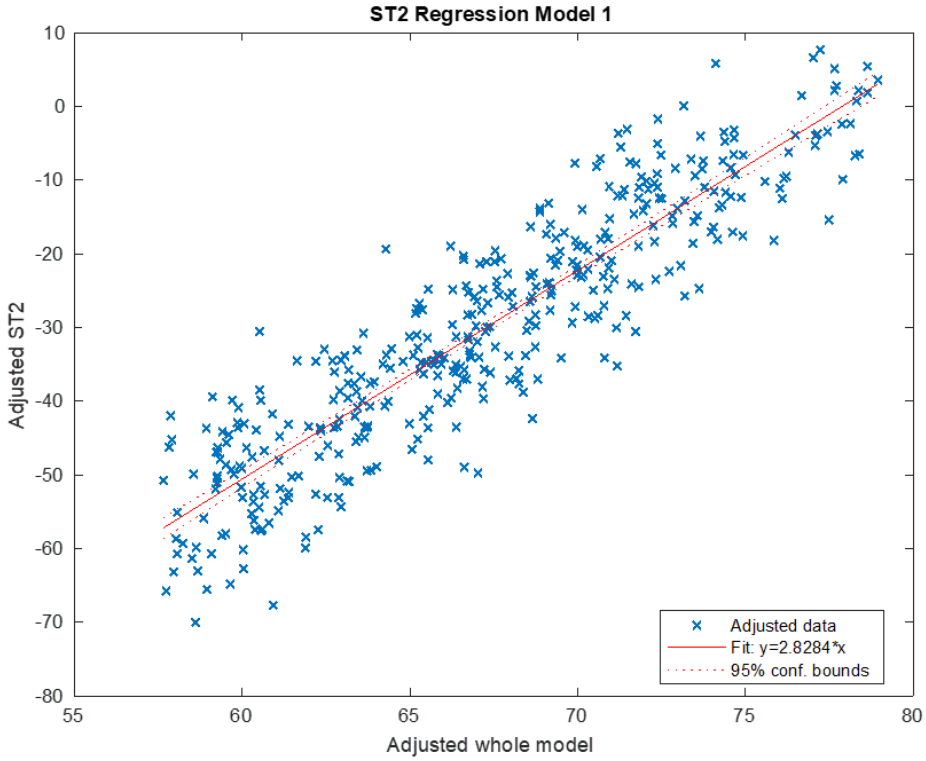

Figure 4.11: Adjusted response function describing the relationship between the fitted ST2 response and the model predictors

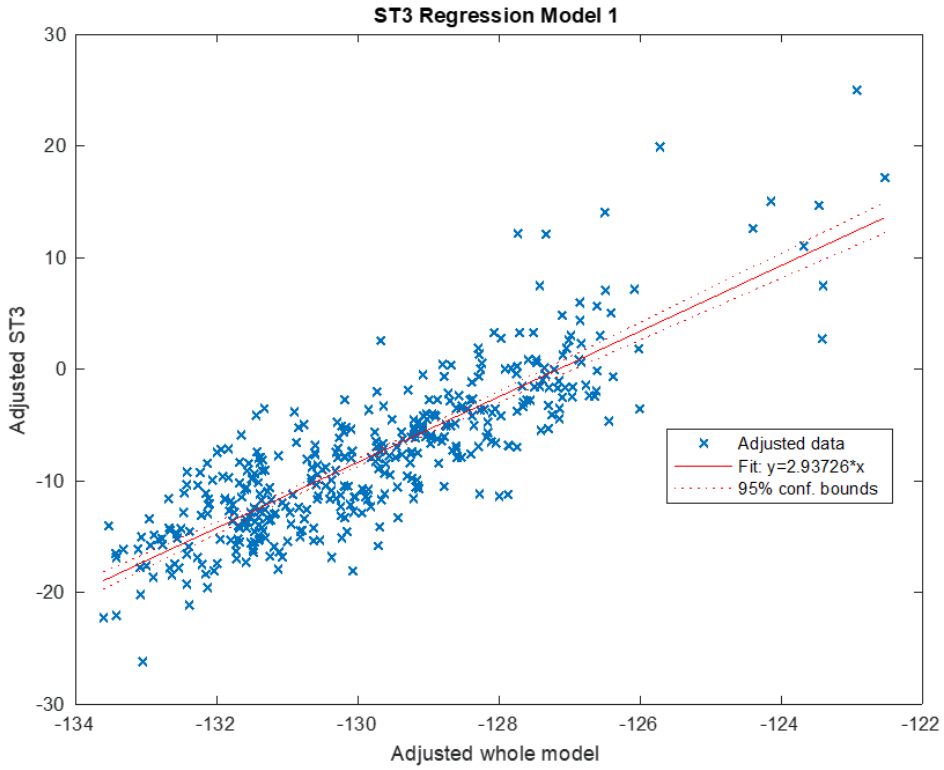

Figure 4.12: Adjusted response function describing the relationship between the fitted ST3 response and the model predictors

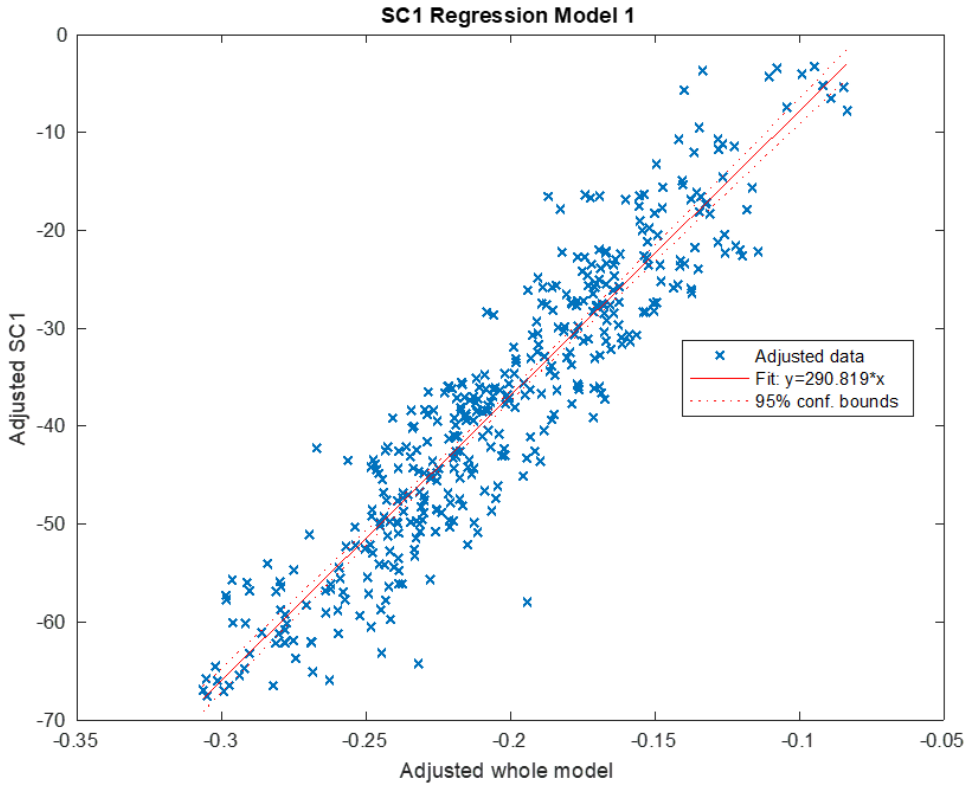

Figure 4.13: Adjusted response function describing the relationship between the fitted SC1 response and the model predictors

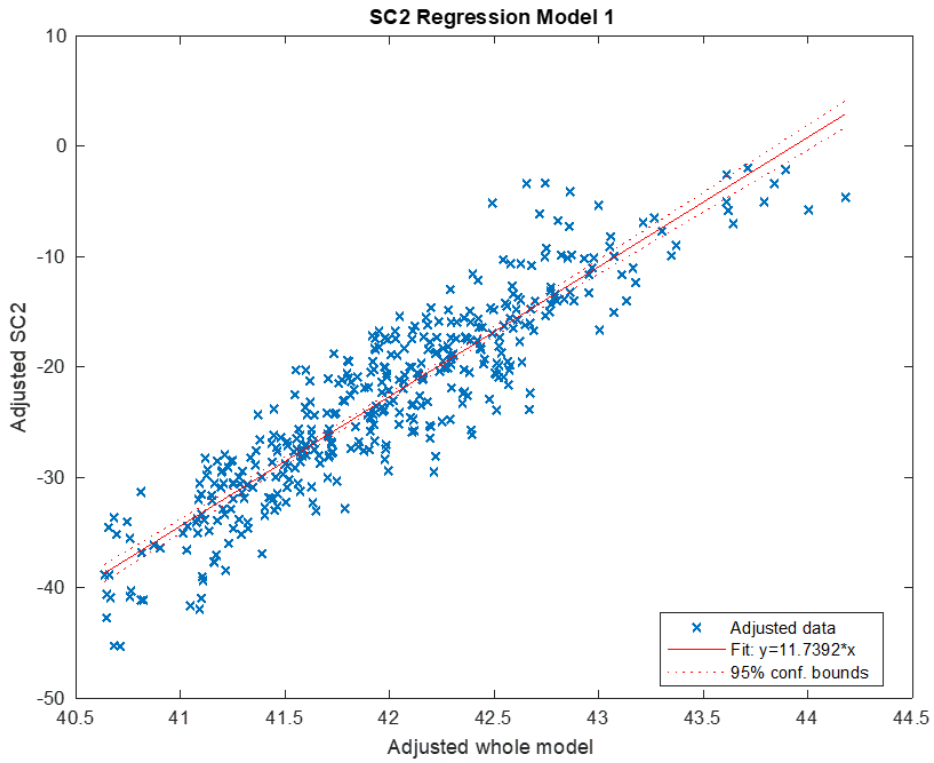

Figure 4.14: Adjusted response function describing the relationship between the fitted SC2 response and the model predictors

The following analysis of the obtained regressions equations aims at a better understanding of the influence of each of the individual factors used as predictor variables.

The model indicated scapular protraction increased with height, decreasing age, decreasing thorax length and increased clavicular length. The scapula medially rotated with increasing age, for elevation planes $> 22º$. For lower elevation planes the scapula posteriorly rotated with increasing age. Increasing clavicular length resulted in increasing medial scapular rotation. Scapula tilts posteriorly with increasing weight, decreasing clavicular length and decreasing length scapular spine.

Clavicular protraction occurred with decreasing height, decreasing thorax length, and with increasing clavicular length. For most humeral configurations the influence of the gender variable resulted in men having decreased clavicular protraction when compared with female subjects. This was the case for all configurations except those in positive elevation planes and very low elevation angles (i.e., very high HT), where men had increased clavicular protraction when compared with female subjects. Clavicular depression occurred with decreasing age, decreasing thorax length, decreasing clavicular length and increasing length scapular spine.

As before, the model's goodness of fit was summarized by the obtained p-values, R^2-values, RMSE, F-statistic vs. constant model and AIC values, shown on Table 4.6.

Table 4.6: The obtained p-values, R-squared (R^2) values, root-mean-square error (RMSE), F-statistic vs. constant model and Akaike information criterion (AIC) values to estimate the scapular and the clavicular angles using Model 1

Model 1	RMSE (°)	R^2	F vs C	p-value	AIC
ST1	6.06	0.62	58	$p < 0.001$	2.63×10^3
ST2	7.09	0.83	168	$p < 0.001$	2.73×10^3
ST3	3.75	0.72	59	$p < 0.001$	2.22×10^3
SC1	5.52	0.86	174	$p < 0.001$	2.53×10^3
SC2	3.64	0.83	144	$p < 0.001$	2.19×10^3

The retraction/protraction of the sternoclavicular joint had the highest R^2 value of 0.86, which means that approximately 86% of the observed variation can be explained by the model's inputs. As with Model 0, retraction/protraction of the scapulothoracic joint had the lowest R^2 value of 0.62 (Table 4.6). The RMSE of the model ranged between 3.75º for the anterior/posterior tilt of the scapula and 7.09º for lateral/medial rotation of the scapula. Anterior/posterior tilt of the scapula had the lowest error in predicting the quantitative data, in both Model 0 and Model 1. The AIC ranged from 2.19×10^3 for clavicular elevation/depression to 2.73×10^3 for lateral/medial scapular rotation. The F vs C ranged from 59 for scapular anterior/posteriro to 174 for clavicular retraction/protraction. The p-value was < 0.001 for all the studied joint angles indicating statistical significance.

4.2.2.1 Validation of Model 1

After applying Model 1 to the validation dataset, the root-mean-square error and the coefficient of determination were calculated to evaluate the predictability of the model, as seen on Table 4.7.

Table 4.7: Validation of Model 1

Model 1	R^2	RMSE (°)
ST1	0.003	8.34
ST2	0.68	10.50
ST3	0.001	6.45
SC1	0.30	11.00
SC2	0.45	5.90

For the validation dataset, the R^2 ranged between 0.003 for the retraction/protraction of the scapula and 0.68 for lateral/medial rotation of the scapula. The RMSE of the models applied to the validation dataset ranged from 5.90° for the clavicular elevation/depression and 11.00° for the retraction/protraction of the clavicle.

A scatter diagram (Figure 4.15) was plotted to visually estimate the correlation between the measured angles and the estimated data computed with the regression equations.

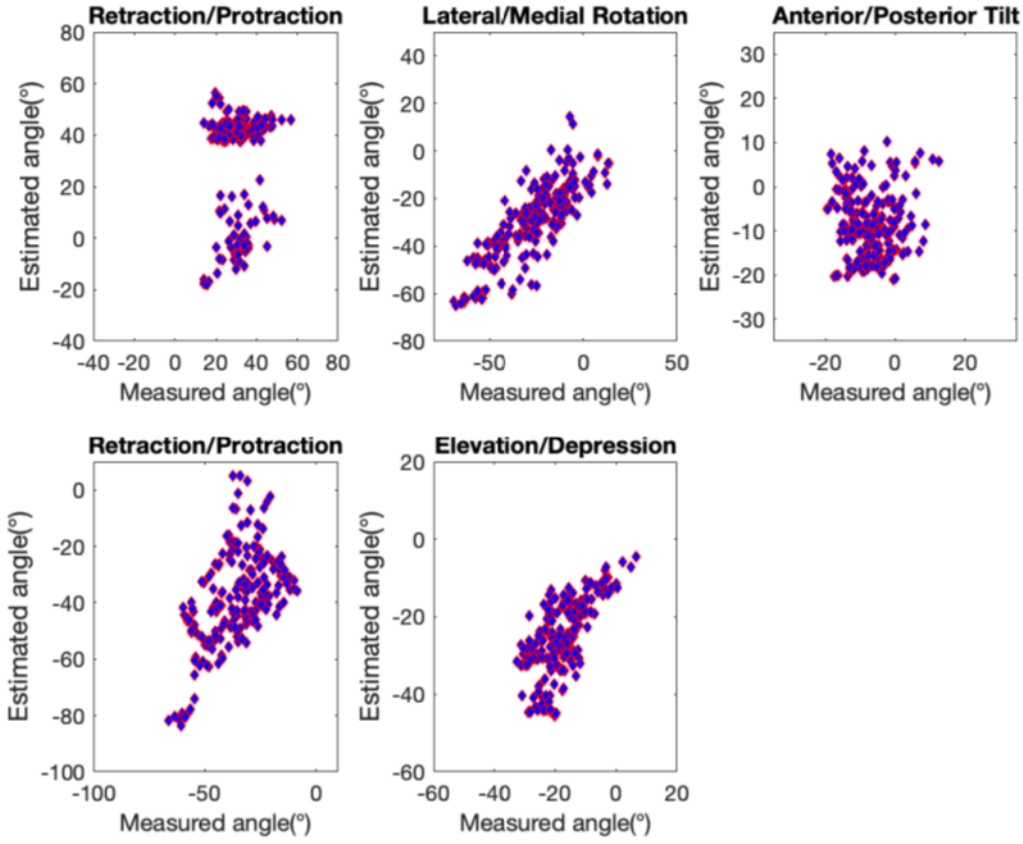

Figure 4.15: The correlation between measured and predicted sternoclavicular and scapulothoracic joint angles for Model 1

For scapular retraction/protraction parameter, the regression equation presented a quadratic term for the height predictor variable. The validation group included a subject whose height was 0.16 m above the average height for the 12 subjects that participated in this study. This explains the two distinct regions of estimated angles, displayed in Figure 4.15, where the higher predicted values correspond to the ones estimated using this subject's anthropometric data. The anterior/posterior tilt model applied to the validation dataset had the second lowest RMSE. Even then both moderate underestimation and overestimation were found in the computed data when compared to the measured angles. The clavicular retraction/protraction also revealed overestimation, especially for the most protracted angles. The model applied to the validation dataset displayed the highest root-mean-square error (RMSE = 11.00°).

4.2.3 Analysis of Model 2

Model 2 included both Belsley collinearity diagnostics (Belsley, 1991) and analysing the Pearson correlation coefficients, in order to reduce multicollinearity among variables.

The first indicated all variables with the exception of the three thoracohumeral angles, i.e., all individual factors were involved in strong dependencies (Figure 4.16).

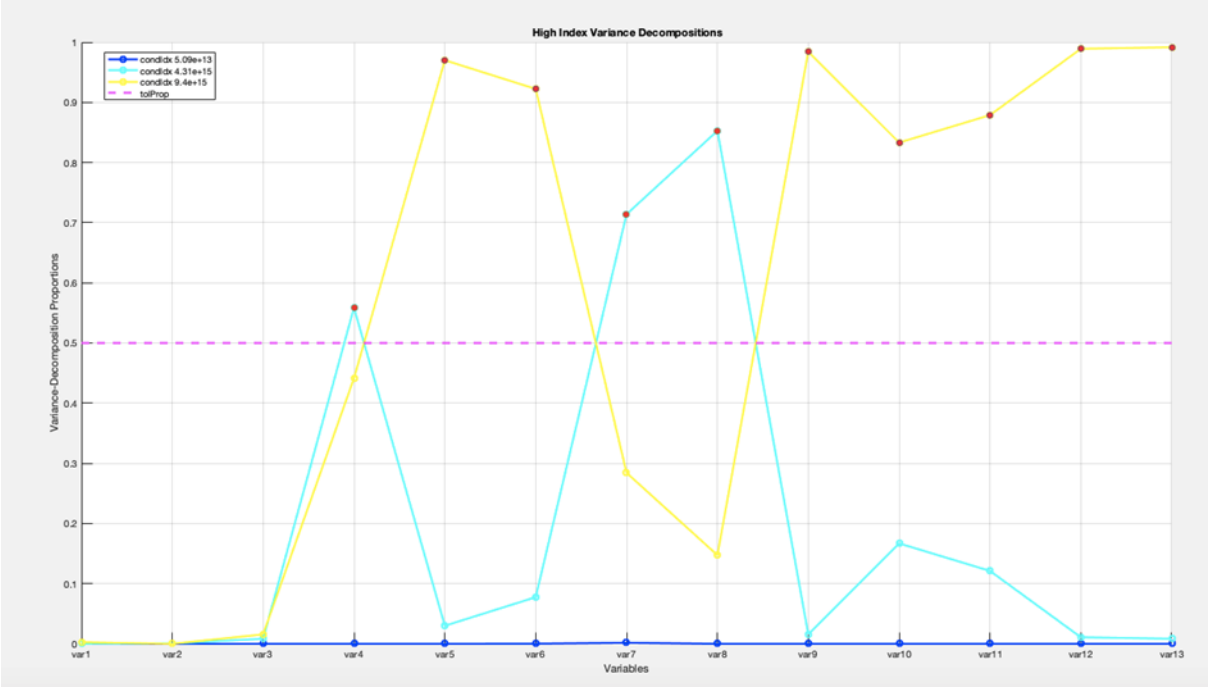

Figure 4.16: The plot corresponds to the values in the last three rows of variance-decomposition proportions, which all presented condition index larger than the default tolerance, 30. Variables 1 to 3 correspond to the thoracohumeral parameters. Variables 1 to 13 denoted, respectively: thoracohumeral angle HT1, thoracohumeral angle HT2, thoracohumeral angle HT3, gender, age, height, weight, thorax length, thorax depth, clavicular length, scapular spine length, scapular length, upper arm length. Variables 4 to 13 correspond to the individual factors which, as shown, all had variance decomposition proportions exceeding the default tolerance, 0.5, indicated by red markers in the plot.

Afterwards, the predictor variables selected to integrate the stepwise regression were decided following an analysis of the Pearson correlation coefficients (Figure 4.17). The only predictors with correlation coefficients (between them) < 0.75 were age, weight, scapular spine length, clavicular length, thorax depth and upper arm length, plus the three thoracohumeral angles, HT1, HT2 and HT3.

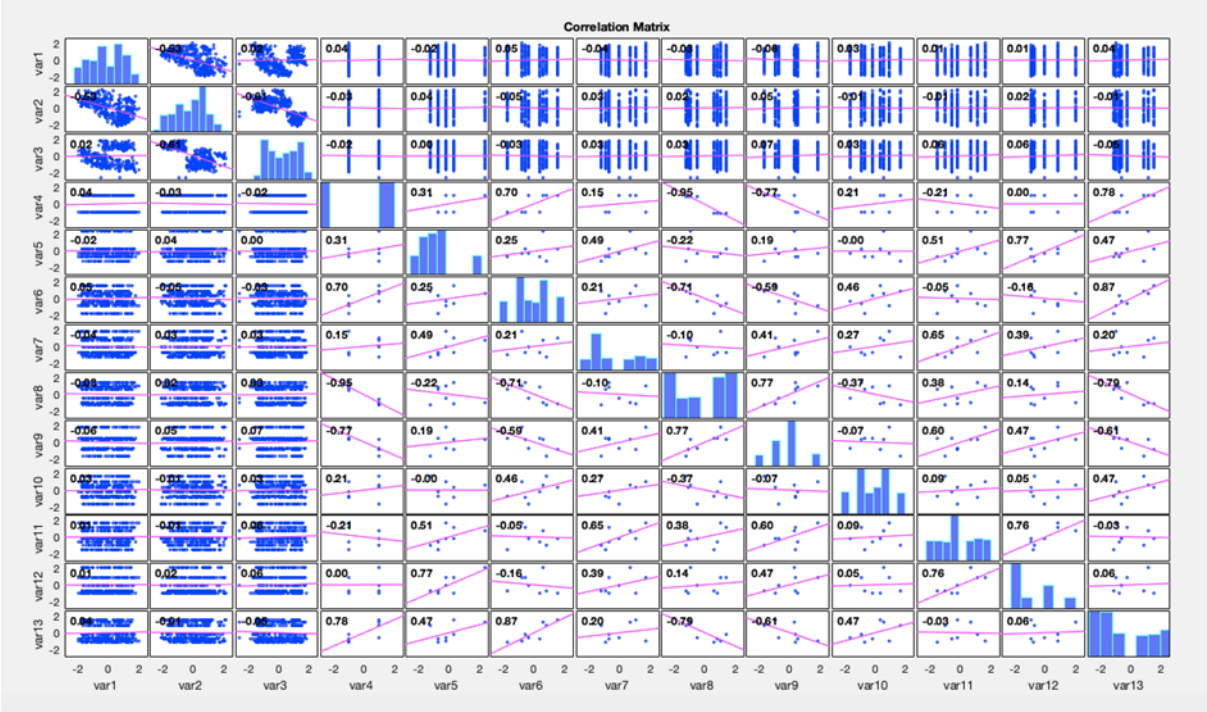

Figure 4.17: Plot of the Pearson's linear correlation coefficients between all pairs of the 13 predictor variables. All the predictors were centred and the *z*-score of each variable´s measurement was calculated. Variables 1 to 13 denoted, respectively: thoracohumeral angle HT1, thoracohumeral angle HT2, thoracohumeral angle HT3, gender, age, height, weight, thorax length, thorax depth, clavicular length, scapular spine length, scapular length, upper arm length The matrix of plots shows the correlations among the pairs of predictor. Histograms of the variables appear along the matrix diagonal; scatter plots of variable pairs appear in the off diagonal. The slopes of the least-squares reference lines in the scatter plots are equal to the displayed correlation coefficients

For the scapular retraction/protraction, the second regression step eliminated HT2 as a predictor, which agrees with the Model 0. Among the individual factors weight and clavicular length were also excluded. For the scapular lateral/medial rotation no thoracohumeral variables were eliminated as predictors during the second regression step, which also coincides with Model 0. The individual factors weight, clavicular length and thorax depth were also excluded.

For the scapular anterior/posterior tilt, the second regression step did not exclude any of the three thoracohumeral angles, in alignment with Model 0. The individual factors weight, scapular spine length and clavicular length were excluded. In this second step no thoracohumeral variables were eliminated as predictors for retraction/posterior of the clavicle, as expected according to Model 0. Weight was eliminated as a predictor.

For the clavicular elevation/depression the second step excluded HT1 as a predictor variable, which is also in agreement with Model 0. Age, scapular spine length and upper arm length were excluded as predictors for retraction/posterior of the clavicle.

Quadratic prediction models were obtained for all sternoclavicular and scapulothoracic joint angles. Figures 4.18, 4.19, 4.20, 4.21 and 4.22 present the plots of the adjusted response functions, describing the relationship between, respectively, the fitted ST1, ST2, ST3, SC1 and SC2 responses and the model predictors.

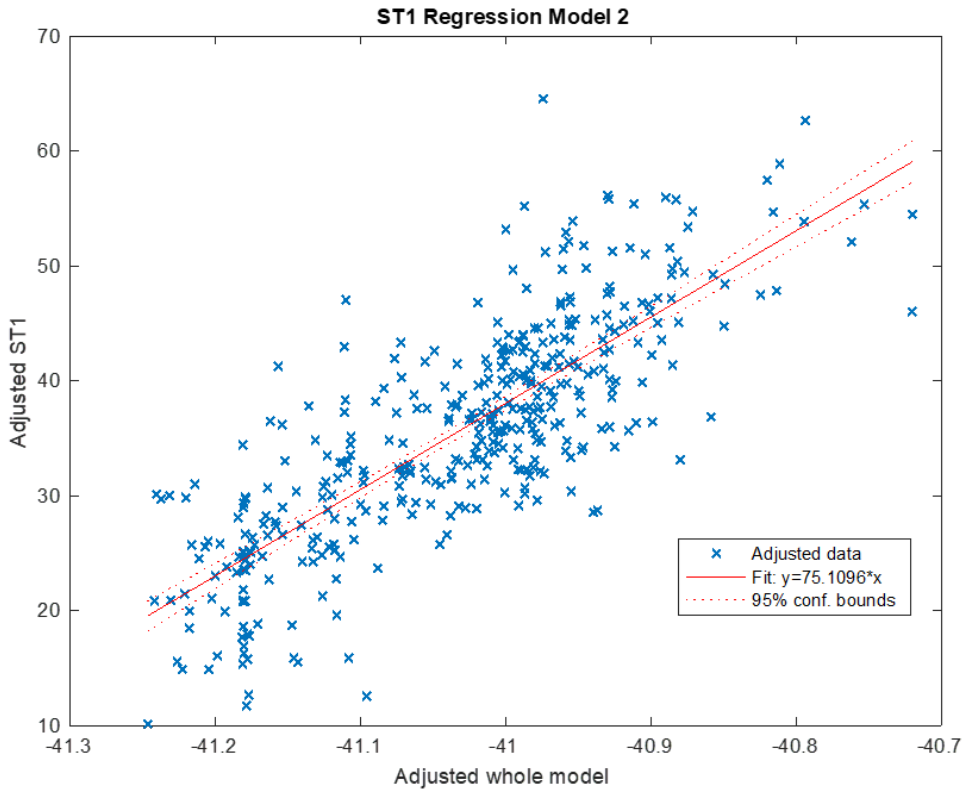

Figure 4.18: Adjusted response function describing the relationship between the fitted ST1 response and the model predictors

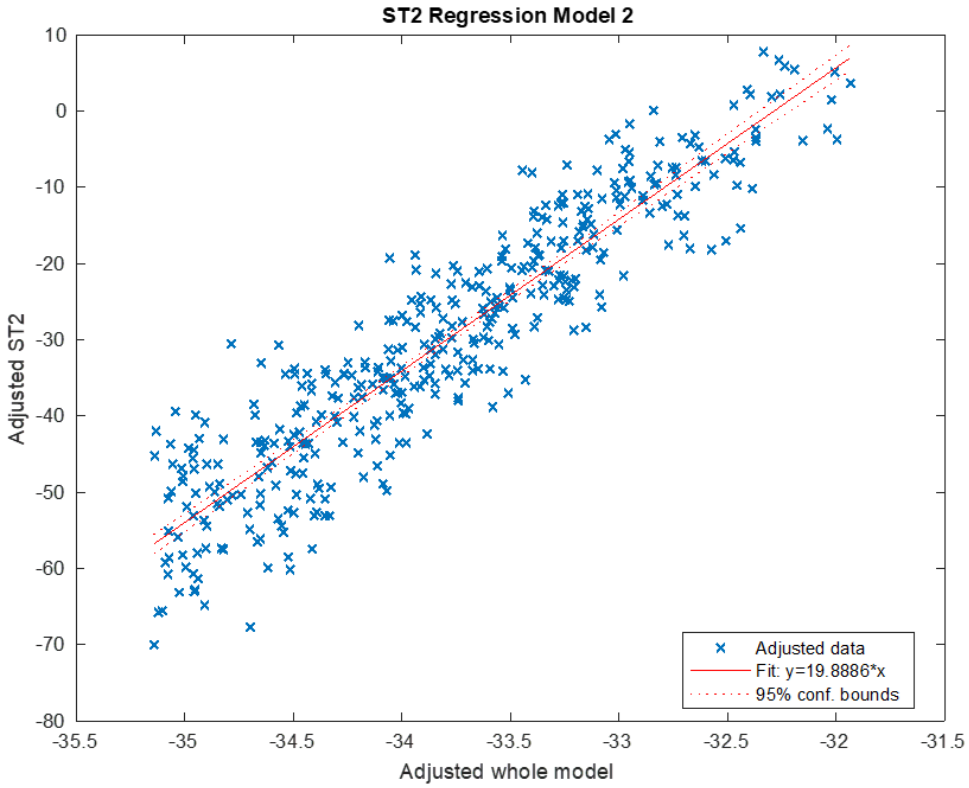

Figure 4.19: Adjusted response function describing the relationship between the fitted ST2 response and the model predictors

Figure 4.20: Adjusted response function describing the relationship between the fitted ST3 response and the model predictors

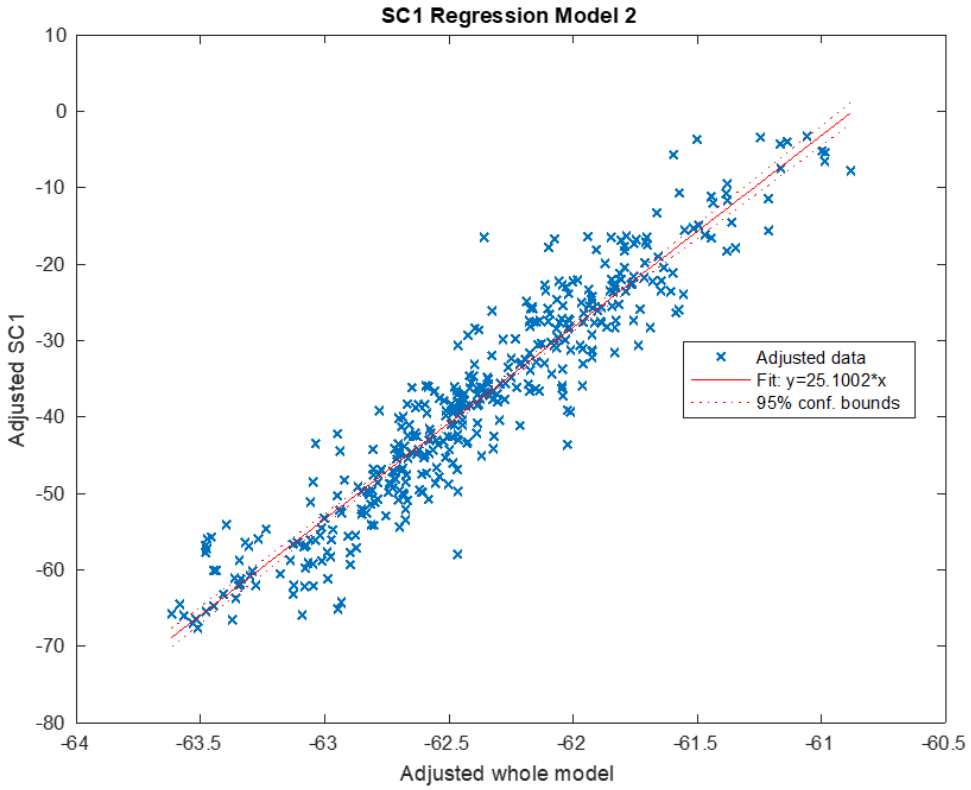

Figure 4.21: Adjusted response function describing the relationship between the fitted SC1 response and the model predictors

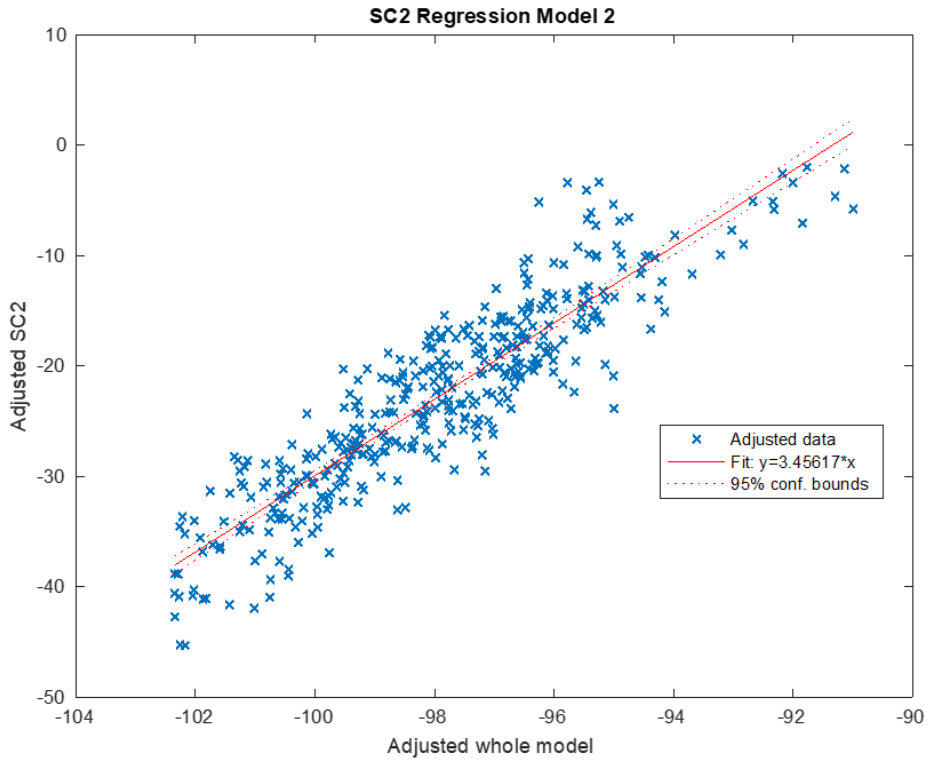

Figure 4.22: Adjusted response function describing the relationship between the fitted SC2 response and the model predictors

The model indicated scapular protraction increased with age, decreasing thorax length, decreasing length scapular spine and decreasing upper arm length The scapula showcased increasing medial rotation with increasing age, except for humeral postures in high (i.e., very positive) elevation planes and with low humeral elevation (i.e., high HT2), where medial rotation increased with decreasing age. Scapular medial rotation lso increased with decreeasing scapular spine length, for HT2 > -131º. For very high humeral elevations, with HT2 below this value, medial rotation increased with increasing scapular spine length. Medial rotation increased with decreasing upper arm length. Scapula tilts posteriorly with increasing age, decreasing thorax depth and increasing upper arm length.

Clavicular protraction occurred with decreasing age, for elevation planes > -43º. For arm postures in elevation planes below this value increasing age resulted in clavicular protraction. Protraction also increased with increasing thorax depth. For clavicular lengths > 155 mm rotraction increased with increasing clavicular length. For clavicular lengths below this value increasing clavicular length resulted in decreasing protraction. Clavicular protraction increased with scapular spine length except for humeral postures with very high HT3 and in very positive elevation planes. Finally, protraction also increased with increasing upper arm length, except for extremely high humeral elevation angles, with HT2 < -144º. Clavicular depression occurred with increasing weight, decreasing thorax depth and decreasing clavicular length.

Table 4.8 summarizes the model's goodness of fit.

Table 4.8: The obtained p-values, R-squared (R^2) values, root-mean-square error (RMSE), F-statistic vs. constant model and Akaike information criterion (AIC) values to estimate the scapular and the clavicular angles using Model 2

Model 2	RMSE (°)	R^2	F vs C	p-value	AIC
ST1	5.87	0.65	55	$p < 0.001$	2.58×10^3
ST2	6.63	0.85	145	$p < 0.001$	2.68×10^3
ST3	3.60	0.74	87	$p < 0.001$	2.18×10^3
SC1	4.97	0.89	164	$p < 0.001$	2.45×10^3
SC2	3.76	0.81	191	$p < 0.001$	2.22×10^3

The retraction/protraction of the sternoclavicular joint had the greatest R^2 value of 0.89, which means that approximately 89% of the observed variation can be explained by the model's inputs. Retraction/protraction of the scapulothoracic joint had the least R^2 value of 0.65 (Table 4.8). The RMSE of the model ranged between 3.60º for the anterior/posterior tilt of the scapula and 6.63º for lateral/medial rotation of the scapula. Similarly to Models 0 and 1, anterior/posterior tilt of the scapula thus had the lowest error in predicting the quantitative data. The AIC ranged from 2.18×10^3 for scapular anterior/posterior tilt to 2.68×10^3 for lateral/medial scapular rotation. The F vs C ranged from 55 for scapular retraction/protraction to 191 for clavicular elevation/depression. The p-value was $p < 0.001$ for all the studied joint angles indicating statistical significance.

4.2.3.1 Validation of Model 2

Table 4.9 summarizes the predictability of Model 2, after applying it to the validation dataset.

Table 4.9: Validation of Model 2

Model 2	R^2	RMSE (°)
ST1	0.10	7.91
ST2	0.70	10.20
ST3	0.43	4.86
SC1	0.13	12.30
SC2	0.60	5.03

For the validation dataset, the minimum R^2 was obtained for scapular retraction/protraction (R^2 = 0.10). A possible explanation for this low R^2 are the underlying multicollinearity problems among the predictor variables. As previously stated, in models showcasing multicollinearity the estimated regression coefficients tend to vary widely from one sample to the another one if the predictor variables are highly correlated. (Kutner et al., 2005). The maximum R^2 was obtained for scapular lateral/medial rotation, R^2 = 0.70. The RMSE of the models applied to the validation dataset ranged from 4.86º for the clavicular elevation/depression and 12.30º for scapular lateral/medial rotation.

The following scatter diagram (Figure 4.23) visually assesses the correlation between the measured angles and the estimated data computed with the regression equations.

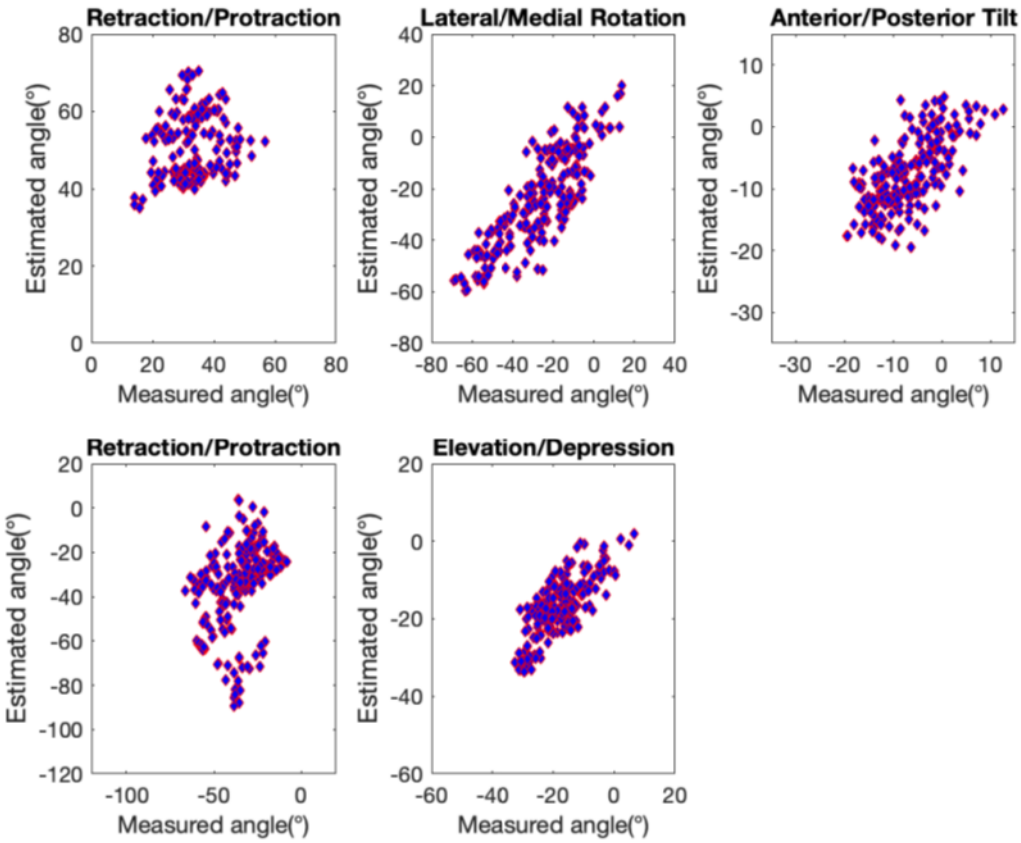

Figure 4.23: The correlation between the measured and the predicted sternoclavicular and scapulothoracic joint angles for Model 2

Scapular retraction/protraction was overestimated for several angles. Lateral/Medial rotation was underestimated for some rotation angles. Anterior/Posterior tilt had the lowest RMSE (RMSE = 4.86° **)** but nevertheless showed underestimation for the more posteriorly tilted angles

The clavicular retraction/protraction model applied to the validation dataset also showed severe underestimation for mid-range joint angles.

4.3 Comparison Between Models

Regarding the predictor variables considered significant, some differences are exhibited between the regression models computed in this study and those from past works (de Groot and Brand, 2001; Grewal and Dickerson, 2013; Xu et al., 2014a). Xu et al. (2014a) considered the three thoracohumeral parameters significant for all joint rotations, with the exception of scapular retraction/protraction. This was not supported by this work or the work of Grewal and Dickerson (2013). Both in their work and in this study, the three thoracohumeral angles were significant predictors for all joint angles except for scapular retraction/protraction and clavicular elevation/depression. In the present study, scapular retraction/protraction was only influenced by HT1 and HT3, which is in agreement with the work of Xu et al. (2014a) but opposes the findings of Grewal and Dickerson (2013), where the two significant angles

were HT1 and HT2. A possible explanation for this could be the more efficient thoracohumeral discretization achieved by the present work and the one from Xu et al. (2014a). In the present work axial rotation was tracked using IMU and Xu et al. (2014a) resorted to frame stabilization. Grewal and Dickerson (2013) did not track the axial rotation configurations, which might have obscured the influence of this parameter angle. In what concerns clavicular elevation/depression both this study and the one from Grewal and Dickerson (2013) considered HT2 and HT3 as the only significant thoracohumeral predictors. All three clavicular elevation/depression regression equations obtained in this work have a squared elevation angle predictor term. This is supported by observed non-linear changes of clavicular elevation with humeral elevation (Barnett et al., 1999; Ludewig et al., 2009; McClure et al., 2001).

Every sternoclavicular and scapulothoracic joint angles had, in models 1 and 2, individual factors as significant predictor variables. This agrees with Xu et al. (2014a), but opposes the findings of other previous works. In de Groot and Brand (2001), gender and anthropometry data were found not to be significant predictors. In Grewal and Dickerson (2013), age, height, and weight were also excluded in the regression model due to lack of predictive power. Xu et al. (2014a) hypothesized that this could be a result of participant selection. In their study, the participants had a larger diversity in terms of age and weight than the participants in those previous studies, which might have contributed to less model predictability and accentuated the effect of the individual factors. All individual factors considered in this study impacted at least one of the joint rotations, with the exception of scapular length, which was always excluded by the statistical processing. Scapular length was shown to be involved in severe multicollinearity. This is in agreement with Campobasso et al. (1998) who found that the scapula could be reliably employed for the estimation of stature in forensic practice.

A difference from past works was the influence of gender on the shoulder rhythm. Xu et al. (2014a) found gender to be a predictor for all joint angles with the exception of clavicular retraction/protraction. In this work, gender was only a predictor for the clavicular retraction/protraction. This reduced influence of gender could be related to the more efficient standardization achieved by the present work's external frame and IMU guidance, detailed in chapter 4.5. The Xu et al. (2014a) hypothesized inter-participant variability could be related to differences in hip width as an individual with greater hip width relative to shoulder width could laterally tilt the trunk to achieve shoulder alignment with the arc centre. This hip width to shoulder width ratio, different according to the gender as broad shoulders and narrow hips tend to be a masculine trait (Kasperk et al., 1997), could increase differences between participants from different gender and thus make this variable a more significant predictor. The SD for the most negative elevation plane was, in the present work, 5.1°, significantly below the SD for the elevation planes found across all postures of the work of Xu et al. (2014b), 11.6°. The frame used in the present work thus reduced inter-participant variability. The more efficient stabilization of the thorax and standardization of the arm postures, , detailed in chapter 4.5, might have reduced the influence of gender in our regression models.

Model 1 showed inferior RMSE when compared to Model 0 for all shoulder rotations. Model 2 further continued this tendency, having the lowest RMSE in all scapular and clavicular movements, with the exception of clavicular elevation/depression. Nevertheless, the RMSE for this joint angle was, in Model

2, only 0.12º above the RMSE of Model 1. Concerning R^2, the same was observed: Model 1 provided a better fit to the dataset than Model 0, and Model 2 had the highest R^2 except for clavicular elevation/depression. The R^2 for this joint angle was, nevertheless, in Model 2, only 0.014 below the R^2 of Model 1. This small difference might be explained by the inclusion of weight and thorax depth as predictors in Model 2. The test group included a subject whose weight was 14.6 kg above the average weight of 66.4 kg (SD: 9.5 kg) for all 8 test subjects. Furthermore, Model 2 included, for this joint angle, thorax depth as a predictor. This variable was included both as an individual term and as an interaction term (interacting with HT2). The same subject's thorax depth was 32.4 mm above the average thorax depth of 243.4 mm for all 8 test subjects. This is a small difference, but for this individual factor the SD was of only SD: 18.7 mm. This, in conjunction with the above average weight, might explain the slightly poorer performance of Model 2 in what concerns clavicular elevation/depression. In conclusion, the highest total variability in the response was accounted by the Model 2. The p-values were also lower in Model 1 than in Model 0 and the lowest in Model 2, making it the most statistically significant model of the three. Again this trend found an exception for clavicular elevation/depression, where Model 2 had a slightly larger p-value than Model 1. The difference is negligible as all the found p-values (for all models and joint angles) are < 0.001 indicating statistical significance. The AIC statistic showcased the same tendency, which indicates that the consecutive model improvements were effective in achieving models that not only better explained the observed variation in the test dataset but that were also increasingly parsimonious

The F vs C found, however, disparate results. Model 0 had the best F vs C statistic for all joint angles, except scapular anterior/posterior tilt, where it was the worst performing model and Model 2 was the best. Finally, the AIC statistic showcased the same tendency. Model 2 was the best performing model for all joint angles and Model 0 the worst, except for clavicular elevation/depression, where Model 1 was the best and Model 0 again the worst. This indicates that the consecutive model improvements were effective in achieving models that not only better explained the observed variation in the test dataset but that were also increasingly parsimonious.

Regarding the application of the developed models to the validation dataset, the scapulothoracic retraction/protraction and anterior/posterior tilt regression models had the lowest RMSE in Model 2 and the highest errors were observed in Model 1. Scapulothoracic lateral/medial rotation and clavicular elevation/depression regression models had the lowest RMSE in Model 2 and the highest errors were observed in Model 0. For clavicular retraction/protraction a different trend was observed, with Model 0 having the lowest differences between values observed and predicted values and Model 2 having the highest observed differences.

Concerning R^2, the regression model for scapular retraction/protraction had the best results when predicted by Model 2 and the worst when computed by Model 1. The same trend was observed for scapular anterior/posterior tilt. Scapular lateral/medial rotation and clavicular elevation/depression had the best results when predicted by Model 2 and the worst when computed by Model 0. Clavicular retraction/protraction, on the other hand, showed the highest R^2 on Model 0 and the lowest R^2 in Model 2.

The models show how the inclusion of individual factors in the regression improves the fit to the data from the test group. This is possibly due to the increase in degrees of freedom (maximum number of logically independent values, which are values that are free to vary). But this inclusion has varying results when the models are applied to the validation dataset. For these data, Model 2 improved Model's 0 estimation of scapulothoracic retraction/protraction and anterior/posterior tilt, but Model 1 performed poorly. For scapular lateral/medial rotation and clavicular elevation/depression both Model 1 and Model 2 better predict the data. However, for clavicular retraction/protraction both models including individual factors provided a worse angle estimation. This is a direct consequence of the multicollinearity among the predictor variables. Multicollinearity causes the estimated regression coefficients to vary widely from one sample to the next. All in all, the inclusion of individual factors worsened the predictability of mainly clavicular retraction/protraction and, for Model 1, scapular anterior/posterior tilt.

For the current model with no individual factors, the RMSE are in a similar range as those found in the works of de Groot and Brand (2001) and Xu et al. (2014a) . The inclusion of individual factors in our model reduced the computed RMSE, which were in general lower than the ones in the literature. The values of R^2 in Model 0 were higher than the ones obtained by Xu et al. (2014a). The inclusion of individual factors in our models further increased R^2.

The models applied to the validation dataset which included individual factors revealed a difference between measured and predicted values in the range of the models derived by de Groot and Brand (2001) and Xu et al. (2014a). The differences were, however, generally larger than the ones found in the work of Grewal and Dickerson (2013), especially those in Model 2. This may be due to the inclusion of a larger selection of anthropometric data in the regression models of this study, which likely increased multicollinearity problems, even when filtered through the analysis of the Variable Inflation Factors (VIF) (Model 1) and the Belsley collinearity diagnostics and Pearson correlation coefficients (Model 2). On the other hand, past regression models were built using a larger number of participants with greater diversity of age, height, weight and anthropometric data. This could explain why the models developed by Grewal and Dickerson (2013) showed better predictive power in the validation stage, as the regression equations were computed using more diverse values of predictor variables.

4.4 Application of Models Present in the Literature to the Validation Dataset

Lastly, the model developed by Xu et al. (2014a) that only included thoracohumeral angles was applied to our validation dataset. The correlation between the measured and predicted joint angles was scatter plotted as depicted in Figure 4.24.

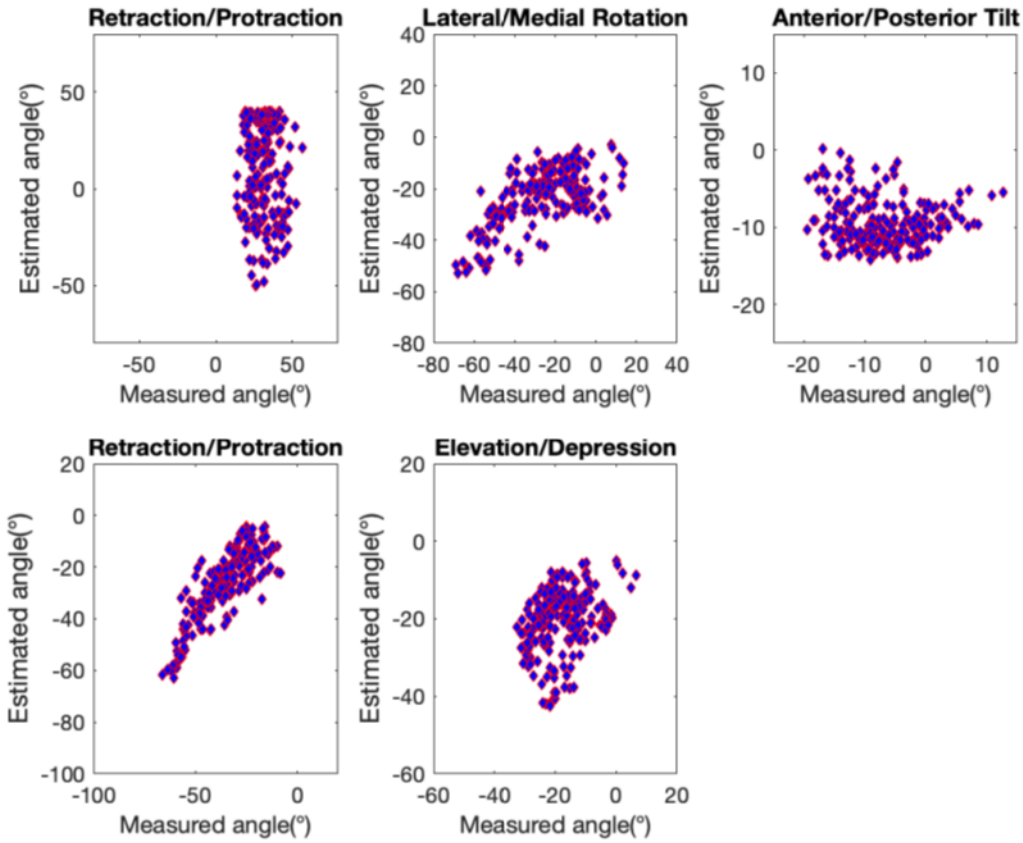

Figure 4.24: Correlation between the measured joint angles and the predicted sternoclavicular and scapulothoracic joint angles obtained using Xu et al. (2014a) model without individual factors

The application of this model to our validation dataset is summarized in Table 4.10.

Table 4.10: Application of the regression equations derived by Xu et al. (2014a) to our validation dataset

Xu et al. (2014a)	R^2	RMSE (°)
ST1	0.002	8.35
ST2	0.44	14.00
ST3	0.01	6.42
SC1	0.70	7.19
SC2	0.13	7.41

The largest error was obtained for the scapular lateral/medial rotation, where the RMSE was 14.00°. The application of Model 0 to the validation dataset also resulted in the largest error for this joint angle, with RMSE = 10.80º. For his own validation dataset, the scapular lateral/medial rotation RMSE obtained by Xu et al. (2014a) was the second highest presented in work, 7.40°. The best prediction using the equations of Xu et al. (2014a) was observed for clavicular retraction/protraction (R^2 = 0.70).

When applied to this work's validation set, Model's 0 highest RMSE was lower (RMSE = 10.80°) and the best R^2 was higher (R^2 = 0.75), than the model developed by Xu et al (2014a) applied to the same dataset. Interestingly, the model developed by Xu et al. (2014a) showed, when applied to our validation dataset, than when applied to his validation set, for clavicular retraction/protraction (in their work, R^2 was 0.47). Also, the RMSE found for their scapular retraction/protraction validation dataset (RMSE = 11.13°). was higher than when applied to our validation dataset (RMSE = 8.35°). This might be a result of the larger validation dataset used in their work, which possibly increased the number of outliers and worsened the prediction of the joint angles.

The same process was done for the model developed by Grewal and Dickerson (2013), applying it to our validation dataset. Figure 4.25 depicts the correlation between the measured and predicted joint angles.

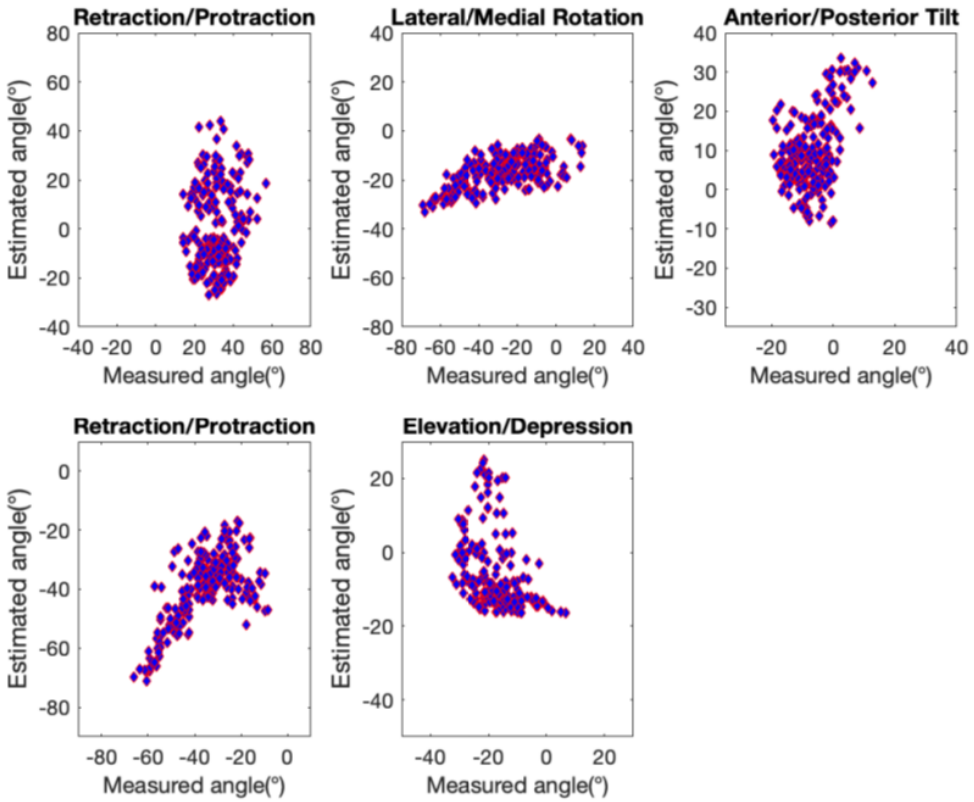

Figure 4.25: Correlation between the measured joint angles and the predicted sternoclavicular and scapulothoracic joint angles obtained using Grewal and Dickerson (2013) model without individual factors

The application to our validation dataset is summarized in Table 4.11.

Table 4.11 Application of the regression equations derived by Grewal and Dickerson (2013) to our validation dataset

Grewal and Dickerson (2013)	R^2	RMSE (°)
ST1	0.02	8.29
ST2	0.40	14.50
ST3	0.22	5.70
SC1	0.45	9.76
SC2	0.14	7.34

The largest error was obtained for the scapular lateral/medial rotation, where the RMSE was 14.50°. It was also the angle where Model 0 presented the highest RMSE. The best prediction using the equations of Grewal and Dickerson (2013) was observed for clavicular retraction/protraction (R^2 = 0.45), which is in agreement with the highest R^2 found in his own work. It was also the joint angle for which the equations from Xu et al. (2014a) provided the best prediction.

This shows the equations developed in these past works have moderate success predicting some of the studied joint angles for wider-ranging humeral postures, including for those in negative elevation planes. These past models are, nevertheless, surpassed by the models developed over the course of this work. It also indicated scapular lateral/medial rotation as the joint angle for which the inclusion of this novel range of motion leads to larger discrepancies. This angle was underlined as an especially difficult one to predict accurately, as indicated by the large errors found during the application of the models (both the ones computed in this work and models present in the literature) to the validation dataset. A possible explanation for this might be the found SD among measured joint angles. In the validation dataset, scapular lateral/medial rotation had a SD = 18.59°, the largest among all measured joint angles. For comparison, the other scapular joint angles, retraction/protraction and anterior/posterior tilt, had a SD of 8.34° and 6.43°, respectively. This large angle variability might explain the increased prediction errors in the validation stage. On the other hand, this extension of the envelope of humeral postures had the smallest impact on the predictability of past clavicular retraction/protraction regression models. Our Model 0 found this joint angle to be the only one where a quadratic model included HT2 as the only squared variable term. The present work had a similar elevation angle discretization to these two past works, and thus similar HT2 values in the validation dataset were expected. This could help understand why the novel range of motion did not stop past regression models from achieving a decent angle estimation.

4.5 Accuracy of the External Frame

All the postures, with the exception of the ones with a thoracohumeral elevation of 0°, were standardized with the aid of the external frame. Two sets of postures proved to be the most difficult to standardize. The highest angle differences occurred at the most negative elevation plane (frame defined plane of -90°), where the average angle difference between frame-defined and measured planes was 17.4°, and at the postures with the highest elevation angle (frame defined elevation angle of 160°). For this

elevation angle, the average angle difference between frame-defined and measured elevation angles was 23.7°. This is a significant improvement to the work of Xu et al. (2014b). Xu et al. (2014b) developed an aluminium external frame and calculated the differences between all frame defined angles and the measured joint angles. His work had a lower maximum elevation angle (150°), for which an average elevation angle difference of 49.2° was found. The average elevation plane angle difference found in the work of Xu et al. (2014b) was 30.1°, also higher than the one found using our developed external frame (17.4°, as previously stated). Furthermore, the frame used in the present work reduced inter-participant variability. This was corroborated by the found SD for the most extreme arm postures. The SD for the most negative elevation plane was 5.1°, significantly below the SD for the elevation planes found across all postures of the work of Xu et al. (2014b), 11.6°. The SD for the maximum elevation angle was 4°, where Xu et al. (2014b) found an SD of 12.1°. Furthermore, in the present work, a wider range of postures was tracked, with special focus on the novel negative planes. This shows an improvement in the standardization of humeral postures even at the most extreme positions of the novel range of motion.

Chapter 5

Conclusion

5.1 Main Conclusions

Regression equations for 3-D multiplanar shoulder rhythms were developed considering a larger envelope of arm postures than the one currently available in the literature. Past studies neglected arm postures in negative planes of elevation, which are particularly prevalent in ample upper limb motions, such as those in swimming activities. An optoelectronic tracking system complemented with the usage of inertial measurement units was used to acquire shoulder kinematics, in a series of arm postures supported by an external frame. This external frame efficiently improved the consistency of arm positioning and the comfort of subjects. A three-pointed palpatory, scapula locator, was 3-D printed to help locate the scapular anatomical landmarks during postures with significant soft tissue displacement.

Software developed in-house was used to generate the anatomical coordinate systems for each bone segment (Quental et al., 2015, 2018). The used upper limb model follows the standardization of the upper limb data proposed by the Standardization and Terminology Committee of the International Society of Biomechanics (ISB) (Wu et al., 2005).

A 3-D regression-based shoulder rhythm approach was developed. Two types of regression models were built to predict the 3-D orientation of clavicle and scapula. The first type used exclusively the orientation of the humerus as a predictor, specified by three Euler angles, HT1, HT2 and HT3. The other type included two regression models that used as input the orientation of the humerus as well as individual factors. Age, gender, height, weight and other readily available anthropometry data were used as predictors. For these individual factors, severe multicollinearity was detected and thus a more detailed statistical study was made using a combination of Belsley collinearity diagnostics (Belsley, 1991), Pearson correlation coefficients and variable inflation factors. The regression models were validated using an independent dataset.

Overall, this work was successful in extending the regression-based 3-D shoulder rhythm equations to a wider range of arm postures. The model without individual factors showed a fit to the data in the range of the preceding study with the highest angular resolution of arm postures (Xu et al., 2014a). This allows the conclusion that an extension of the 3-D regression models to ranges of motion including negative planes of humeral elevation was possible, without compromising the models predictability.

The impact of individual factors on the regression models requires, however, a more careful approach. The models with individual factors showed a better fit to the initial test dataset than the model without, possibly due to the increase in degrees of freedom. The application of the models to the validation dataset showed, on the other hand, that the inclusion of individual factors in the models has varying results in the quality of angle estimation. This can be explained by the high multicollinearity found among the predictor variables, which causes the computed regression coefficients to be very sensitive to small

changes in the model. Even after a preselection of the individual factors through a statistical study, multicollinearity was still found. The anthropometrical data include segments that are constrained by their relation in a closed chain mechanism and thus a degree of variable dependency is unavoidable.

5.2 Limitations and Future Work

This study had important limitations. First and foremost, the subjects were selected from an homogenous group. This lack of diversity might have confounded the influence of personal factors. The COVID-19 pandemic exerted high pressure on the participants' recruitment. Furthermore, and even with the usage of the scapula locator, skin deformation may have led to inaccuracies in the placement of markers. This is an intrinsic limitation of using a non-invasive procedure with cutaneous markers. Another difficulty during the data acquisition was the falling of markers when switching from one posture to the other. This was particularly prevalent among the three scapular markers which, due to the constant adjustment in each position (with the aid of the scapula locator) had poor adhesion to the subject's skin. The external frame helped standardizing the arm postures among participants. However, differences between the frame defined angles and measured thoracohumeral angles were observed, especially at the most negative elevation plane (frame defined plane of -90°) and at the postures with the highest elevation angle (frame defined elevation angle of 160°). An external frame which provided more thorax stabilization could improve the consistency of recorded joint angles.

There are other limitations to generalizing the results. The models from the validation dataset indicated differences between observed and estimated data, especially for scapular lateral/medial rotation and clavicular retraction/protraction. High multicollinearity was detected among predictor variables, and the computed regression coefficients were very sensitive to small changes in the model. Additionally, the effects of force exertion on shoulder rhythm were not studied. Substantial external loads, such as those that occur during complex sportive movements may lead to discrepancies when applying the current model to novel humeral postures under the action of forces. A future study should consider these external forces in conjunction with the newly-tested negative planes of humeral elevation.

Another point of future interest is the definition of the body orientations. This study used Euler angles, in alignment, and to allow comparison, with the existing literature. These orientation angles are computed from a given rotation matrix by performing an inverse transformation. The inverse transformation problem has, however, two solutions for which two of the Euler angles, describe the same rotation and cannot be computed separately, and thus one degree of freedom is lost (Project, 1986). This problem can be solved using Euler parameters to parametrize the rotation matrix. These parameters are unit quaternions and consist of four real parameters, of which the first is a scalar and the other three are a vector in a three-dimensional space. The use of Euler parameters in the study of multibody dynamics has proved to be a success due to the singularity-free and fast calculation of rotational motion (Schwab et al., 2006). It would therefore be interesting to see a 3-D regression model that studied the shoulder rhythm using as predictors thoracohumeral positions represented by these

Euler parameters. This could help generalize the prediction of the shoulder rhythm from the positions of the thorax and the arm.

Finally, advances in the motion capture system are expected. A point of current concern is the interference between close markers, such as the ones located at the AC and AI, which leads to occlusions and data loss. A more capable shielding of the markers from the others' reflections, can help lead the way to more detailed 3-D modelling systems, and therefore to a better understanding of the intricacies of shoulder kinematics.

6. References

Ackland, D. C., Roshan-Zamir S., Richardson M., Pandy M.G. 2010. Moment arms of the shoulder musculature after reverse total shoulder arthroplasty. *Journal of Bone & Joint Surgery*, **92**(5), 1221–30.

Ackland, D. C., Patel, M., & Knox, D. 2015. Prosthesis design and placement in reverse total shoulder arthroplasty. *Journal of Orthopaedic Surgery and Research*, **10(**1), 1–9. https://doi.org/10.1186/s13018-015-0244-2.

Aiken, L. S., & West, S. G. 1991. *Multiple regression: Testing and interpreting interactions.* Sage Publications, Inc.

Alderink, G. J. 2006. Joint Structure and Function: A Comprehensive Analysis, ed 4. *Physical Therapy*, **86**(4), 598–599. https://doi.org/10.1093/ptj/86.4.598a.

Anglin, Carolyn, & Wyss, Urs P. 2000. Arm motion and load analysis of sit-to-stand, stand-to-sit, cane walking and lifting. *Clinical Biomechanics*, **15**(6), 441–448.

Barnett, N.D., Duncan, R.D.D., Johnson, G.R., 1999. The measurement of three dimensional scapulohumeral kinematics—a study of reliability. *Clinical Biomechanics***. 14**, 287–290.

Belsley, D.A. 1991. A guide to using the collinearity diagnostics. *Computer Science in Economics and Management*, **4**(1), 33-50.

Braman, Jonathan P. 2010. In Vivo Assessment of Scapulohumeral Rhythm During Unconstrained Overhead Reaching in Asymptomatic Subjects. *Journal of Bone & Joint Surgery.*, **18**(6), 960–967.

Brochard, S., Lempereur, M., Remy-Neris, O. 2011. Double calibration: an accurate, reliable and easy-to-use method for 3D scapular motion analysis. *Journal of Biomechanics*. **44** (4), 751–754.

Burstein A.H., Reilly D.T., Martens M. 1976. Aging of bone tissue: mechanical properties. *The Journal of Bone and Joint surgery*. American Volume. 1976 Jan; **58**(1):82-86. PMID: 1249116.

Campobasso, C.P., G. Di Vella, and F. Introna, Jr.1998. Using Scapular Measurements in Regression Formulae for the Estimation of Stature. Bollettino della Societa Italiana di Biologia Sperimentale **74**(7-8):75-82.

Cappozzo, A., Catani, F., Della Croce, U., & Leardini, a. 1995. Position and orietnation in space of bones during movement. *Clinical Biomechanics*, **10**(4), 171–178.

Cau N., Cimolin V., Brugliera L., Ventura G., Galli M., Capodaglio P. 2017. Range of motion limitations of the upper body in obese female workers. *Med. Lav*., **108**(6), (Dec 14, 2017), 455-465. doi: 10.23749/mdl. v108i6.6339. PMID: 29240042.

Chang, L.Y., Pollard, N.S. 2007. Constrained least-squares optimization for robust estimation of center of rotation. *Journal of Biomechanics*, **40**(6), 1392-1400.

Clarkson, H. M. 1999. Musculoskeletal assessment: joint range of motion and manual muscle strength. 2.nd edition. Philadelphia (PA): Lippincott Williams and Wilkins.

Cook, Thomas M., Paula, Ludewig M., Ludewig, Paula M., Shields, Richard K., & Paula, Ludewig M. 2002. Occupational and Environmental Health Publications Comparison of Surface Sensor and Bone-Fixed Measurement of Humeral Motion Comparison of Surface Sensor and Bone-Fixed Measurement of Humeral Motion. *Public Health*, **18**, 163–170.

Copeland, K. A. F. 1997. Applied Linear Statistical Models. In *Journal of Quality Technology*, **29**(2). https://doi.org/10.1080/00224065.1997.11979760.

Costigan, P. A., Wyss, U. P., Deluzio, K. J., & Li, J. 1992. Semiautomatic three-dimensional knee motion assessment system. *Medical and Biological Engineering and Computing*, **30**(3), 343–350.

Culham, E., Peat, M. 1993. Functional anatomy of the shoulder complex. *Journal of Orthopaedic and Sports Physical Therapy*, **18**(1), 342-350.

De Groot, J.H. 1998. The shoulder: a kinematic and dynamic analysis of motion and loading [doctoral thesis]. [Delft (NL)]: Technical University of Delft.

De Groot, J. H., & Brand, R. 2001. A three-dimensional regression model of the shoulder rhythm. *Clinical Biomechanics*, **16**(9), 735–743. https://doi.org/10.1016/S0268-0033(01)00065-1.

Drake, R.A. A, Vogl, W., & Mitchell, A.W.M. W. M. 2009. Gray's Anatomy for Students E-Book.

Ehrig, R. M., Taylor, W.R., Duda, G.N., Heller, M.O. 2006. A survey of formal methods for determining the centre of rotation of ball joints. *Journal of Biomechanics*, **39**(15), 2798-2809.

Engin, A., Peindl, R., Berme, N., & Kaleps, I. 1984. Kinematic and force data collection by means of sonic emitters - I. Kinematic data collection methodology. *Journal of Biomechanical Engineering*, **106**(August 1984), 204–211.

Farron, A., Terrier, A., Buchler, P. 2006. Risks of loosening of a prosthetic glenoid implanted in retroversion. *Journal of Shoulder and Elbow Surgery*, 15(4), 521-526.

Favre, P., Snedeker, J.G., Gerber, C., 2009. Numerical modelling of the shoulder for clinical applications. *Philosophical Transactions of the Royal Society*, **A 367**(1895), 2095-2118.

Finnoff, J.T., Doucette, S., Hicken, G. 2004. Glenohumeral instability and dislocation. *Physical Medicine and Rehabilitation Clinics of North America*, **15**(3), v-vi, 575-605.

Forte, F. C., de Castro, M.P., de Toledo, J.M., Ribeiro, D.C., Loss, J.F. 2009. Scapular kinematics and scapulohumeral rhythm during resisted shoulder abduction – implications for clinical practice. *Physical Therapy in Sport*, **10**(3), 105-111.

Gamage, S. S. H. U., & Lasenby, J. 2002. New least squares solutions for estimating the average centre of rotation and the axis of rotation. *Journal of Biomechanics*, **35**(1), 87–93. https://doi.org/10.1016/S0021-9290(01)00160-9.

Gray, H., Lewis, W. H. 1918. Anatomy of the human body. 20th edition. Philadelphia (PA): Lea and Febiger.

Grewal, T. J., & Dickerson, C. R. 2013. A novel three-dimensional shoulder rhythm definition that includes overhead and axially rotated humeral postures. *Journal of Biomechanics*, **46**(3), 608–611. https://doi.org/10.1016/j.jbiomech.2012.09.028.

Gupta, Miti, Dashottar, Amitabh, & Borstad, John D. 2013. Scapula kinematics differ by body mass index. *Journal of Applied Biomechanics*, **29**(4), 380–385.

Halvorsen, K. 2003. Bias compensated least squares estimate of the center of rotation. *Journal of Biomechanics*, **36**(7), 999-1008.

Harryman D. T., Sidles J.A., Clark J.M., McQuade K.J., Gibb T.D., Matsen F.A. 1990. Translation of the humeral head on the glenoid with passive glenohumeral motion. *Journal of Bone & Joint Surgery*, **72-a**, 1334–1343.

Hatze, H. The Meaning of the Term “Biomechanics”. *Journal of Biomechanics* 1974, 7, 189–190.

Hendrickson, Thomas. 2009. “Chapter 6: The Shoulder - Anatomy, Function, and Dysfunction of the Shoulder Complex.” p. 239–91 in Massage and Manual Therapy for Orthopedic Conditions.

Hogfors, C., Peterson, B., Sigholm, G., Herberts, P. 1991. Biomechanical model of the human shoulder joint.2. The shoulder rhythm. *Journal of Biomechanics*, **24**, 699–709.

Hosseinimehr, Seyed Hossein, Anbarian, Mehrdad, Norasteh, Ali Asghar, Fardmal, Javad, & Khosravi, Mohammad Taghi. 2015. The comparison of scapular upward rotation and scapulohumeral rhythm between dominant and non-dominant shoulder in male overhead athletes and non-athletes. *Manual Therapy*, **20**(6), 758–762.

Inman, V. T., Saunders, J. B., Abbott, L.C. 1944. Observations on the function of the shoulder joint. *Journal of Bone and Joint Surgery*, **26**(1), 1-30.

Innocenti B. 2018. Biomechanics: a fundamental tool with a long history (and even longer future!). Muscles, ligaments and tendons journal, 7(4), 491–492. https://doi.org/10.11138/mltj/2017.7.4.491

Jackson, M., Michaud, B., Tétreault, P., & Begon, M. 2012. Improvements in measuring shoulder joint kinematics. *Journal of Biomechanics*, **45**(12), 2180–2183. https://doi.org/10.1016/j.jbiomech.2012.05.042.

Johnson, G. R., & Anderson, J. M. 1990. Measurement of three-dimensional shoulder movement by an electromagnetic sensor. *Clinical Biomechanics*, **5**(3), 131–136.

Johnson, G.R., Stuart, P.R., Mitchell, S., 1993. A method for the measurement of three-dimensional scapular movement. *Clinical Biomechanics*, **8** (5), 269–273.

Karduna, A. R., McClure, P.W., Michener, L.A., Sennett, B. 2001. Dynamic measurements of three-dimensional scapular kinematics: a validation study. *Journal of Biomechanical Engineering*, **123** (2), 184–190.

Kasperk, C., Helmboldt, A., Börcsök, I., Heuthe, S., Cloos, O., Niethard, F., & Ziegler, R. 1997. Skeletal Site-Dependent Expression of the Androgen Receptor in Human Osteoblastic Cell Populations.

Calcified Tissue International, *61*(6), 464–473. https://doi.org/10.1007/s002239900369

Kebaetse, M., Mcclure, P., & Pratt, N. 1999. Thoracic position effect on shoulder range of motion, strenght, and three-Dimensional scapular Kinematics. *Archives of physical Medicine and rehabilitation*, **80**(8), 945–950.

Kibler, W. Ben. 1998. The Role of the Scapula in Athletic Shoulder Function. *The American Journal of Sports Medicine*, **26**(2).

Kim, J. 2019. Multicollinearity and misleading statistical results. *Korean Journal of Anesthesiology*, *72*. https://doi.org/10.4097/kja.19087.

Krishnan, R., Björsell, N., Gutierrez-Farewik, E. M., & Smith, C. 2019. A survey of human shoulder functional kinematic representations. *Medical and Biological Engineering and Computing*, **57**(2), 339–367. https://doi.org/10.1007/s11517-018-1903-3.

Kutner, M., Christopher, Nachtsheim, J. C., Neter, J., & Li, W. 2005. In Applied Linear Statistical Models. In *Building the regression model II: Diagnostics*.

Langrana, N. A. 1981. Spatial kinematic analysis of the upper extremity using a biplanar videotaping method. *Journal of Biomechanical Engineering*, **103**(1), 11–17.

Lawrence, Rebekah L., Braman, Jonathan P., Laprade, Robert F., Ludewig, Paula M., Braman, O C S Jonathan P, Staker, Justin L., Laprade, Robert F., Ludewig, Paula M., Braman, Jonathan P., Laprade, Robert F., Ludewig, Paula M., Staker, Justin L., Laprade, Robert F., & Ludewig, Paula M. 2014. Com-parison of 3-Dimensional Shoulder Complex Kinematics in Individuals With and Without Shoulder Pain, Part 2: Glenohumeral Joint. *Journal of Orthopaedic & Sports Physical Therapy*, **44**(9), 636-A8.

Leardini, A., Chiari, A., Della Croce, U., & Cappozzo, A. 2005. Human movement analysis using stereophotogrammetry Part 3. Soft tissue artifact assessment and compensation. *Gait and Posture*, **21**(2), 212–225. https://doi.org/10.1016/j.gaitpost.2004.05.002.

Lempereur, M., Leboeuf, F., Brochard, S., Rousset, J., Burdin, V., Rémy-Néris, O. 2010. In vivo estimation of the glenohumeral joint centre by functional methods: accuracy and repeatability assessment. *Journal of Biomechanics*, **43**(2), 370-374.

Levangie P.K., Norkin C.C. 2006. Joint Structure and Function : A Comprehensive Analysis. 4th ed. India: JAYPEE.

Lippert, L. S. 2006. Clinical kinesiology and anatomy. 4th edition. Philadelphia (PA): F.A. Davis Company.

Ludewig, P. M., & Cook, T. M. 2000. Alterations in shoulder kinematics and associated muscle activity in people with symptoms of shoulder impingement. *Physical therapy*, **80**(3), 276–291.

Ludewig, P. M., Phadke, V., Braman, J. P., Hassett, D. R., Cieminski, C. J., & Laprade, R. F. 2009. Motion of the shoulder complex during multiplanar humeral elevation. *Journal of Bone and Joint Surgery - Series A*, **91**(2), 378–389. https://doi.org/10.2106/JBJS.G.01483.

Makhsous, M., Högfors, C., Siemieński, A., & Peterson, B. 1999. Total shoulder and relative muscle strength in the scapular plane. *Journal of Biomechanics*, **32**(11), 1213–1220. https://doi.org/10.1016/s0021-9290(99)00049-4.

Matsui, K., Shimada, K., Andrew, P.D. 2006. Deviation of skin marker from bone target during movement of the scapula. *Journal of Orthopaedic Science*, **11** (2), 180–184.

Meskers C. G., van der Helm F.C., Rozendaal L.A., Rozing P.M. 1998. In vivo estimation of the glenohumeral joint rotation centre from scapular bony landmarks by linear regression. *Journal of Biomechanics*, **31**(1), (Jan 1998), 93-6. doi: 10.1016/s0021-9290(97)00101-2. PMID: 9596544.

Meskers, C. G. M., van de Sande, M. A. J., & de Groot, J. H. 2007. Comparison between tripod and skin-fixed recording of scapular motion. *Journal of Biomechanics*, **40**(4), 941–946. https://doi.org/10.1016/j.jbiomech.2006.02.011.

McClure, P. W., Michener, L. A., Sennett, B.J., Karduna, A.R. 2001. Direct 3-dimensional measurement of scapular kinematics during dynamic movements in vivo. *Journal of Shoulder and Elbow Surgery*, **10**(3), 269-277.

McMahon, P. J., Jobe, F.W., Pink, M. M., Brault, J. R., Perry, J. 1996. Comparative electromyographic analysis of shoulder muscles during planar motions: anterior glenohumeral instability versus normal. *Journal of Shoulder and Elbow Surgery*, **5**(2), 118-123.

McQuade, K. J., Smidt, G.L. 1998. Dynamic scapulohumeral rhythm: the effects of external resistance during elevation of the arm in the scapular plane. *Journal of Orthopaedic and Sports Physical Therapy***, 27**(2), 125-133.

Moore, K.L., Dalley, A.F., Agur, A.M.R. 2010. Clinically oriented anatomy. 6.th edition. Philadelphia (PA): Lippincott Williams and Wilkins.

Moore, Keith L., Dalley, Arthur F., & Agur, Anne M.R. 2014. *Moore Clinically Oriented Anatomy*.

Nelson E. L., Berthier N.E., Konidaris G.D. 2018. Handedness and Reach-to-Place Kinematics in Adults: Left-Handers Are Not Reversed Right-Handers. *Journal of Motor Behavior*, **50**(4), (Jul-Aug 2018), 381-391. doi: 10.1080/00222895.2017.1363698. Epub 2017 Sep 6. PMID: 28876178.

Neumann D. A. 2009. Kinesiology of the musculoskeletal system: Foundations for Physical Rehabilitation.2nd Ed. Elsevier Health Sciences.

Nunes, J. 2019. *Biomechanical Analysis of the Shoulder Joint Motion in Patients with Rotator Cuff Tendinopathy*. 1-90.

Oatis, C. A. 2004. Kinesiology: the mechanics and pathomecanics of human movement. 5th edition. Philadelphia (PA): Lippincott Williams & Wilkins.

Ogston, Jena B., & Ludewig, Paula M. 2007. Differences in 3-dimensional shoulder kinematics be-tween persons with multidirectional instability and asymptomatic controls. *American Journal of Sports Medicine*, **35**(8), 1361–1370.

Palastanga, N., Field, D., Soames, R. 2002. Anatomy and human movement: Structure and function. 4th edition. Edinburgh (UK): Butterworth-Heinemann.

Peat, M. 1986. Functional anatomy of the shoulder complex. *Journal of the American Physical Therapy Association*, **66**(12), 1855-1865.

Prinold, J.A., Shaheen, A.F., Bull, A.M. 2011. Skin-fixed scapula trackers: a comparison of two dynamic methods across a range of calibration positions. *Journal of Biomechanics*. **44** (10), 2004–2007.

Project, P. A. 1986. Production automation. *Data Processing*, **28**(8), 441. https://doi.org/10.1016/0011-684x(86)90434-x.

Pronk, G. M. 1991. The shoulder girdle: analysed and modelled kinematically [doctoral thesis]. [Delft (NL)]: Technical University of Delft.

Quental, C., Folgado, J., Fernandes, P.R., Monteiro, J. 2012a. Bone remodelling analysis of the humerus after a shoulder arthroplasty. *Medical Engineering and Physics*, **34**(8), 1132-1138.

Quental, C., Folgado, J., Ambrósio, J., Monteiro, J. 2012b. A multibody biomechanical model of the upper limb including the shoulder girdle. Multibody System Dynamics, **28**(1-2), 83-108.

Quental, C. 2013. *Biomechanical Tools for the Analysis of the Native and Prosthetic Shoulders*. 1–310.

R. John Runciman. 1993. Biomechanical model of the shoulder joint. Ph.D. thesis.

Rettig, O., Fradet, L., Kasten, P., Raiss, P., Wolf, S.I. 2009. A new kinematic model of the upper extremity based on functional joint parameter determination for shoulder and elbow. *Gait and Posture* **30**(4), 469-476.

Robertson, D. D., Yuan, J., Bigliani, L.U., Flatow, E.L., Yamaguchi, K. 2000. Three dimensional analysis of the proximal part of the humerus: relevance to arthroplasty. *Journal of Bone and Joint Surgery American*, **82-A**(11), 1594-1602.

Rouvière, Henri, & Delmas, André. 2005. Anatomía Humana Descriptiva, Topograficá y Funcional.

Salehi, S., Bleser, G., Reiss, A., & Stricker, D. 2015. Body-IMU autocalibration for inertial hip and knee joint tracking. *BodyNets International Conference on Body Area Networks*, *1*. https://doi.org/10.4108/eai.28-9-2015.2261522.

Schepers H., Koopman H., Veltink P. 2009. Ambulatory Assessment of Ankle and Foot Dynamics. *Biomedical Engineering*, IEEE Transactions on, **54**(5), 895-902.

Schwab, A. L., & Meijaard, J. P. 2006. How to draw Euler angles and utilize Euler parameters. *Proceedings of the ASME Design Engineering Technical Conference*. https://doi.org/10.1115/detc2006-99307.

Scibek, Jason S., Mell, Amy G., Downie, Brian K., Carpenter, James E., Hughes, Richard E., & Arbor, Ann. 2008. Shoulder kinematics in patients with full-thickness rotator cuff tears after a subacromial injection. *Journal of Shoulder and Elbow Surgery*, **17**(1), 172–181.

Scibek, J. S., Carcia, C. R. 2012. Assessment of scapulohumeral rhythm for scapular plane shoulder elevation using a modified digital inclinometer. *World Journal of Orthopedics*, **3**(6), 87- 94.

Silva, M. P. T., Ambrósio, J.A.C. 2002. Kinematic data consistency in the inverse dynamic analysis of biomechanical systems. Multibody System Dynamics, **8**(2), 219-239.

Standring, S. 2008. Gray's anatomy: The anatomical basis of clinical practice. 40th edition. (ES): Churchill Livingstone Elsevier.

Struyf, Filip, Nijs, Jo, Brussel, Vrije Universiteit, Baeyens, Jean-pierre, Brussel, Vrije Universiteit, & Mottram, Sarah. 2011. Scapular positioning and movement in unimpaired shoulders , shoulder impingement syndrome , and glenohumeral instability. *Scandinavian Journal of Medicine and Science in Sports*.

Taylor, Craig L., & Blaschke, Alfred C. 1951. A Method for Kinematic Analysis of Motions of the Shoulder, Arm, and Hand Complex. *Annals of the New York Academy of Sciences*, **51**(7), 1251–1265.

Terry, G. C., Chopp, T. M. 2000. Functional anatomy of the shoulder. *Journal of Athletic Training*, **35**(3), 248-255.

Tortora, Gerard J., & Derrickson, Bryan. 2017. Principles of Anatomy and Phisiology.

Turnbull, J.R. 1998. Acromioclavicular joint disorders. *Medicine & Science In Sports & Exercise*, **30**, S26-32.

Turgut, Elif, Pedersen, Øyvind, Duzgun, Irem, & Baltaci, Gul. 2016. Three-dimensional scapular kinematics during open and closed kinetic chain movements in asymptomatic and symptomatic subjects. *Journal of Biomechanics*, **49**(13), 2770–2777.

Wakimoto K., Dakeshita T., Wakimoto J., et al. 2018. Effects of triple-treatment trunk stretching on physical fitness and curvature of the spine. *Heliyon*, **4**(12), (Dec 1, 2018), e00985. doi: 10.1016/j.heliyon.2018.e00985.

Wilk, K .E., Arrigo, C. A., Andrews, J.R. 1997. Current concepts: the stabilizing structures of the glenohumeral joint. *Journal of Orthopaedic and Sports Physical Therapy*, **25**(6), 364-379.

Wilk, K. E., Reinold, M. M., Andrews, J.R. 2009. The athlete's shoulder. 2.nd edition. Philadelphia (PA): Churchill Livingstone.

Wilkinson, G., & Rogers, C. 1973. Symbolic Description of Factorial Models for Analysis of Variance. *Journal of the Royal Statistical Society. Series C (Applied Statistics),* **22**(3), 392-399. doi:10.2307/2346786.

Woltring, H. J., Huiskes, R., de Lange, A., Veldpaus, F.E. 1985. Finite centroid and helical axis estimation from noisy landmark measurement in the study of human joint kinematics. *Journal of Biomechanics*, **18**(5), 379-389.

Wu, G., van der Helm, F. C., Veeger, H. E., Makhsous, M., van Roy, P., Anglin, C., Nagels, J., Karduna, A. R., McQuade, K., Wang, X., Werner, F. W., Buchholz, B. 2005. ISB recommendation on definitions of joint coordinate systems of various joints for the reporting of human joint motion. Part II. Shoulder, elbow, wrist and hand. *Journal of Biomechanics*, **38**(5), 981-992.

Van Andel, C., van Hutten, K., Eversdijk, M., Veeger, D. J., & Harlaar, J. 2009. Recording scapular

motion using an acromion marker cluster. *Gait and Posture*, **29**(1), 123–128. https://doi.org/10.1016/j.gaitpost.2008.07.012.

VandenBerghe, G., Hoenecke, H.R., Fronek, J. 2005. Glenohumeral joint instability: the orthopaedic approach. *Seminars in Musculoskeletal Radiology*, **9**(1), 34-43.

Van der Helm, F.C.T. 1994a. Analysis of the kinematic and dynamic behavior of the shoulder mechanism. *Journal of Biomechanics***, 27**(5), 527-550.

Van der Helm, F.C.T. 1994b. A finite-element musculoskeletal model of the shoulder mechanism. *Journal of Biomechanics*, **27**(5), 551-569.

Van der Helm, F.C.T., Pronk, G.M. 1995. Three-dimensional recording and description of motions of the shoulder mechanism. *Journal of Biomechanical Engineering*, **117**(1), 27-40.

Veeger H.E. 2000. The position of the rotation centre of the glenohumeral joint. *Journal of Biomechanics*, **33**(12), (Dec, 2000), 1711-5. doi: 10.1016/s0021-9290(00)00141-x. PMID: 11006398.

Vizniak, N. A. 2010. Muscle manual. Burnaby (BC): Professional Health Systems.

Xu, X., Lin, J. hua, & McGorry, R. W. 2014a. A regression-based 3-D shoulder rhythm. *Journal of Biomechanics*, **47**(5), 1206–1210. https://doi.org/10.1016/j.jbiomech.2014.01.043.

Xu, X., McGorry, R. W., & Lin, J. hua. 2014b. The accuracy of an external frame using ISB recommended rotation sequence to define shoulder joint angle. *Gait and Posture*, **39(**1), 662–668. https://doi.org/10.1016/j.gaitpost.2013.08.032.

Yoshizaki, Kunio, Hamada, Junichiro, Tamai, Kazuya, Sahara, Ryo, Fujiwara, Takayuki, & Fujimoto, Tetsuya. 2009. Analysis of the scapulohumeral rhythm and electromyography of the shoulder muscles during elevation and lowering: Comparison of dominant and nondominant shoulders. *Journal of Shoulder and Elbow Surgery*, **18**(5), 756–763.

Zatsiorsky, V. M. 1998. *Kinematics of human motion*. Champaign, IL: Human Kinetics.

Zhou H., Stone T., Hu H., Harris N. 2008. Use of multiple wearable inertial sensors in upper limb motion tracking. *Medical Engineering & Physics*, **30**(1), 123-133.